

AD-A258 914



AFIT/GSO/ENS/92D-3

①

DTIC
ELECTE
JAN 7 1993
S c D

ANALYSIS OF KRIGING APPLIED TO
RESOLUTION ENHANCEMENT OF
DIGITAL SATELLITE IMAGERY

THESIS

David John Blaufuss
Captain, USAF

AFIT/GSO/ENS/92D-3

012225

93-00192



139
R5

Approved for public release; distribution unlimited

93 1 04 092

Thesis Approval

STUDENT: Capt. David J. Blaufuss

CLASS: GSO-92D

THESIS TITLE: Analysis of Kriging Applied to Resolution
Enhancement of Digital Satellite Imagery

DEFENSE DATE: December 1, 1992

COMMITTEE: NAME/DEPARTMENT

SIGNATURE

Advisor Thomas S. Kelso, PhD, Lt Col, USAF
Assistant Professor of Space Operations

Thomas S. Kelso

Reader David G. Robinson, PhD, Maj, USAF
Associate Professor of Aeronautical
and Systems Engineering

David G. Robinson

DTIC QUALITY INSPECTED 8

Accession For	
NTIS GTRAI	<input checked="checked" type="checkbox"/>
DTIC TAB	<input type="checkbox"/>
Unannounced	<input type="checkbox"/>
Justification	
By	
Distribution/	
Availability Codes	
Dist	Avail and/or Special
A-1	

AFIT/GSO/ENS/92D-3

ANALYSIS OF KRIGING APPLIED TO
RESOLUTION ENHANCEMENT OF
DIGITAL SATELLITE IMAGERY

THESIS

Presented to the Faculty of the School of Engineering
of the Air Force Institute of Technology

Air University

In Partial Fulfillment of the
Requirements for the Degree of
Master of Science in Space Operations

David John Blaufuss, B.S.

Captain, USAF

December 1992

Approved for public release; distribution unlimited

Acknowledgements

This topic was a very fastinating and rewarding one for me. It concluded my studies of remote sensing technology by concentrating on the ground processing aspect of remote sensing.

I would like to thank Lt Col Thomas S. Kelso for the incredible amount of work he performed as well as the guidance given me over the last year of research. Without his help, this research would have never been completed. I would also like to thank Maj David Robinson for answers to my questions about kriging theory.

I would also like to thank David Koster for his help with programming, statistics advice, and all the other things done for me, David Wilsey for his programming help, and Jeff Berger for help his help with Mathematica.

David John Blaufuss

Table of Contents

	Page
Acknowledgements	ii
Table of Contents	iii
List of Figures	vii
List of Tables	xii
Abstract	xiv
I. Introduction	1-1
1.1 Background	1-1
1.2 Research Objective	1-2
1.3 Summary of Current Knowledge	1-2
1.4 Scope	1-4
II. Literature Review	2-1
2.1 Introduction	2-1
2.2 Digital Imagery	2-1
2.2.1 Resolution Enhancement.	2-2
2.3 Imaging System Resolution	2-2
2.3.1 Airy Pattern.	2-2
2.3.2 Rayleigh Criterion.	2-3
2.3.3 Resolution Example.	2-4
2.4 Current Resolution Enhancement Techniques	2-7
2.4.1 Nearest-Neighbor.	2-7
2.4.2 Bilinear Interpolation.	2-7
2.4.3 Cubic Convolution.	2-8

	Page
2.5 Kriging	2-9
2.5.1 Structural Analysis.	2-11
2.5.2 Ordinary Kriging.	2-18
2.5.3 Ordinary Kriging Example.	2-20
2.5.4 Universal Kriging.	2-22
2.5.5 Universal Kriging Example.	2-23
2.6 Conclusions	2-26
III. Methodology	3-1
3.1 Image Data	3-1
3.1.1 Image Used.	3-1
3.1.2 Sub-Sampling.	3-1
3.2 Current Methods	3-2
3.2.1 Neighborhood.	3-2
3.3 Kriging Implementation	3-2
3.3.1 Structural Analysis.	3-2
3.3.2 Kriging Equations.	3-3
3.4 Program Operation	3-3
3.5 Tests	3-4
3.6 Statistical Analysis	3-4
3.6.1 Variance Test.	3-5
3.6.2 Mean Test.	3-5
3.7 Summary	3-6
IV. Results	4-1
4.1 Structural Analysis.	4-1
4.1.1 Model Determination.	4-1
4.1.2 Anisotropy.	4-1

	Page
4.1.3 Range.	4-1
4.2 Enhanced Images	4-1
4.2.1 Test Statistics.	4-2
4.2.2 Comparisons of Two Population Variances.	4-2
4.2.3 Comparisons of Two Population Means.	4-2
4.2.4 Regression/No Regression Comparison.	4-3
4.3 Summary	4-4
V. Recommendations	5-1
5.1 Program Improvements.	5-1
5.1.1 Model Estimation.	5-1
5.2 Summary	5-1
Appendix A. Image Sections	A-1
Appendix B. Program Operation	B-1
B.1 Flags	B-1
B.1.1 Regression.	B-1
B.1.2 Models.	B-1
B.1.3 Nugget Effect.	B-1
B.1.4 Kriging.	B-2
B.2 Image Data	B-2
B.3 Regression	B-2
B.4 Semi-Variogram	B-3
B.4.1 Calculations and Model Formulation.	B-3
B.4.2 Data and Plot Generation.	B-4
B.4.3 Output Files.	B-4
B.5 Kriging Equations	B-5
B.5.1 Ordinary Kriging.	B-5

	Page
B.5.2 Universal Kriging.	B-6
B.5.3 Right-Hand-Side.	B-6
B.5.4 Solution.	B-7
B.6 Cubic Convolution	B-7
B.7 Recombination	B-8
B.8 Image Comparison	B-8
Appendix C. Semi-Variograms of Residuals	C-1
C.1 Variograms	C-1
C.2 Exponential Model	C-13
C.3 Spherical Model	C-25
C.4 Nugget (Exponential Model).	C-37
C.5 Nugget (Spherical Model).	C-43
Appendix D. Test Statistics (Mean and Standard Deviation)	D-1
D.1 Kriging and Cubic Convolution Comparison	D-1
D.2 Interpolation and Spherical Model Comparison	D-3
D.3 Interpolation and Exponential Model Comparison	D-5
D.4 Non-Nugget and Nugget Comparison	D-7
D.4.1 Spherical Model.	D-7
D.5 Non-Nugget and Nugget Comparison	D-8
Appendix E. Program	E-1
E.0.1 Exponential Model.	E-1
E.1 Program Listing	E-1
E.2 Quinn-Curtis Routine Description	E-12
Bibliography	BIB-1
Vita	VITA-1

List of Figures

Figure	Page
2.1. Airy Pattern	2-3
2.2. Airy Disk	2-4
2.3. Rayleigh Criterion	2-5
2.4. Imaging System Geometry	2-6
2.5. Bilinear Interpolation	2-8
2.6. Cubic Convolution	2-10
2.7. Data on a grid for the calculation of an experimental semi-variogram	2-12
2.8. Cross-Section Through the Iron Ore Deposit	2-13
2.9. Identifying all Pairs at 100 ft Apart in the East-West Direction	2-14
2.10. Identifying all Pairs at 200 ft Apart in the East-West Direction	2-15
2.11. Experimental Semi-Variograms in 0° and 90° Directions	2-16
2.12. Linear Model	2-16
2.13. Spherical Model	2-17
2.14. Exponential Model	2-18
2.15. Experimental Semi-Variograms in 0° and 90°	2-19
2.16. Water table elevations (meters) at three observation wells	2-20
2.17. Water table elevations (meters) at five observation wells	2-24
3.1. Neighborhood Pixels	3-4
B.1. GNUPLOT Example.	B-5
C.1. Offset 000,210; First Order, SPOT 1 Channel 2	C-1
C.2. Offset 108,168; First Order, SPOT 1 Channel 2	C-2
C.3. Offset 365,370; First Order, SPOT 1 Channel 2	C-2
C.4. Offset 390,130; First Order, SPOT 1 Channel 2	C-3
C.5. Offset 090,250; First Order, SPOT 2 Channel 2	C-3

Figure	Page
C.6. Offset 100,130; First Order, SPOT 2 Channel 2	C-4
C.7. Offset 100,470; First Order, SPOT 2 Channel 2	C-4
C.8. Offset 100,570; First Order, SPOT 2 Channel 2	C-5
C.9. Offset 150,100; First Order, SPOT 2 Channel 2	C-5
C.10. Offset 290,050; First Order, SPOT 2 Channel 2	C-6
C.11. Offset 258,000; First Order, SPOT 2 Channel 2	C-6
C.12. Offset 258,000; First Order, SPOT 2 Channel 3	C-7
C.13. Offset 000,210; First Order, SPOT 1 Channel 3	C-7
C.14. Offset 108,168; First Order, SPOT 1 Channel 3	C-8
C.15. Offset 365,370; First Order, SPOT 1 Channel 3	C-8
C.16. Offset 390,130; First Order, SPOT 1 Channel 3	C-9
C.17. Offset 090,250; First Order, SPOT 2 Channel 3	C-9
C.18. Offset 100,130; First Order, SPOT 2 Channel 3	C-10
C.19. Offset 100,130; First Order, SPOT 2 Channel 3	C-10
C.20. Offset 100,470; First Order, SPOT 2 Channel 3	C-11
C.21. Offset 100,570; First Order, SPOT 2 Channel 3	C-11
C.22. Offset 150,100; First Order, SPOT 2 Channel 3	C-12
C.23. Offset 290,050; First Order, SPOT 2 Channel 3	C-12
C.24. Offset 000,210; First Order, SPOT 1 Channel 2, Exponential model	C-13
C.25. Offset 108,168; First Order, SPOT 1 Channel 2, Exponential model	C-13
C.26. Offset 365,370; First Order, SPOT 1 Channel 2, Exponential model	C-14
C.27. Offset 390,130; First Order, SPOT 1 Channel 2, Exponential model	C-14
C.28. Offset 090,250; First Order, SPOT 2 Channel 2, Exponential model	C-15
C.29. Offset 100,130; First Order, SPOT 2 Channel 2, Exponential model	C-15
C.30. Offset 100,470; First Order, SPOT 2 Channel 2, Exponential model	C-16
C.31. Offset 100,570; First Order, SPOT 2 Channel 2, Exponential model	C-16
C.32. Offset 150,100; First Order, SPOT 2 Channel 2, Exponential model	C-17

Figure	Page
C.33.Offset 290,050; First Order, SPOT 2 Channel 2, Exponential model	C-17
C.34.Offset 258,000; First Order, SPOT 2 Channel 2, Exponential model	C-18
C.35.Offset 258,000; First Order, SPOT 2 Channel 3, Exponential model	C-19
C.36.Offset 000,210; First Order, SPOT 1 Channel 3, Exponential model	C-19
C.37.Offset 108,168; First Order, SPOT 1 Channel 3, Exponential model	C-20
C.38.Offset 365,370; First Order, SPOT 1 Channel 3, Exponential model	C-20
C.39.Offset 390,130; First Order, SPOT 1 Channel 3, Exponential model	C-21
C.40.Offset 090,250; First Order, SPOT 2 Channel 3, Exponential model	C-21
C.41.Offset 100,130; First Order, SPOT 2 Channel 3, Exponential model	C-22
C.42.Offset 100,130; First Order, SPOT 2 Channel 3, Exponential model	C-22
C.43.Offset 100,470; First Order, SPOT 2 Channel 3, Exponential model	C-23
C.44.Offset 100,570; First Order, SPOT 2 Channel 3, Exponential model	C-23
C.45.Offset 150,100; First Order, SPOT 2 Channel 3, Exponential model	C-24
C.46.Offset 290,050; First Order, SPOT 2 Channel 3, Exponential model	C-24
C.47.Offset 000,210; First Order, SPOT 1 Channel 2, Spherical Model	C-25
C.48.Offset 108,168; First Order, SPOT 1 Channel 2, Spherical Model	C-25
C.49.Offset 365,370; First Order, SPOT 1 Channel 2, Spherical Model	C-26
C.50.Offset 390,130; First Order, SPOT 1 Channel 2, Spherical Model	C-26
C.51.Offset 090,250; First Order, SPOT 2 Channel 2, Spherical Model	C-27
C.52.Offset 100,130; First Order, SPOT 2 Channel 2, Spherical Model	C-27
C.53.Offset 100,470; First Order, SPOT 2 Channel 2, Spherical Model	C-28
C.54.Offset 100,570; First Order, SPOT 2 Channel 2, Spherical Model	C-28
C.55.Offset 150,100; First Order, SPOT 2 Channel 2, Spherical Model	C-29
C.56.Offset 290,050; First Order, SPOT 2 Channel 2, Spherical Model	C-29
C.57.Offset 258,000; First Order, SPOT 2 Channel 2, Spherical Model	C-30
C.58.Offset 258,000; First Order, SPOT 2 Channel 3, Spherical Model	C-31
C.59.Offset 000,210; First Order, SPOT 1 Channel 3, Spherical Model	C-31

Figure	Page
C.60.Offset 108,168; First Order, SPOT 1 Channel 3, Spherical Model	C-32
C.61.Offset 365,370; First Order, SPOT 1 Channel 3, Spherical Model	C-32
C.62.Offset 390,130; First Order, SPOT 1 Channel 3, Spherical Model	C-33
C.63.Offset 090,250; First Order, SPOT 2 Channel 3, Spherical Model	C-33
C.64.Offset 100,130; First Order, SPOT 2 Channel 3, Spherical Model	C-34
C.65.Offset 100,130; First Order, SPOT 2 Channel 3, Spherical Model	C-34
C.66.Offset 100,470; First Order, SPOT 2 Channel 3, Spherical Model	C-35
C.67.Offset 100,570; First Order, SPOT 2 Channel 3, Spherical Model	C-35
C.68.Offset 150,100; First Order, SPOT 2 Channel 3, Spherical Model	C-36
C.69.Offset 290,050; First Order, SPOT 2 Channel 3, Spherical Model	C-36
C.70.Offset 000,210; First Order, SPOT 1 Channel 2, Spherical Model	C-37
C.71.Offset 108,168; First Order, SPOT 1 Channel 2, Exponential model	C-37
C.72.Offset 365,370; First Order, SPOT 1 Channel 2, Exponential model	C-38
C.73.Offset 390,130; First Order, SPOT 1 Channel 2, Exponential model	C-38
C.74.Offset 090,250; First Order, SPOT 2 Channel 2, Exponential model	C-39
C.75.Offset 100,130; First Order, SPOT 2 Channel 2, Exponential model	C-39
C.76.Offset 100,470; First Order, SPOT 2 Channel 2, Exponential model	C-40
C.77.Offset 100,570; First Order, SPOT 2 Channel 2, Exponential model	C-40
C.78.Offset 150,100; First Order, SPOT 2 Channel 2, Exponential model	C-41
C.79.Offset 290,050; First Order, SPOT 2 Channel 2, Exponential model	C-41
C.80.Offset 258,000; First Order, SPOT 2 Channel 2, Exponential model	C-42
C.81.Offset 000,210; First Order, SPOT 1 Channel 2, Spherical Model	C-43
C.82.Offset 108,168; First Order, SPOT 1 Channel 2, Spherical Model	C-43
C.83.Offset 365,370; First Order, SPOT 1 Channel 2, Spherical Model	C-44
C.84.Offset 390,130; First Order, SPOT 1 Channel 2, Spherical Model	C-44
C.85.Offset 090,250; First Order, SPOT 2 Channel 2, Spherical Model	C-45
C.86.Offset 100,130; First Order, SPOT 2 Channel 2, Spherical Model	C-45

Figure	Page
C.87.Offset 100,470; First Order, SPOT 2 Channel 2, Spherical Model	C-46
C.88.Offset 100,570; First Order, SPOT 2 Channel 2, Spherical Model	C-46
C.89.Offset 150,100; First Order, SPOT 2 Channel 2, Spherical Model	C-47
C.90.Offset 290,050; First Order, SPOT 2 Channel 2, Spherical Model	C-47
C.91.Offset 258,000; First Order, SPOT 2 Channel 2, Spherical Model	C-48

List of Tables

Table	Page
2.1. Water Table Elevation Data for the Ordinary Kriging Example.	2-21
2.2. Distances Between Wells and Point p (Ordinary Kriging).	2-21
2.3. Semi-Variograms for Distances Between Wells and Point p for the Ordinary Kriging Example.	2-21
2.4. Water Table Elevation Data for the Universal Kriging Example.	2-23
2.5. Distances Between Wells and p for the Universal Kriging Example.	2-24
2.6. Semi-Variograms for Distances Between Wells and Point p for the Universal Kriging Example.	2-25
A.1. Image Sections Tested, SPOT 1 Channel 2	A-1
A.2. Image Sections Tested, SPOT 1 Channel 3	A-1
A.3. Image Sections Tested, SPOT 2 Channel 2	A-2
A.4. Image Sections Tested, SPOT 2 Channel 3	A-2
D.1. Comparison Data, SPOT 1, Channel 2	D-1
D.2. Comparison Data, SPOT 1, Channel 3	D-1
D.3. Comparison Data, SPOT 2, Channel 2	D-2
D.4. Comparison Data, SPOT 2, Channel 3	D-2
D.5. Comparison Data, SPOT 1, Channel 2	D-3
D.6. Comparison Data, SPOT 1, Channel 3	D-3
D.7. Comparison Data, SPOT 2, Channel 2	D-3
D.8. Comparison Data, SPOT 2, Channel 3	D-4
D.9. Comparison Data, SPOT 1, Channel 2	D-5
D.10. Comparison Data, SPOT 1, Channel 3	D-5
D.11. Comparison Data, SPOT 2, Channel 2	D-6
D.12. Comparison Data, SPOT 2, Channel 3	D-6

Table	Page
D.13.Comparison Data, SPOT 1, Channel 2, Spherical Model.	D-7
D.14.Comparison Data, SPOT 2, Channel 2, Spherical Model	D-7
D.15.Comparison Data, SPOT 1, Channel 2, Exponential Model	D-8
D.16.Comparison Data, SPOT 2, Channel 2, Exponential Model	D-8

Abstract

To aid the viewer in interpreting the information contained in an image, spatial resolution of the image can be increased. One way to increase the resolution is to improve the optics and sensors of the imaging system. Another is to process the data on the ground by computer. Enhancement techniques can be employed to alter the image and extract necessary data. Current techniques to manipulate and enlarge an image are nearest-neighbor, bilinear interpolation, and cubic convolution which can give greater clarity and readability. To satisfy the growing demand for quality (high-resolution) remotely sensed images, new techniques to enhance images need to be developed.

Kriging is the geostatistical spatial estimation technique developed by Matheron that optimally predicts spatial data using observations at nearby locations. Kriging can be applied to many specialties and applications such as lead contamination in the soil near a smelter or prevalence of AIDS within a population viewed geographically.

This research investigates the application of kriging as a technique of digital image resolution enhancement by adapting its use for the personnel computer and validating its capability and reliability. Twenty-seven percent of the images tested produced significantly lower means for kriging than cubic convolution with 45 percent of the kriged images producing lower variances. When universal and ordinary kriging were tested, no difference was found between the means and variances while no significant differences between the use of a model and linear interpolation for semi-variogram estimation was found.

ANALYSIS OF KRIGING APPLIED TO RESOLUTION ENHANCEMENT OF DIGITAL SATELLITE IMAGERY

I. Introduction

This research continues the efforts of Captain Donald W. McGee, Jr. and investigates the application of statistical kriging to digital image resolution enhancement. This research builds on the theoretical background of McGee and further adapts the technique of kriging by taking advantage of the regular nature of satellite imagery to simplify processing.

Kriging is the geostatistical spatial estimation technique developed by Matheron that optimally predicts spatial data using observations at nearby locations (18:1259). Christensen states "the object of kriging is the prediction of unobserved spatial random variables based on the values of observed random variables" (4:267) and adds, "there are innumerable situations in which data are collected at various locations in space and thus innumerable potential application for methods of analysis for spatial data" (4:262). Kriging can be applied to many specialties and applications such as lead contamination in the soil near a smelter or prevalence of AIDS within a population viewed geographically (4:263) or resolution enhancement of digital imagery. This paper provides background, objectives, summary of current knowledge, scope, and methodology of the research to apply kriging to digital image resolution enhancement.

1.1 Background

The traditional method for extracting data from images is manual interpretation (3:719). With the invention of the charge-coupled device (CCD) and advances in computer technology, quick and easy spatial resolution enhancement is now possible. Spatial resolution is the degree of discernible detail of an image or the ability to distinguish between spatial elements within an image (17:36). Because increasing the spatial resolution of imagery extracts the most information possible from the image, it has become major concern of remote sensing specialists, astronomers, and the intelligence community. Resolution may be increased in two ways:

1. Optics and sensors of the imaging system can be improved (larger optics, lower altitudes, or larger CCD arrays) to increase the spatial resolution of the images produced. Changing

the imaging system is undesirable because it is costly and produces massive amounts of data creating problems with data handling and distribution.

2. Image data can be processed on the ground to enhance resolution. Processing involves enlarging the original image (through the addition of blank pixels to produce a larger image) and then estimating and assigning new values to the coordinates of the blank pixels to reproduce the image. This enhancement method is preferred due to its lower cost and relative simplicity.

Though processing of the images to enhance their resolution is preferred, problems exist with the current techniques. Three processing methods are commonly used to estimate pixel values: they are nearest-neighbor, bilinear interpolation, and cubic convolution. The nearest-neighbor technique leaves images blocky in appearance while bilinear interpolation tends to blur the image. Neither result is desirable.

This research will continue the development of kriging as a viable and preferred image resolution enhancement technique. On kriging's ability of spatial estimation, Cressie states "In all comparisons, on real and simulated data, universal kriging generally did as well or better than the other methods" (6:202). Kriging can perform as well or better than current enhancement techniques because it is an exact method of estimation. In digital image terms, the gray values of the original image are reproduced exactly with no error while estimating new spatial data. Kriged images will not have the blocky appearance of nearest-neighbor nor blurs the image as does bilinear interpolation (20:112). It is the best of all processing techniques and is truly a best linear unbiased predictor (4:262).

1.2 Research Objective

This research investigates the application of kriging as a technique of digital image resolution enhancement by adapting its use for the personnel computer and validating its capability and reliability.

Ultimate goals of the research are streamlining the kriging approach (to keep processing times low) and validation of previous work by testing the technique over image varying in terrain and spectral qualities.

1.3 Summary of Current Knowledge

Many techniques of generating new pixel values from old are available but processing costs and quality control the choice of method.

The nearest-neighbor technique of resolution enhancement is the simplest method in use today. The value of the new pixel takes the value of the original pixel nearest to its location. The nearest-neighbor technique has two main advantages: it is fast (takes little processor time) and preserves the exact pixel values in the input image (17:138). This method introduces spatial errors into the image and shifts the original pixel from its current location (3:734). The resultant image has a blocky appearance and can be difficult to read.

Bilinear interpolation uses the gray levels of the four nearest neighbors to estimate the new pixel values. This is done by taking the gray levels of the four nearest neighbors and interpolating the new values to estimate the new points. This technique fills the desired pixels and produces smoother images (13:301).

Cubic convolution is "based on the fitting of a two-dimensional, third-degree polynomial surface to the region surrounding the point" (17:141) of the form $(\sin x)/x$ and produces a smooth estimate of the gray level (13:300). Mather states, this technique "gives a more natural-looking image without the blockiness of the nearest-neighbor [technique] or the over-smoothing of the bilinear method [but loses some data in the process]" (17:141). One problem in the implementation of this method is that it requires an infinite amount of data to accurately estimate the $(\sin x)/x$ function (2:55). This method takes more processing time to achieve the desired results than the previous methods and is currently the "best" technique in use today.

The application of kriging to the problem of digital image resolution enhancement has produced promising results. McGee states "quantitative comparison of the kriging and cubic convolution techniques indicates that image enhancement by universal punctual kriging can produce images which are more faithful than cubic convolution to the original image" (19:4-30). Kriging produced image differences that were 6.4 times smaller than the mean difference produced by cubic convolution with a standard deviation of 4.73 times smaller (in the cases examined) (19). "Kriging methods were clearly superior to the convolution methods in recreating the original image" (19).

Other potential applications of kriging to image enhancement suggested by McGee include noise reduction and as a method of edge detection. "Noise elimination using kriging should produce better results than other methods and should improve image classification and the forecasts made for the enhanced imagery" (19:5-2). When compared to the original image, the concentration of error produced at the perimeter of objects within an image suggests that kriging has potential as a method of edge detection for pattern recognition (19:5-2).

1.4 Scope

This research will be limited to the application of kriging to the enhancement of image resolution. Current techniques to enhance image resolution such as nearest-neighbor, bilinear interpolation, and cubic convolution will be compared to kriging. Validation, consolidation, and streamlining of processing will be the main emphasis of the approach. The statistical background of kriging and application of kriging for data reduction, noise reduction, or edge detection will not be covered within the scope of this analysis. Due to technique limitations, visual image will not be included in the research with the statistical analysis be the limit of the results.

II. Literature Review

2.1 Introduction

Remote sensing is the measurement and collection of spectral data (reflected or emitted electromagnetic (EM) radiation) from a planet's surface or atmosphere from a remote distance (17:1). The images that are produced from this data are representations that vary in brightness, color, or reflectance and can be described mathematically by a function of two variables (14:9). This two-dimensional light-intensity function $f(x, y)$ gives the brightness of the image (13:28).

To aid the viewer in interpreting the information contained in an image, spatial resolution of the image can be increased. One way to increase the resolution is to improve the optics and sensors of the imaging system. Another is to process the data on the ground by computer. Enhancement techniques can be employed to alter the image and extract necessary data. Current techniques to manipulate and enlarge an image are nearest-neighbor, bilinear interpolation, and cubic convolution which can give greater clarity and readability. These techniques have their problems though, either leaving the image blocky in appearance or blur the image (20:112).

To satisfy the growing demand for quality (high-resolution) remotely sensed images, new techniques need to be developed. According to McGee, the geostatistical estimating technique of kriging "can perform well in image enhancement by improving the resolution of satellite imagery" and "can produce images which are more faithful than cubic convolution to the original image" but leave the original image unchanged (19:4-30).

This chapter is a review of literature dealing with the basic makeup of digital imagery, resolution of imaging systems, current digital enhancement techniques and the application of kriging as applied to digital image enhancement.

2.2 Digital Imagery

Mather (17:153) defines a digital image as "a numerical record of the radiance leaving each of a large number of rectangular areas" called picture elements (pixels). The radiance values can be stored as six, seven, eight, or ten-bit words for later access. (17:153). As examples, the Advanced Very High Resolution Radiometer (AVHRR) on the Television and Infrared Observation Satellite (TIROS) weather satellites use a ten-bit word where the Landsat Thematic Mapper uses eight-bit words. All pixels discussed for particular techniques in this research will be eight-bit words. Associated with each pixel is a value that corresponds to the relative radiance of the area being studied. The pixel typically assumes a gray (or brightness) level value ranging from 0 to 255 where

0 represents black and 255 white. A digital image can be considered a three-dimensional array where the x and y axes are the spatial representations of the image and the z axis is the radiance value of the pixel (17:153). A computer displays the monochromatic image on an output device by assigning the gray level to pixels on the device.

2.2.1 Resolution Enhancement. Magnification of an image is enlargement of part of an image to increase its resolution. Resolution is the degree of discernible detail and is dependent on its dimensions (13:33). The goal of the magnification is to make features noticeable that were not noticeable in the original image (19:2-2). A simple way to enhance the resolution of an image is to copy the original gray level pixel values and duplicate each pixel by a factor called the zoom or magnification factor. The magnification factors are usually limited to two, four, and eight (17:95). This makes for crude images that can be worse than the original. A better technique than this copy-and-repeat method would be an interpolator.

2.3 Imaging System Resolution

One method to increase the spatial resolution of an image is to improve the optical system used to collect the EM radiation that forms the image. Larger optics and advanced CCD arrays will decrease the field of view (FOV) of each sensor element but not without problems and limitations.

2.3.1 Airy Pattern. The irradiance on the focal plane of an imaging system from a point source takes the shape of a Bessel function or "Airy pattern" (named after Sir George Airy) not a point as one might expect (10:137). See Figure 2.1 for a graphical representation of an Airy pattern. This diffraction pattern forms a three-dimensional Airy disk (Figure 2.2), on the sensor array with 84 percent of the EM radiation entering the sensor contained in the center ring.

The radius r of the center circle depends on the diameter D and focal length f of the collecting optics and the wavelength λ of the collected radiation by the following relationships (10:138):

$$r \approx 1.22f\lambda/D \quad (2.1)$$

which can be represented as:

$$\alpha \approx 1.22\lambda/D \quad (2.2)$$

with α representing the angular resolution.

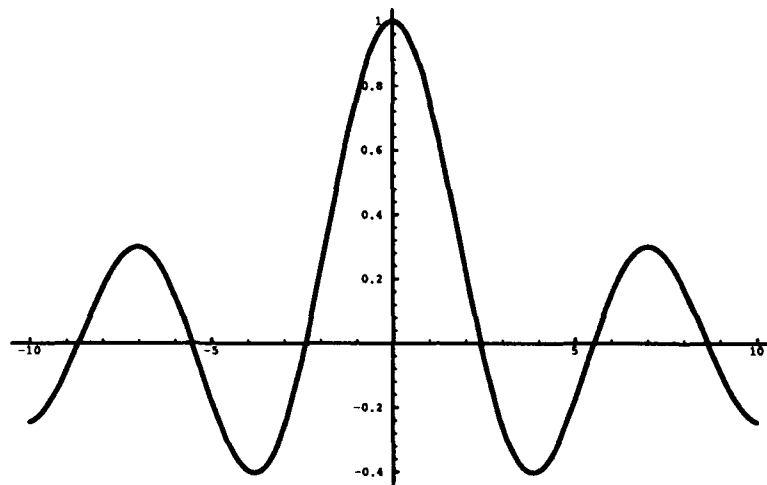


Figure 2.1. Airy Pattern. (10:139)

2.3.2 Rayleigh Criterion. Spatial resolution can then be defined as the minimum separation between the center peaks of two adjacent Airy disks. This “Rayleigh criterion” (Figure 2.3) can be applied to satellite images and is considered the best possible resolution that an imaging system can attain. A satellite at an altitude A , viewing the surface of the earth with an angle ϕ from nadir, has a linear separation of S on the ground given by (10:140):

$$S \approx (1.22 f \lambda A / D) \sec \phi \quad (2.3)$$

2.3.2.1 Diffraction-Limited. The Rayleigh criterion represents the best possible resolution an imaging system can achieve and is called diffraction-limited resolution. In reality, resolution will be limited by many other factors besides diffraction. Physical size and spacing of the detector elements in an array place additional limits on the imaging system. Elements must be small enough to distinguish between the two Airy disks. Further reductions in resolution are caused by lack of stability in the space platform, observation geometry providing non-uniform FOV, atmospheric turbulence, and aberrations in the focusing mirrors.

To obtain improvement in the resolution of the imaging system, alterations in focal length, diameter of optics, CCD element size, satellite altitude, or observed wavelength are required. Figure 2.4 illustrates the geometry of the FOV of one pixel in a satellite imaging system. Since minimum altitude is limited by orbital mechanics and wavelength is controlled by the specific application of the system, changes in the optics and array are the only options available to satellite designers to

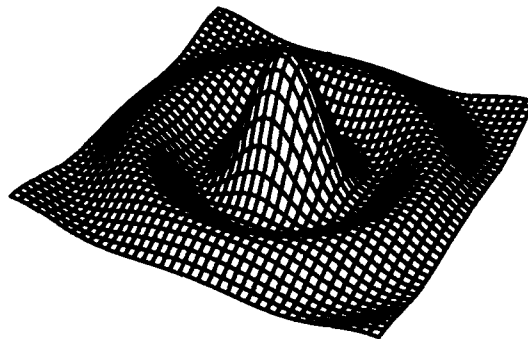


Figure 2.2. Airy Disk. (10:140)

maximize resolution. Focal length, mirror diameter, or CCD element size may be altered to achieve the required resolution.

2.3.3 Resolution Example. The following is an example illustrating the limits of current state-of-the-art imaging systems. This example is adapted from class notes from for PHYS 621, Electro-Optical Space Systems Technology (11).

2.3.3.1 Element Size. If the Hubble Telescope were pointed toward Earth to image and distinguish characters on an automobile license plate, what size detectors and optics would be required? To satisfy the Rayleigh criterion, the system must resolve, in this case, objects (plate characters) 2 cm apart, so using the following Hubble optics dimensions:

$$D = 2.4\text{m}$$

$$f = 6.4\text{m}$$

$$A = 700\text{km}$$

$$S = 2\text{cm}$$

and the previous equations would result in:

$$\begin{aligned}\alpha_{full} &= S/A \\ &= .02\text{m}/7 \times 10^5\text{m}\end{aligned}$$

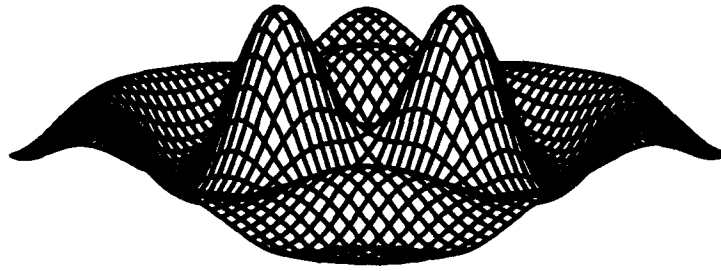


Figure 2.3. Rayleigh Criterion. (10:140)

$$= 2.86 \times 10^{-8} \text{rad}$$

then

$$\begin{aligned} r &= \alpha f \\ &= (2.86 \times 10^{-8} \text{rad})(6.4 \text{m}) \\ &= 0.183 \mu\text{m} \end{aligned}$$

These results show that the CCD elements must be smaller in size than the wavelength of the received light (visible range of $.4\mu\text{m}$ to $.7\mu\text{m}$) in order to distinguish characters on the plate. Current state-of-the-art Si CCD elements are $13\mu\text{m}$ in size.

2.3.3.2 Diffraction-Limited. For diffraction-limited resolutions (the best resolution possible for the Hubble Telescope), the smallest distinguishable distance projected upon the CCD array is:

$$\begin{aligned} r &\approx 1.22 f \lambda / D \\ &\approx 1.22(6.4 \text{m})(.5 \mu\text{m}) / 2.4 \text{m} \\ &\approx 1.63 \mu\text{m} \end{aligned}$$

(2.4)

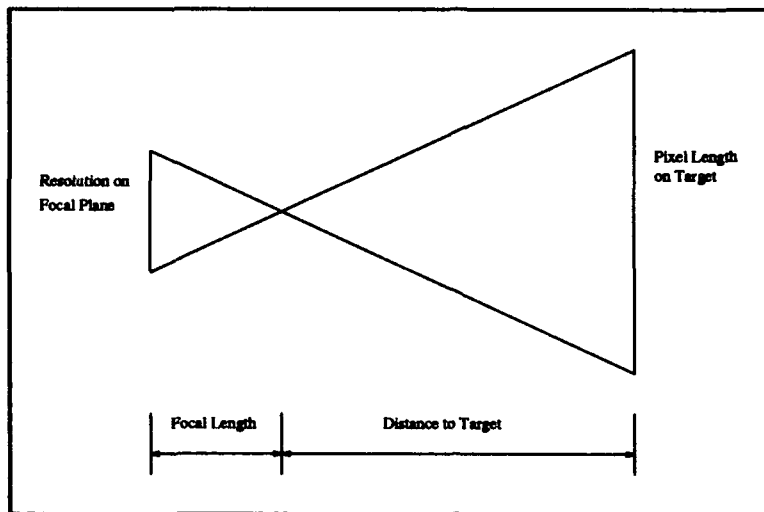


Figure 2.4. Imaging System Geometry. (10:140)

This result is larger than the r necessary to identify the plate numbers. In other words, the Hubble Telescope's mirror must be altered to perform this task. To accomplish this task, the Hubble Telescope's mirror must have the following diameter D :

$$\begin{aligned}
 D &\approx 1.22f\lambda/r \\
 &\approx 1.22(6.4\text{m})(.183\mu\text{m})/2.4\text{m} \\
 &\approx 21.3\text{m}
 \end{aligned}$$

The diameter of optics to perform the task would be unmanageable in space as well as being beyond current technology.

This example demonstrates the changes required to alter a satellites optical system to increase the resolution of the imagery produced by the system. The problems associated with such a change include:

1. CCD element size. State-of-the-art CCD technology cannot produce the necessary element size.
2. Mirror diameter. To compensate for the larger element size, the mirror of the satellite must be very large which would make it unmanageable in space as well as being beyond current technology.

2.4 Current Resolution Enhancement Techniques

An alternative to altering the optics of an imaging system is to use ground software to enhance the resolution of an image. This method is considerably cheaper and is without the problems associated with increasing the power of the optics. For software magnification, the portion of interest within the image is selected and this area is expanded (pixels are spaced out) and new pixels are added between the original pixels. Gray levels are then estimated and assigned to the coordinates of the new pixels. Currently three processing methods are used today to estimate pixel values and they are:

- Nearest-neighbor
- Bilinear interpolation
- Cubic convolution

2.4.1 Nearest-Neighbor. The nearest-neighbor technique of image magnification is the simplest method in use today. The value of the new pixel takes the value of the original pixel nearest to its location. It assigns the gray level of the closest pixel (DN_{kj}) to the new pixel (Z_{il}) (3:734). The nearest neighbor is found by:

$$k = \text{integer part of } (i+0.5) \quad (2.5)$$

$$l = \text{integer part of } (j+0.5) \quad (2.6)$$

and then

$$Z_{ij} = Z_{kl} \quad (2.7)$$

Nearest-neighbor has two main advantages: it is fast (takes little processor time) and ensures that the pixel values in the enlarged image directly relate to the original image (17:138). This technique is not without its problems. Bernstein states that "the major drawback to nearest neighbor assignment is the discontinuities which are introduced by its zero-order interpolation" which causes a stairstep or blocky appearance to the image (1:6-4).

2.4.2 Bilinear Interpolation. The bilinear interpolation method uses the gray levels of the four nearest neighbors to estimate the new pixel values. Many algorithms to implement bilinear interpolation are possible (1:6-4).

Bernstein describes an algorithm developed by IBM which minimizes the programming complexity and maintains high accuracy:

$$Z_{uv} = Z_{11} + d(Z_{12} - Z_{11}) + d'[Z_{21} + d(Z_{22} - Z_{21}) - d(Z_{12} - Z_{11})] \quad (2.8)$$

where Z_{uv} is the intensity of the new pixel and Z_{11} , Z_{12} , Z_{21} , and Z_{22} are the four nearest neighbors and are selected as shown in Figure 2.5. This technique fills the desired pixels and

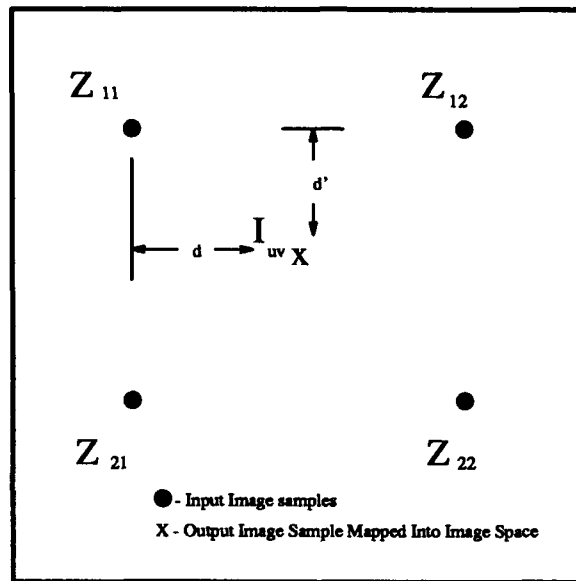


Figure 2.5. Bilinear Interpolation. (1:6-5)

produces smoother images but tends to blur the image (20:112).

2.4.3 Cubic Convolution. Cubic convolution got its name because it is “based on the fitting of a two-dimensional, third-degree polynomial surface to the region surrounding the point” (17:141). Gonzalez says “smoother results can be obtained by using more sophisticated techniques, . . . which fit a surface of the $(\sin x)/x$ type through a much larger number of neighbors . . .” (13:300). This means that the 16 nearest pixel gray levels are used to estimate the value of the new pixel. This technique gives a more natural-looking image without the blockiness of the nearest-neighbor or the over-smoothing of the bilinear method (17:141). One problem in the implementation of the adaptation of this method is that it requires an infinite amount of data to accurately estimate the $(\sin x)/x$ function (2:55).

Bernstein describes an algorithm used for cubic convolution which uses four input points (horizontal interpolation points) and 16 neighbors in the following way:

$$Z'_k = Z_{k1}[4 - 8(1 + d) + 5(1 + d)^2 - (1 + d)^3] \quad (2.9)$$

$$\begin{aligned} & + Z_{k2}(1 - 2d^2) + d^3) \\ & + Z_{k3}[(1 - 2(1 - d)^2 + (1 - d)^3] \\ & + Z_{k4}[4 - 8(2 - d) + 5(2 - d)^2 - (2 - d)^3] \\ = & d\{d[Z_{k4} - Z_{k3} + Z_{k2} - Z_{k1}) \\ & + (-Z_{k4} + Z_{k3} - 2Z_{k2} + 2Z_{k1})] \\ & + (Z_{k3} - Z_{k1})\} + Z_{k2} \end{aligned} \quad (2.10)$$

where

$$\begin{aligned} Z'_k = & d\{d[Z_{k4} - Z_{k3} + Z_{k2} - Z_{k1}) + (Z_{k3} - Z_{k4} \\ & - 2Z_{k2} + 2Z_{k1})] + (Z_{k3} - Z_{k1})\} - Z_{k2} \end{aligned} \quad (2.11)$$

then the final pixel values are solved using the following equation:

$$\begin{aligned} Z_{uv} = & d'\{d'[d'(Z'_4 - Z'_3 + Z'_2 - Z'_1) \\ & + (Z'_3 - Z'_4 - 2Z'_2 + 2Z'_1)] + (Z'_3 - Z'_1)\} - Z'_2 \end{aligned} \quad (2.12)$$

See Figure 2.6 for an illustration of the pixel configuration.

2.5 Kriging

Kriging is a spatial estimation technique developed by Matheron in the early 1960s to estimate ore reserves from spatial core samples. Journel describes kriging as "a local estimation technique which provides the best linear unbiased estimator of the unknown characteristics studied" (15:304). Clark describes kriging as "the optimal prediction in space using observations taken at known nearby locations" and is a weighted average where the weights depend on the location of the points used in the prediction (7:240). The estimator is of the form:

$$\hat{Z}^* = \omega_1 Z_1 + \omega_2 Z_2 + \omega_3 Z_3 + \cdots + \omega_n Z_n \quad (2.13)$$

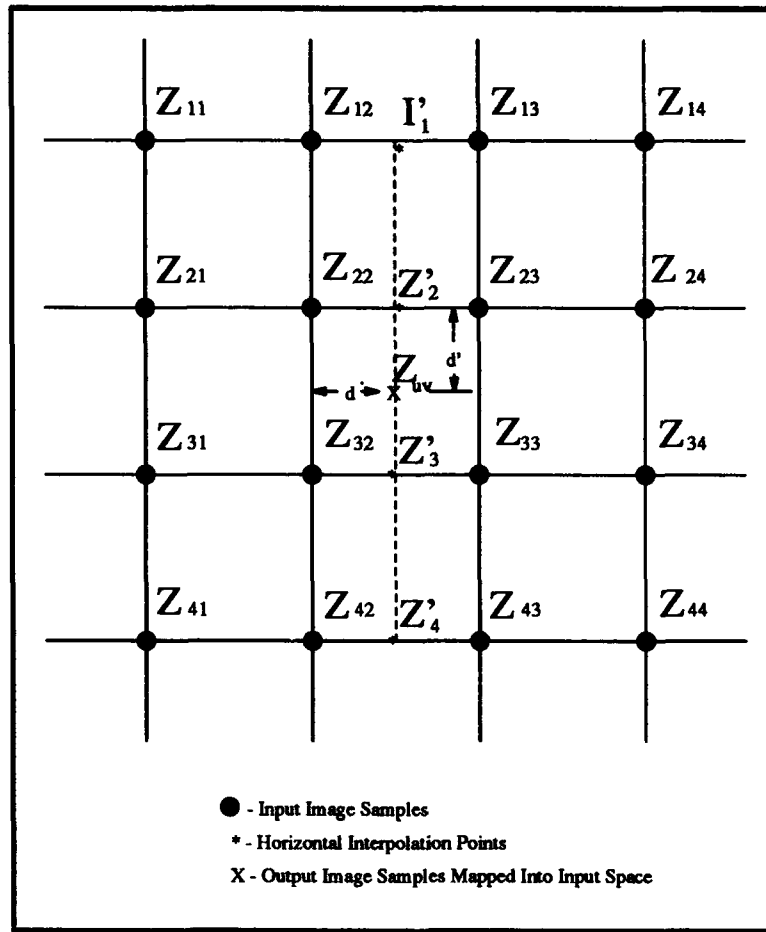


Figure 2.6. Cubic Convolution. (1:6-7)

where the ω_n are the weights, Z_n are the values of the surrounding data, and Z^* is the unbiased estimator (5:99). If the weights used for the estimates sum to one and there is no drift, the estimates are considered unbiased (9:384). The weights are found by using the following kriging equations in general matrix notation:

$$\begin{bmatrix} 0 & 1 & 1 & \cdots & 1 \\ 1 & \gamma(h_{11}) & \gamma(h_{12}) & \cdots & \gamma(h_{1n}) \\ 1 & \gamma(h_{21}) & \gamma(h_{22}) & \cdots & \gamma(h_{2n}) \\ \vdots & \vdots & \vdots & \ddots & \vdots \\ 1 & \gamma(h_{n1}) & \gamma(h_{n2}) & \cdots & \gamma(h_{nn}) \end{bmatrix} \cdot \begin{bmatrix} \lambda \\ w_1 \\ w_2 \\ \vdots \\ w_n \end{bmatrix} = \begin{bmatrix} 1 \\ \gamma(h_{1p}) \\ \gamma(h_{2p}) \\ \vdots \\ \gamma(h_{np}) \end{bmatrix} \quad (2.14)$$

where $\gamma(h_{ij})$ are the calculated semi-variograms between the points in the neighborhood, $\gamma(h_{ip})$ are calculated semi-variograms between the points in the neighborhood and the estimated point, and λ is a Lagrange multiplier used to solve the simultaneous equations.

In this research, kriging is used for spatial prediction of image pixel values during the enhancement of imagery resolution.

2.5.1 Structural Analysis. Structural analysis attempts to find the size, shape, orientation, and spatial arrangement of samples and constitutes the variation of the pixels in an image (9:239). Determination of the variogram, anisotropy, and trend constitute the structural analysis of an image.

2.5.1.1 Variogram. Any discussion of kriging must start with a discussion of the variogram which represents the degree of continuity or correlation of a data set (18:1250). The variogram describes the variance of the difference of samples within the data set and is calculated by the following equation:

$$2\gamma^*(h) = \frac{1}{n} \sum_{i=1}^n [z(x_i) - z(x_i + h)]^2 \quad (2.15)$$

where $z(x)$ is the value of the data at point x and $z(x+h)$ is the value at a point a lag h from x . The semi-variogram is one-half the value of the variogram. We now have a measure of the correlation between data values h apart. As will be seen later, these calculations are easily displayed in graphical form with lags plotted on the horizontal axis and the calculation of the semi-variogram on the vertical axis.

Variogram Example. The following example is used to illustrate the calculation of an experimental semi-variogram (adapted from Clark (5:11-16)).

The data shown in Figure 2.7 represents a stratiform iron deposit in which holes are bored perpendicular to the dip (direction ore deposit travels into the earth) of the ore (see Figure 2.8). In this case, h depends on the distance between sample pairs and the orientation of drilling provides a convenient square grid with holes 100 feet apart (h). The data given is the average value of the iron (percentage by weight) over the bore sample.

Semi-variogram calculations can take place and will be calculated for multiples of 100 feet in the east-west (0 degree) direction. When $h = 0$, $\gamma^*(0) = 0$. When $h = 100$ feet, all pairs 100 feet apart in the 0 degree direction must be found (Figure 2.9) and the semi-variogram $\gamma^*(100)$ is calculated by Equation 2.16.

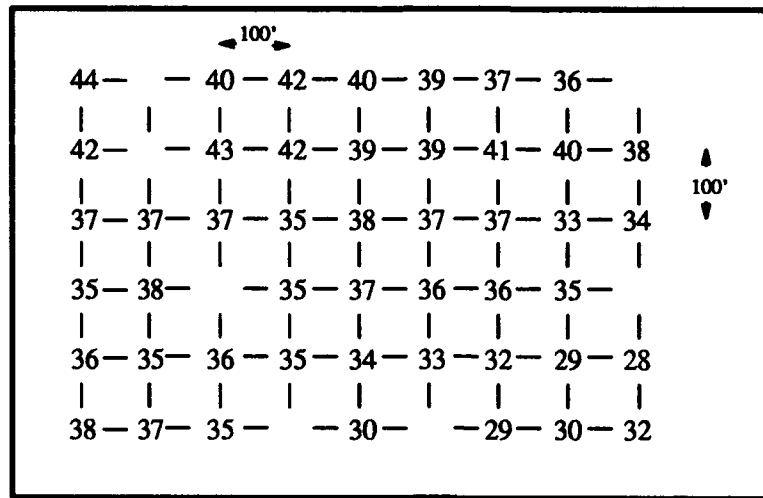


Figure 2.7. Data on a grid for the calculation of an experimental semi-variogram. (5:11)

$$\begin{aligned}
 \gamma^*(100) = & [(40 - 42)^2 + (42 - 40)^2 + (40 - 39)^2 + (39 - 37)^2 \\
 & + (37 - 36)^2 + (43 - 42)^2 + (42 - 39)^2 + (39 - 39)^2 \\
 & + (39 - 41)^2 + (41 - 40)^2 + (40 - 38)^2 + (37 - 37)^2 \\
 & + (37 - 37)^2 + (37 - 35)^2 + (35 - 38)^2 + (38 - 37)^2 \\
 & + (37 - 37)^2 + (37 - 33)^2 + (33 - 34)^2 + (35 - 38)^2 \\
 & + (35 - 37)^2 + (37 - 36)^2 + (36 - 36)^2 + (36 - 35)^2 \\
 & + (36 - 35)^2 + (35 - 36)^2 + (36 - 35)^2 + (35 - 34)^2 \\
 & + (34 - 33)^2 + (33 - 32)^2 + (32 - 29)^2 + (29 - 28)^2 \\
 & + (38 - 37)^2 + (37 - 35)^2 + (29 - 30)^2 \\
 & + (30 - 32)^2] \div (2 \times 36) \\
 \gamma^*(100) = & 1.46
 \end{aligned}
 \tag{2.16}$$

This gives a value for γ^* at $h = 100$ for the graph. Now, find all points 200 feet apart (Figure 2.10) and calculate $\gamma^*(200)$ as in Equation 2.17.

$$\gamma^*(200) = [(44 - 40)^2 + (40 - 40)^2 + (42 - 39)^2 + (40 - 37)^2] \tag{2.17}$$

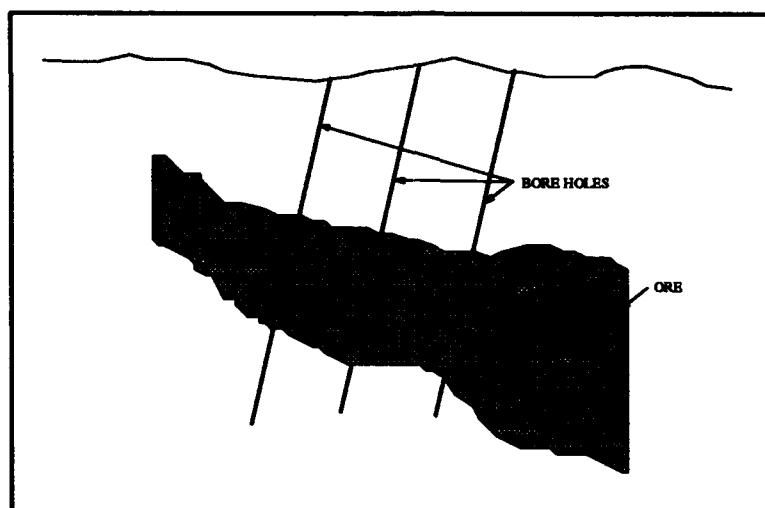


Figure 2.8. Cross-Section Through the Iron Ore Deposit. (5:12)

$$\begin{aligned}
 &+(39-36)^2 + (42-43)^2 + (43-39)^2 + (42-39)^2 \\
 &+(39-41)^2 + (39-40)^2 + (41-38)^2 + (37-37)^2 \\
 &+(37-35)^2 + (37-38)^2 + (35-37)^2 + (38-37)^2 \\
 &+(37-33)^2 + (37-34)^2 + (38-35)^2 + (35-36)^2 \\
 &+(37-36)^2 + (36-35)^2 + (36-36)^2 + (35-35)^2 \\
 &+(36-34)^2 + (35-33)^2 + (34-32)^2 + (33-29)^2 \\
 &+(32-28)^2 + (38-35)^2 + (35-30)^2 + (30-29)^2 \\
 &+(29-32)^2] \div (2 \times 33)
 \end{aligned}$$

$$\gamma^*(200) = 3.30$$

This gives a second point to graph. Calculations can continue up to $h = 800$ feet but Clark states, "In practice, we rarely go past about half the total sample extent." North-south (90 degree) calculations can be made and both plotted on the same graph (Figure 2.11).

If there is a large difference between the plots of the two directions, this means that more information is needed to find the axis of the anisotropy (this will be described later).

Sill And Range. As samples become farther apart, the correlation between these points decrease and the calculated semi-variogram value will increase. Eventually, in the ideal case, the samples will become independent and the semi-variogram value will remain constant (5:6). The lag at which the samples become independent is called the range (a) and the calculated semi-variogram

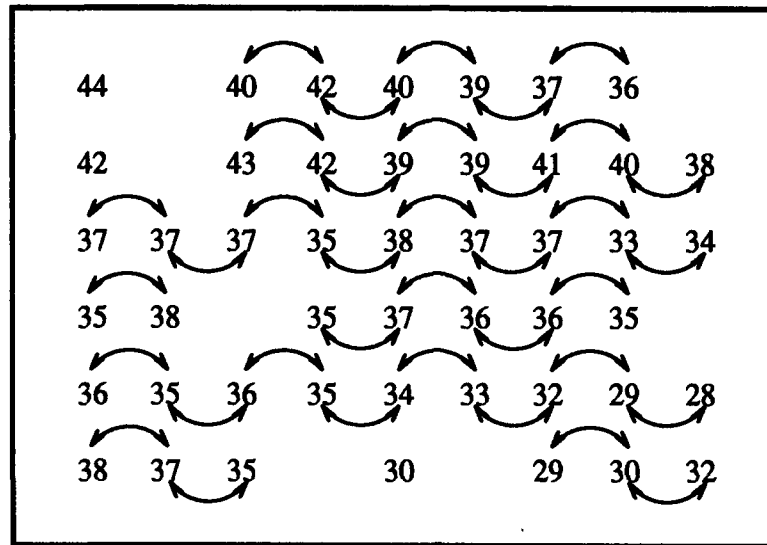


Figure 2.9. Identifying all Pairs at 100 ft Apart in the East-West Direction. (5:13)

where this occurs is called the sill (C). The sill is where the correlation between data points is negligible and defined as the ordinary variance of the sample data (5:7):

$$s^2 = \frac{1}{n-1} \sum_{i=1}^n (z_i - \bar{z})^2 \quad (2.18)$$

where

$$\bar{z} = \frac{1}{n} \sum_{i=1}^n (z_i) \quad (2.19)$$

Nugget Effect. Davis describes the nugget effect:

“...the nugget effect arises because the regionalized variable is so erratic over a very short distance that the semi-variogram goes from zero to the level of the nugget effect in a distance less than the sampling interval.” (9:246)

The nugget effect (C_o) is random in nature and is represented by a spherical model with a very small range (5:9).

Models. The experimental data above must be fit to a model to estimate points for the later kriging equations. A model that matches the experimental data must be selected and fit to the semi-variogram curve.

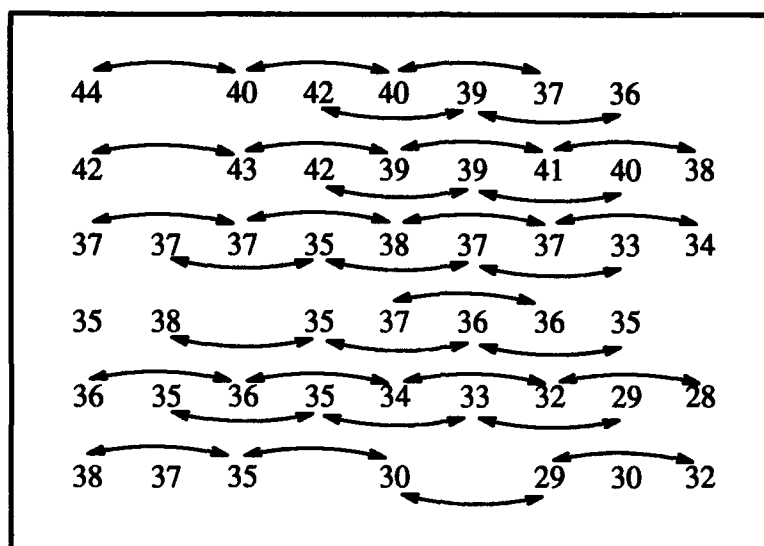


Figure 2.10. Identifying all Pairs at 200 ft Apart in the East-West Direction. (5:14)

Linear Model. The data for the previous ore example suggests that a linear model would fit. The linear model is the simplest with only the slope (m) describing the shape. The following equation describes its shape.

$$\gamma(h) = \begin{cases} mh + C_0 & \text{for } h < a \\ C & \text{for } h \geq a \end{cases}$$

For lags less than the range, the linear model makes a satisfactory estimate of the semi-variogram (9:246-247). The shape of the linear model is displayed in Figure 2.12.

Spherical. An ideal model to describe the semi-variogram begins at the origin and rises to a limit (the sill) and then levels out to a constant value (9:246). The spherical model, described by the following equation, matches this description:

$$\gamma(h) = \begin{cases} C[(3/2)(h/a) - (1/2)(h^3/a^3)] + C_0 & \text{for } h \leq a \\ C + C_0 & \text{for } h > a \end{cases}$$

The range is the corresponding lag (h) where the sill occurs. Figure 2.13 represents the shape of the spherical model showing the range and sill.

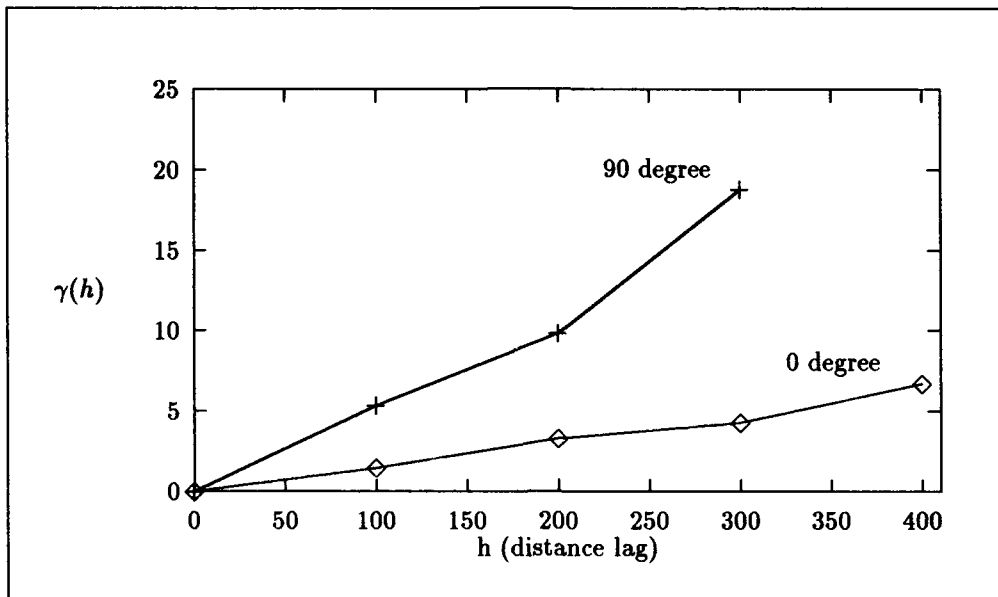


Figure 2.11. Experimental Semi-Variograms in 0° and 90° Directions. (5:15)

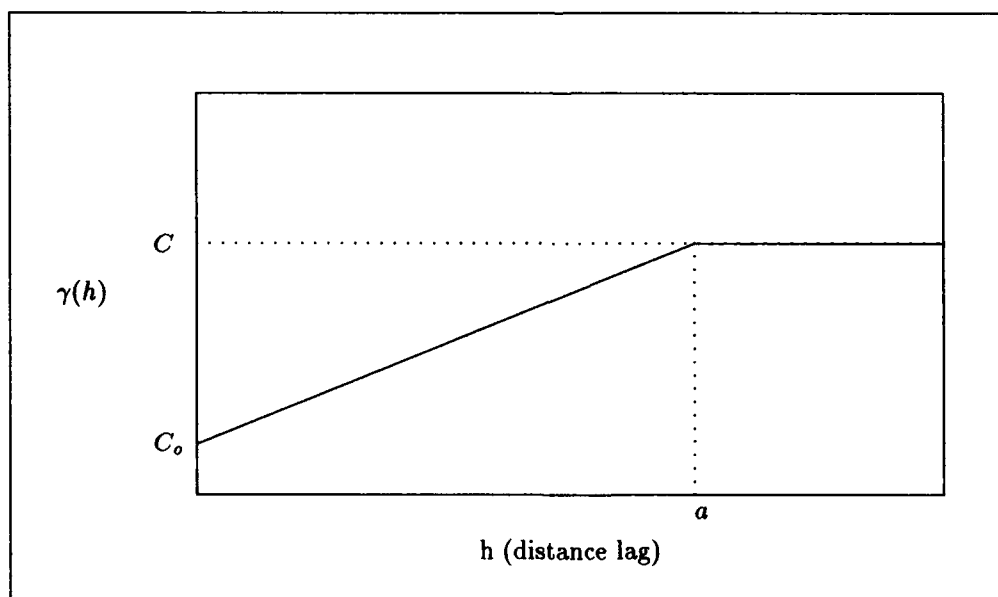


Figure 2.12. Linear Model.

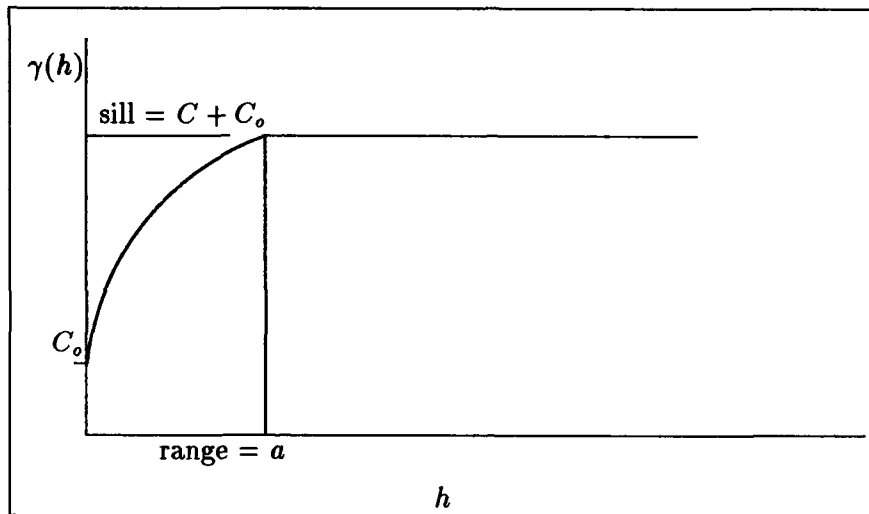


Figure 2.13. Spherical Model. (19:2-13)

Exponential. The exponential model is similar in nature to the spherical model though it never levels out to a constant value or sill and is described by the following equation:

$$\gamma(h) = A [1 - e^{-h/a}] + C_0 \quad (2.20)$$

Figure 2.14 shows the exponential model.

2.5.1.2 Trend. Trends in the data occur when samples in a particular direction demonstrate regional fluctuations. Since stationarity (the mean and covariance of the regionalized variable are known to exist and are constant over the area (8:92)) is assumed prior to kriging, the trend must be removed from the sample data to prevent biased results (5:120). The trend can be removed by fitting a linear or polynomial function to the data and performing the structural analysis on the remaining residuals.

2.5.1.3 Anisotropy. Anisotropy explains differences in semi-variograms calculated in different directions and results from non-isotropic data. Geometric anisotropy occurs when variations in semi-variogram values in differing directions are the same for lags that are multiples of each other (19:2-15). The semi-variograms will have the same sill but differing ranges. A correction factor, k , can be used to equalize the ranges. The spherical model can then be corrected as in the following:

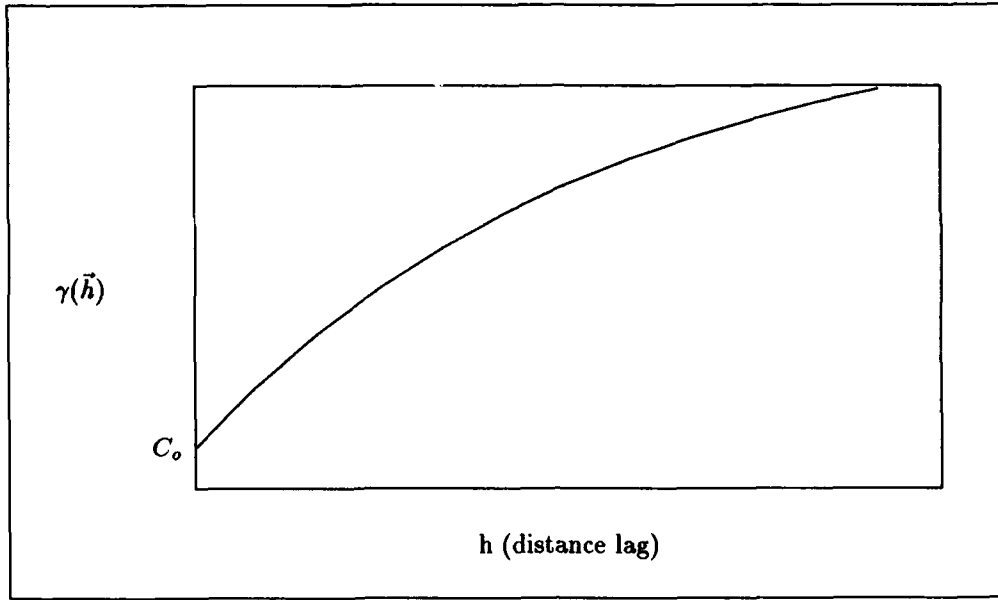


Figure 2.14. Exponential Model.

$$\gamma_1(h) = C \left(\frac{3h}{2a} - \frac{h^3}{2a^3} \right) + C_o \quad (2.21)$$

to

$$\gamma_2(h) = C \left(\frac{3kh}{2a} - \frac{k^3 h^3}{2a^3} \right) + C_o \quad (2.22)$$

which makes the two equations equal.

Figure 2.15 graphically demonstrates geometric anisotropy by plotting zero and ninety-degree semi-variograms for an image from Channel One of the SPOT multi-spectral sensor. The differences between the two plots is due to the anisotropy and represents the non-isotropic nature of the image.

2.5.2 Ordinary Kriging. Ordinary kriging, a form of punctual kriging (predicting values of a stationary regionalized point variable), solves for the new spatial data by weighting the nearest neighbors (size of 16, 20, 25 ... dependent on the range of influence) and substituting into the estimator. Ordinary kriging solves for the pixel values by the following estimator equation:

$$Z^* = \sum_{i=1}^n \omega_i Z_i \quad (2.23)$$

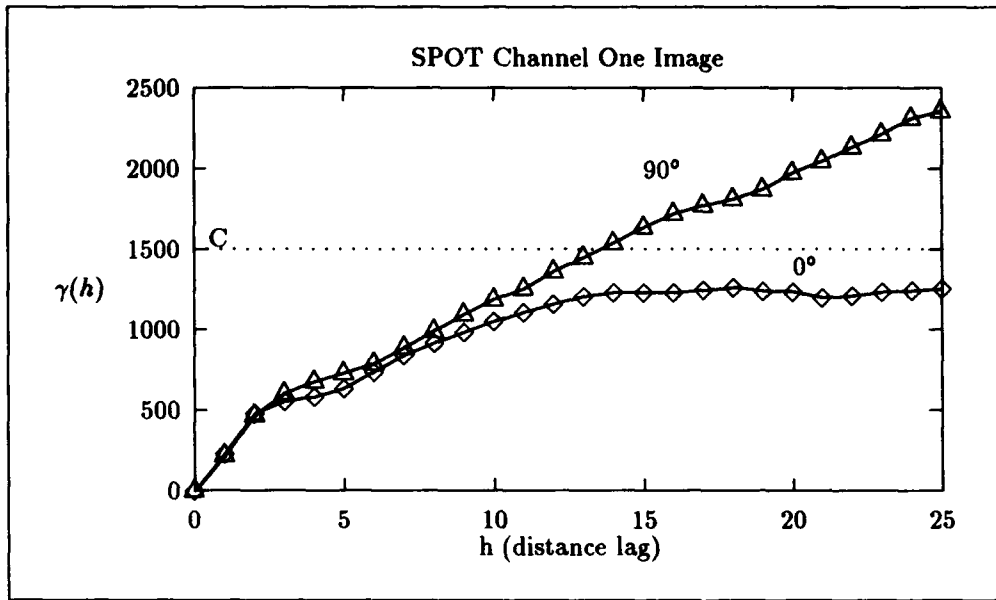


Figure 2.15. Experimental Semi-Variograms in 0° and 90°.

where

$$\sum_{i=1}^n \omega_i = 1 \quad (2.24)$$

If the weights sum to one and no trend exists, then Z^* is considered an unbiased estimator. This is a linear estimator because it is a linear combination of the samples (5:99). To determine the weights necessary, a system of equations must be derived. If there are n samples within the neighborhood used to estimate a point, the following linear equations will result:

$$\begin{array}{rcl} 0 & + & w_1 + w_2 + w_3 + \dots + w_n = 1 \\ \lambda & + & w_1\gamma(h_{11}) + w_2\gamma(h_{12}) + w_3\gamma(h_{13}) + \dots + w_n\gamma(h_{1n}) = \gamma(h_{1p}) \\ \lambda & + & w_1\gamma(h_{21}) + w_2\gamma(h_{22}) + w_3\gamma(h_{23}) + \dots + w_n\gamma(h_{2n}) = \gamma(h_{2p}) \\ \lambda & + & w_1\gamma(h_{31}) + w_2\gamma(h_{32}) + w_3\gamma(h_{33}) + \dots + w_n\gamma(h_{3n}) = \gamma(h_{3p}) \\ \vdots & + & \vdots + \vdots + \vdots + \ddots + \vdots = \vdots \\ \lambda & + & w_1\gamma(h_{n1}) + w_2\gamma(h_{n2}) + w_3\gamma(h_{n3}) + \dots + w_n\gamma(h_{nn}) = \gamma(h_{np}) \end{array}$$

where ω_i is the weight at point i of the neighborhood to the estimated point p and $\gamma(h_{ij})$ is the semi-variogram estimate from points i to j . The regular grid nature of the images simplify the calculations of the semi-variograms limiting the number of equation systems. These equations are solved for the weights and used to estimate the new pixel value Z^* as in Equation 2.23.

To solve the system of equations, matrices are developed as:

$$\begin{bmatrix} 0 & 1 & 1 & \cdots & 1 \\ 1 & \gamma(h_{11}) & \gamma(h_{12}) & \cdots & \gamma(h_{1n}) \\ 1 & \gamma(h_{21}) & \gamma(h_{22}) & \cdots & \gamma(h_{2n}) \\ \vdots & \vdots & \vdots & \ddots & \vdots \\ 1 & \gamma(h_{n1}) & \gamma(h_{n2}) & \cdots & \gamma(h_{nn}) \end{bmatrix} \cdot \begin{bmatrix} \lambda \\ w_1 \\ w_2 \\ \vdots \\ w_n \end{bmatrix} = \begin{bmatrix} 1 \\ \gamma(h_{1p}) \\ \gamma(h_{2p}) \\ \vdots \\ \gamma(h_{np}) \end{bmatrix} \quad (2.25)$$

The weights are calculated for all estimated points and equations are generated to produce the estimator.

2.5.3 Ordinary Kriging Example. Davis demonstrates the technique of ordinary kriging by estimating the elevation of the water table at Point p on the map in Figure 2.16 (9:386-389). In estimating Point p, three measured elevations will be used, with their coordinates given in Table 2.1. The semi-variogram produced from this data is linear with a slope of 4.0 m²/km for a

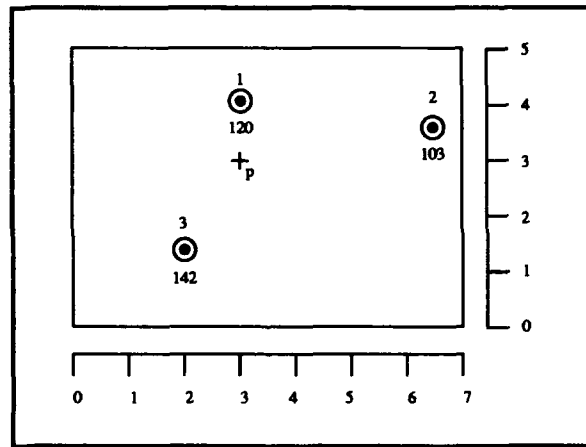


Figure 2.16. Water table elevations (meters) at three observations wells. (9:394)

neighborhood of 20 km. The distances (h) between the points are shown in Table 2.2 with the corresponding semi-variograms values, $\gamma(h_{ij})$, listed in Table 2.3. The kriging matrix will be as

Table 2.1. Water Table Elevation Data for the Ordinary Kriging Example.

Location	X Coordinate	Y Coordinate	Water Table Elevation
Well 1	3.0	4.0	120.0
Well 2	6.3	3.4	103.0
Well 3	2.0	1.3	142.0
Point p	3.0	3.0	

Table 2.2. Distances Between Wells and Point p (Ordinary Kriging).

Location	Well 1	Well 2	Well 3	Point p
Well 1	0	3.35	2.88	1.00
Well 2		0	4.79	3.32
Well 3			0	1.97

Table 2.3. Semi-Variograms for Distances Between Wells and Point p for the Ordinary Kriging Example.

Location	Well 1	Well 2	Well 3	Point p
Well 1	0	13.42	11.52	4.00
Well 2		0	19.14	13.30
Well 3			0	7.89

follows:

$$\begin{bmatrix} 0.0 & 1 & 1 & 1 \\ 1 & \gamma(h_{11}) & \gamma(h_{12}) & \gamma(h_{13}) \\ 1 & \gamma(h_{21}) & \gamma(h_{22}) & \gamma(h_{23}) \\ 1 & \gamma(h_{31}) & \gamma(h_{32}) & \gamma(h_{33}) \end{bmatrix} \cdot \begin{bmatrix} \lambda \\ w_1 \\ w_2 \\ w_3 \end{bmatrix} = \begin{bmatrix} 1 \\ \gamma(h_{1p}) \\ \gamma(h_{2p}) \\ \gamma(h_{3p}) \end{bmatrix}$$

Substituting data from Table 2.3 into the previous kriging equations results in the following system of equations in matrix form:

$$\begin{bmatrix} 0.0 & 1 & 1 & 1 \\ 1 & 0.0 & 13.4 & 11.5 \\ 1 & 13.4 & 0.0 & 19.1 \\ 1 & 11.5 & 19.1 & 0.0 \end{bmatrix} \cdot \begin{bmatrix} \lambda \\ w_1 \\ w_2 \\ w_3 \end{bmatrix} = \begin{bmatrix} 1 \\ 4.0 \\ 13.3 \\ 7.9 \end{bmatrix}$$

The diagonal of the matrix has all zero values and the matrix is symmetrical as discussed earlier, resulting from semi-variogram calculations $\gamma(h_{ij})$ within the neighborhood. Solving this system of equations result in the following weights:

$$\begin{bmatrix} \lambda \\ w_1 \\ w_2 \\ w_3 \end{bmatrix} = \begin{bmatrix} -0.7267 \\ 0.6039 \\ 0.0868 \\ 0.3093 \end{bmatrix}$$

To predict the value of Point p, the preceding weights are substituted into the estimator and the result is as follows:

$$\begin{aligned} Z_p^* &= \sum_{i=1}^3 w_i Z_i \\ &= 0.6039(120.0) + 0.0868(103.0) + 0.3093(142.0) \\ &= 125.3 \text{ meters} \end{aligned}$$

Ordinary kriging can be used if no drift exists within the image or sample data.

2.5.4 Universal Kriging. As discussed earlier, the data must be stationary (no drift) for the kriging process to be effective and unbiased. Davis states:

"The drift consists of the average or expected value of the regionalized variable within a neighborhood, and is a slowly varying, nonstationary part of the surface. The residual is the difference between the actual measurements and the drift." (9:393)

After the drift is removed, the residuals must be stationary and can be kriged. After kriging, the residuals are combined with the drift to retrieve the necessary data. Universal kriging is similar to ordinary kriging but relates the semi-variogram of the residuals of the drift, the size of the neighborhood, and the drift model into the equations. From this interrelationship, the following matrix results:

$$\begin{bmatrix} 0 & 0 & 0 & 1 & 1 & \dots & 1 \\ 0 & 0 & 0 & X_1 & X_2 & \dots & X_n \\ 0 & 0 & 0 & Y_1 & Y_2 & \dots & Y_n \\ 1 & X_1 & Y_1 & \gamma(h_{11}) & \gamma(h_{12}) & \dots & \gamma(h_{1n}) \\ 1 & X_2 & Y_2 & \gamma(h_{21}) & \gamma(h_{22}) & \dots & \gamma(h_{2n}) \\ \vdots & \vdots & \vdots & \vdots & \vdots & \ddots & \vdots \\ 1 & X_n & Y_n & \gamma(h_{n1}) & \gamma(h_{n2}) & \dots & \gamma(h_{nn}) \end{bmatrix} \cdot \begin{bmatrix} \lambda \\ \alpha_1 \\ \alpha_2 \\ w_1 \\ w_2 \\ \vdots \\ w_n \end{bmatrix} = \begin{bmatrix} 1 \\ X_p \\ Y_p \\ \gamma(h_{1p}) \\ \gamma(h_{2p}) \\ \vdots \\ \gamma(h_{np}) \end{bmatrix}$$

where X_i and Y_i are coordinates of the neighborhood points with X_p and Y_p the coordinates of the estimated point. These coordinates are measured relative to a control point within the neighborhood.

2.5.5 Universal Kriging Example. Davis demonstrates the technique of universal kriging by continuing the estimation of the previous example for the elevation of the water table at point p on the map in Figure 2.17 (9:386-389). In estimating Point p for this case, five known elevations will be used, with their coordinates given in Table 2.4.

Table 2.4. Water Table Elevation Data for the Universal Kriging Example.

Location	X Coordinate	Y Coordinate	Water Table Elevation
Well 1	3.0	4.0	120.0
Well 2	6.3	3.4	103.0
Well 3	2.0	1.3	142.0
Well 2A	3.8	2.4	115.0
Well 5	1.0	3.0	148.0
Point p	3.0	3.0	

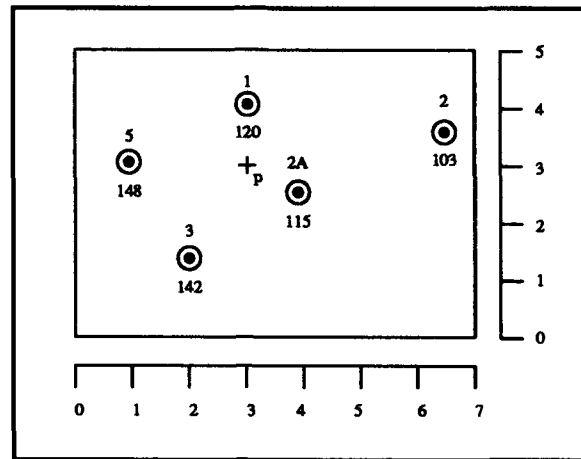


Figure 2.17. Water table elevations (meters) at five observation wells. (9:394)

The semi-variogram produced from this data is the same as the ordinary kriging and is linear with a slope of $4.0 \text{ m}^2/\text{km}$ for a neighborhood of 20 km. The distances (h_{ij}) between the points are shown in Table 2.5 with the corresponding semi-variogram values, $\gamma(h_{ij})$, listed in Table 2.6.

Table 2.5. Distances Between Wells and p for the Universal Kriging Example.

Location	Well 1	Well 2	Well 3	Well 2A	Well 5	Point p
Well 1	0	3.35	2.88	1.79	2.24	1.00
Well 2		0	4.79	2.69	5.32	3.32
Well 3			0	2.11	1.97	1.97
Well 2A				0	2.86	1.00
Well 5					0	2.00

Table 2.6. Semi-Variograms for Distances Between Wells and Point p for the Universal Kriging Example.

Location	Well 1	Well 2	Well 3	Well 2A	Well 5	Point p
Well 1	0	13.42	11.52	7.16	8.96	4.00
Well 2		0	19.16	10.76	21.28	13.28
Well 3			0	8.44	7.88	7.88
Well 2A				0	11.44	4.00
Well 5					0	8.00

The kriging matrix will be as follows:

$$\begin{bmatrix}
 0 & 0 & 0 & 1 & 1 & \cdots & 1 \\
 0 & 0 & 0 & X_1 & X_2 & \cdots & X_5 \\
 0 & 0 & 0 & Y_1 & Y_2 & \cdots & Y_5 \\
 1 & X_1 & Y_1 & \gamma(h_{11}) & \gamma(h_{12}) & \cdots & \gamma(h_{15}) \\
 1 & X_2 & Y_2 & \gamma(h_{21}) & \gamma(h_{22}) & \cdots & \gamma(h_{25}) \\
 1 & \vdots & \vdots & \vdots & \vdots & \ddots & \vdots \\
 1 & X_5 & Y_5 & \gamma(h_{51}) & \gamma(h_{52}) & \cdots & \gamma(h_{55})
 \end{bmatrix} \cdot \begin{bmatrix} \lambda \\ \alpha_1 \\ \alpha_2 \\ w_1 \\ w_2 \\ \vdots \\ w_5 \end{bmatrix} = \begin{bmatrix} 1 \\ X_p \\ Y_p \\ \gamma(h_{1p}) \\ \gamma(h_{2p}) \\ \vdots \\ \gamma(h_{5p}) \end{bmatrix}$$

Substituting data from Table 2.6 into the previous kriging equations result in the following system of equations in matrix form:

$$\begin{bmatrix}
 0 & 0 & 0 & 1 & 1 & 1 & 1 & 1 \\
 0 & 0 & 0 & 0 & 3.3 & -1.0 & 0.8 & -2.0 \\
 0 & 0 & 0 & 1.0 & 0.4 & -1.0 & -0.6 & 0 \\
 1 & 0 & 1.0 & 0 & 13.4 & 11.52 & 7.16 & 8.94 \\
 1 & 3.3 & 0.4 & 13.4 & 0 & 19.16 & 10.76 & 21.28 \\
 1 & -1.0 & -1.0 & 11.52 & 19.16 & 0 & 8.44 & 7.88 \\
 1 & 0.8 & -0.6 & 7.16 & 10.76 & 8.44 & 0 & 11.45 \\
 1 & -2.0 & 0 & 8.94 & 21.28 & 7.88 & 11.44 & 0
 \end{bmatrix} \cdot \begin{bmatrix} \lambda \\ \alpha_1 \\ \alpha_2 \\ w_1 \\ w_2 \\ w_3 \\ w_4 \\ w_5 \end{bmatrix} = \begin{bmatrix} 1 \\ 0 \\ 0 \\ 4.0 \\ 13.28 \\ 7.88 \\ 4.0 \\ 8.0 \end{bmatrix}$$

Solving this system of equations result in the following weights:

$$\begin{bmatrix} \lambda \\ \alpha_1 \\ \alpha_2 \\ w_1 \\ w_2 \\ w_3 \\ w_4 \\ w_5 \end{bmatrix} = \begin{bmatrix} -0.7275 \\ 0.0826 \\ -0.2555 \\ 0.3797 \\ -0.0171 \\ 0.1115 \\ 0.4356 \\ 0.0903 \end{bmatrix}$$

To predict the value of Point p, the preceding weights are substituted into the estimator and the result is as follows:

$$\begin{aligned} Z^* &= 0.3797(120) - 0.0171(103) + 0.1117(142) + 0.4356(115) + 0.0903(148) \\ &= 123.09 \text{ meters} \end{aligned}$$

2.6 Conclusions

This chapter reviewed basic concepts in resolution, current resolution enhancement techniques, and kriging. Resolution depends upon the optics of an imaging system. In order to increase the resolution of an image, the optics of the systems must be altered. Extensive alterations to optical and sensing systems are extremely expensive and difficult from a technological standpoint.

Ground processing of images can improve resolution without the costs associated with changing an imaging system. Current techniques used are nearest-neighbor, bilinear interpolation, and cubic convolution. Kriging can be applied to enhance resolution of digital satellite imagery because it is an unbiased spatial predictor. Ordinary and universal kriging were discussed as the preferred methods but if trends exist in the data, universal kriging is the single preferred method.

III. Methodology

The following chapter summarizes the steps taken to complete the objectives listed in previous chapters. The methodology includes data, implementation of current methods, kriging implementation, program operation, and output.

3.1 Image Data

The image data used in this research was collected from various sources ranging from satellites to digitized aerial photographs. The predominant image type used was from the French *Systems Pour l'Observation de la Terre* (SPOT) satellite system. The SPOT-1 satellite has a circular, sun-synchronous orbit with an altitude of 832 km and an inclination of 98.7° with its orbit repeating every 26 days (16:581-582).

The sensor provides multi-spectral data from three 3000-element arrays at 20m resolution digitized in eight-bit words and transmitted at 25 Mbps (16:584). Channel One views over a spectral range of 0.50 to $0.59\mu\text{m}$, Channel Two over 0.61 to $0.68\mu\text{m}$, and Channel Three over 0.79 to $0.89\mu\text{m}$. The system uses a push-broom scanner which samples the detectors along the array and then forms the image by assembling successive scans as the satellite travels over the earth. This system eliminates geometric errors due to variations in speed caused by similar mirror systems as well improving the signal-to-noise performance by increasing the dwell over the target area (16:582). The images used were corrected for geometric distortions due to earth curvature and nonlinearities in the sensor sweep (16:612).

3.1.1 Image Used. Images were chosen to provide a variety of terrain and spectral qualities. The goal was to test the techniques with as many varying spectral qualities to verify kriging's and cubic convolution's ability to handle varying imagery.

Multi-spectral data was used from Channels One, Two, and Three from SPOT's multi-spectral scanning system. Images tested were taken from all channels to verify each techniques ability to handle variations in spectral information. Sections of water were chosen for their isotropic characteristics and urban areas were selected due to their non-isotropic nature. This was done to fully test kriging's ability to handle many image characteristics. A cross reference of image, sizes, statistics on the pixels within the image sections, see Appendix 5.2.

3.1.2 Sub-Sampling. The image sections used were sub-sampled to test the techniques. For the purposes of this research, sub-sampling consist of the removal of every other row and column.

These will be reconstructed by the estimation techniques tested. The original image, four times the size of that specified when running the program, is read out to a file for future comparison.

3.2 Current Methods

Cubic convolution was used as the method to test against kriging.

3.2.1 Neighborhood. For testing purposes, a fixed 4 by 4 neighborhood was chosen for its simplicity as well as matching that neighborhood used by the cubic convolution algorithm. In an operational program, the neighborhood should be responsive to the range where the diagonal radius will equal the range (19:3-10).

3.3 Kriging Implementation

Both, ordinary and universal kriging were implemented within the test program to see if any differences exist between the two techniques for image resolution enhancement. A flag within the program can be set to change kriging method.

3.3.1 Structural Analysis. Structural analysis describes the size, shape, orientation, and spatial arrangement of samples and constitutes the variation of the pixels in an image (9:239). Usually, this relates to the physical description of an ore structure underground but can be applied to the data of an image. Determination of the variogram, anisotropy, and trend constitute the structural analysis of data. Structural analysis was performed only on the specific image sections, not the overall image, to limit the trend and anisotropy of the sub-sampled image and maximize the accuracy of the final results.

3.3.1.1 Trend. An option to remove trend within the data by the use of least squares regression method was included. The result of the technique was a set residuals, one for each data point. It is this residual data that creates the semi-variogram and subsequently kriged. The resulting kriged image is then recreated by calculating the final pixel values using the regression equation and the residual data.

3.3.1.2 Anisotropy. Zonal and geometric anisotropy was not corrected for in this research. Preliminary results indicated that little geometric anisotropy exist within the images. See Chapter 4 for further details of this data.

3.3.1.3 Nugget. From previous research, the nugget was set to zero for all calculations. McGee states, "a model which fit well near the origin of the variogram [was needed] . . . the nugget effect of the spherical model was, therefore, set to zero (19:4-9)."

3.3.2 Kriging Equations. Both ordinary and universal kriging were used for this research to determine the best suited method. Both techniques are used to solve for the following weight estimator:

$$\hat{Z}^* = \omega_1 Z_1 + \omega_2 Z_2 + \omega_3 Z_3 + \cdots + \omega_n Z_n$$

which will be used throughout the image to calculate the necessary pixel values. If the weights sum to one and no trend exists, then \hat{Z}^* is considered an unbiased estimator.

3.3.2.1 Ordinary Kriging. If no trend exists within the image or section of image to be kriged, the simpler form of kriging called ordinary kriging may be used which solves for the weights using the system of equations found in Section 2.5.2. The weights are calculated for all points within the neighborhood and equations are generated to produce the estimator.

3.3.2.2 Universal Kriging. If data has a drift, universal kriging is used to compensate. Universal kriging is similar to ordinary kriging but relates the semi-variogram of the residuals of the drift, the size of the neighborhood, and the drift model into the equations. In this research, pixel one in the upper left hand side (Figure 3.1) represents the zero control point.

3.4 Program Operation

See Appendix A for a detailed treatment of the makeup and operation of the test program.

3.4.0.3 Weights. Due to the regular grid nature of the images, only three systems of weights were needed to estimate the points. These weights can then be used throughout the image section to and estimate all necessary points. See Figure 3.1 for the position of the points estimated within the neighborhood. Due to the size of the neighborhood, a border around the test image is required to estimate all points. This research developed a border within the test image to supply these points.

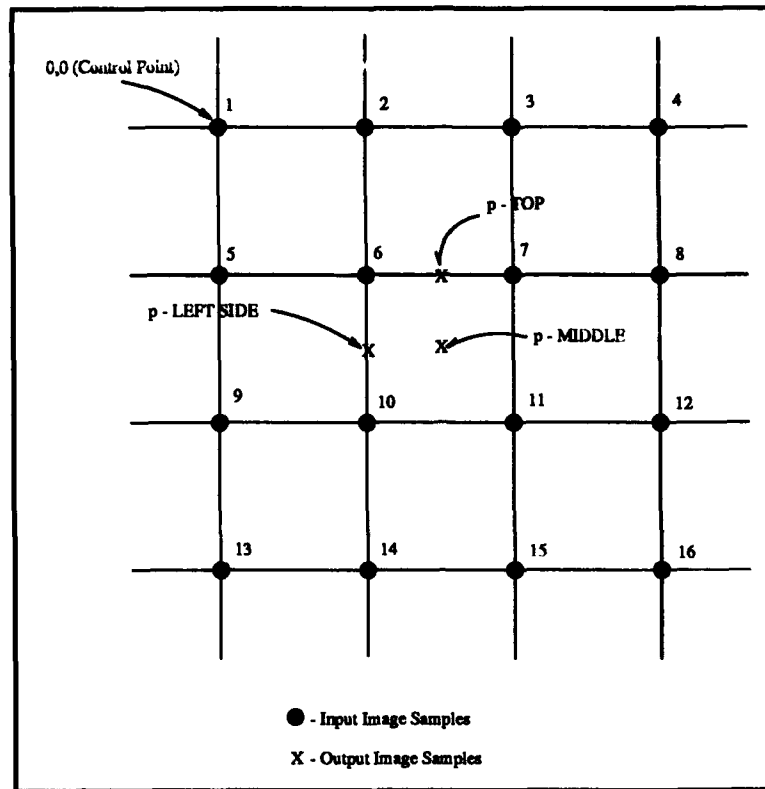


Figure 3.1. Neighborhood Pixels.

3.5 Tests

Comparison tests were made to compare universal and ordinary kriging with regression, kriging with cubic convolution, interpolation with the spherical and exponential model, nugget and no nugget, and regression and no regression.

3.6 Statistical Analysis

To compare images, statistical test are required. The estimated pixels are subtracted from the original image pixels and a difference is found. The absolute value of this difference is found and a sample mean and standard deviation of the differences is determined. These are found by the following:

$$\bar{z} = \frac{\sum_{i=1}^n |z_i|}{n}$$

and

$$s = \sqrt{\frac{n(\sum_{i=1}^n z_i^2) - (\sum_{i=1}^n z_i)^2}{n(n-1)}}$$

3.6.1 Variance Test. Variances are then compared to see if they are considered equal to determine which t test to use. An F statistic is calculated as a comparison with the theoretical. The experimental statistic is calculated by the following:

$$F_o = \frac{S_1^2}{S_2^2}$$

If $F_o > F_{\alpha, n_1-1, n_2-1}$, you reject the hypothesis that the variances are equal. This is the critical region for testing the null hypothesis $s_1^2 = s_2^2$ against the alternative hypothesis $s_1^2 > s_2^2$. To test the null hypothesis against the alternative hypothesis that $s_1^2 < s_2^2$, then $F_o < F_{1-\alpha}$ where $F_{1-\alpha} = 1/F_{\alpha, n_1-1, n_2-1}$ (21:263).

3.6.2 Mean Test. With the means determined, two-sided tests concerning the mean are constructed (21:11). A t statistic is calculated to perform the test as in the following (12:241):

$$t = \frac{(\bar{z}_1 - \bar{z}_2)}{\sqrt{\frac{\sigma_1^2}{n_1} + \frac{\sigma_2^2}{n_2}}} \quad (3.1)$$

We assumed that we are sampling normal populations and that we can apply the central limit theorem so we can approximate σ_1 and σ_2 with s_1 and s_2 when n_1 and n_2 are both greater or equal to 30 (12:242). In this case, they are equal to 867 for our 40 by 40 images.

$$H_o : \mu_1 = \mu_2 \quad (3.2)$$

$$H_a : \mu_1 \neq \mu_2 \quad (3.3)$$

The results of these tests are found in Appendix C.5.

Comparisons are made between cubic convolution and kriging, universal kriging and ordinary kriging, the exponential and spherical models and interpolation, and nugget/non-nugget models.

3.7 Summary

Image data used for enhancement was sub-sampled from various sources including SPOT imagery and digitized aerial photographs. The test program allows the operator to set various flags within the code to vary the test conditions. Some of the conditions that can be changed are the semi-variogram model to be used and the method of kriging to test. Drift is removed by least-squares regression technique and the resulting residuals generate semi-variograms and are then kriged. The kriged image is recombined with the regression equation and compared with the original image. Statistics are generated on the comparison and are compared with like statistics from the cubic convolution technique to determine the best technique.

IV. Results

Cubic convolution, ordinary, and universal kriging were applied to various digital image sections from two SPOT satellite images each with 20m resolution from the system's multi-spectral scanner. See Appendix 5.2 for description of the images. Each image section was cut from two different channels with the following spectral ranges:

- Channel 2 - 0.61 to 0.68 μ m
- Channel 3 - 0.79 to 0.89 μ m

Each technique was used on all channels to test their ability to handle varying spectral conditions (since each spectral channel varies significantly). This chapter contains results from initial structural analysis to determine the proper model to use and see if any anisotropy exists within the images.

4.1 Structural Analysis.

Semi-variograms of residual data were plotted to perform a structural analysis on the images to determine the proper model to incorporate within the program and to determine whether any anisotropy exists within the image. Semi-variograms are displayed in Appendix B.8.

4.1.1 Model Determination. Most semi-variograms plotted for this research indicate the use of no specific model for use in estimation of the kriging equations. The plots show linear tendencies for lags below the maximum distance of a 4×4 neighborhood ($\sqrt{18}$).

4.1.2 Anisotropy. The differences between the 0° and 90° directions are minor, especially for lags less than that used for neighborhood calculations, suggesting no significant anisotropy exists for the images tested.

4.1.3 Range. Most ranges for the semi-variograms were ideal for the 4×4 neighborhoods used with some smaller indicating a small neighborhood could be used in some instances.

4.2 Enhanced Images

With the modified mean calculation, runs were repeated for the image previously enhanced as well as runs on the remaining image sections not enhanced in the initial runs. Image pixel mean and standard deviation was collected from the original image data. This data is displayed in Appendix 5.2.

4.2.1 *Test Statistics.* Tests were performed to test universal and ordinary kriging as well as kriging with cubic convolution.

4.2.2 *Comparisons of Two Population Variances.* To determine the test to perform on the means of the two populations, a test of the variances was performed for those cases to be compared. The F_o statistics are recorded in Appendix C.5. We would reject H_o ($s_1^2 = s_2^2$) against ($s_1^2 > s_2^2$) if $F_o > F_{\alpha/2, n_1-1, n_2-1}$. $F_{\alpha/2, n_1-1, n_2-1}$ for an $\alpha = .05$, equals 1.16. This number is the theoretical value and can be obtained from tables or a statistical computer package. We reject the null hypothesis that the variances are considered equal if the experimental statistic $F_o > 1.16$. For the comparisons of kriging and cubic convolution, for all but two variances, the hypothesis is rejected. For the comparison of interpolation and the spherical model, 10 reject the hypothesis while 12 accept the hypothesis. For the comparison of interpolation and the exponential model, 11 reject the hypothesis while 11 accept the hypothesis.

4.2.3 *Comparisons of Two Population Means.* At this point a test was needed to compare the means to see if they were statistically different. An experimental t value was calculated using the experimental means and variances. A 95 percent confidence level was used making $\alpha = .05$. The two sided test used test the following hypothesis:

$$\mu_1 = \mu_2 \quad (4.1)$$

against

$$\mu_1 \neq \mu_2$$

with a 95 percent confidence interval of $-t_{\alpha/2, n-1} < t < t_{\alpha/2, n-1}$. If t is within the interval, you accept H_o and if not, you reject H_o and accept H_a . Data from all tests are displayed in Appendix C.5. The confidence interval for the data is $-1.965 < t < 1.965$. If the test statistic (t) is within the interval, the means are considered equal and outside the interval, they are not equal.

4.2.3.1 *Universal/Ordinary Kriging Comparison.* Runs were made to collect data on both universal and ordinary kriging. Data on mean difference and standard deviation were collected

at the end of each run. No difference between the two methods was noticed to two decimal points of accuracy. This data is not included within this document.

4.2.3.2 Kriging/Cubic Comparison. The variances for kriging were consistently smaller than that produced by cubic convolution. Many were not statistically different than that produced by cubic convolution but many were when making the F_0 statistic comparison.

Data on mean difference and standard deviation were collected at the end of each run. This data is displayed in Appendix C.5. Kriging consistently produced means better than cubic convolution for the images tested. All images produced by kriging had lower means than cubic convolution though only four of the images produced t statistics that concluded that kriging is better. All remaining t statistics were within the confidence interval concluding that the means were the same.

4.2.3.3 Interpolation/Spherical Model Comparison. Data on mean difference and standard deviation were collected at the end of each run. This data is displayed in Appendix C.5. The data indicates that there is no significant difference between the techniques with the interpolation method producing better results for images with little or no anisotropy.

4.2.3.4 Interpolation/Exponential Model Comparison. Data on mean difference and standard deviation were collected at the end of each run. This data is displayed in Appendix C.5. Results of these test were similar to the comparison of interpolation and the spherical model.

4.2.3.5 Nugget/No Nugget Comparison. Images produced using the nugget effect have significantly high means differences than that produced with no nugget effect.

4.2.4 Regression/No Regression Comparison. Images were produced to see if the inclusion of the regression section of the code was necessary to improve the mean difference. Data showed no difference between the kriging with regression and that without. This data is not included in this document to avoid redundancy.

4.2.4.1 Regression/Universal Kriging Comparison. Images produced by the elimination of the regression function and then using universal kriging produced similar results than that produced using the regression. Only slight differences (one to two hundredths) were noticed. This data was not included since it varied little with the original data.

4.3 Summary

Semi-variograms produced from the kriged images show large fluctuations in the range of influence causing difficulty automating the structural analysis function of the program though little anisotropy exists within the images especially for lower lags. The lower lags are used to estimate the kriging equations. No differences between the use of universal and ordinary kriging were seen when drift was removed prior to kriging. Kriging consistently produced images with lower means differences than that produced by cubic convolution. Twenty-seven percent of the images tested produced significantly better means for kriging while 45 percent of the images produced lower variances. Comparisons did not produce significant differences between the different models while the inclusion of a nugget produced larger mean differences. The final comparison between the use of regression and without it (using universal kriging) produced images with the same means as those produced with the regression function included in the program. This would speed the processing considerably since the regression is the most time consuming aspect of the program.

V. Recommendations

The recommendations in this chapter suggest improvements to the image processing program to further improve the speed and performance of the dedicated kriging image enhancement as well as a suggestion for a further use of the semi-variogram plots.

5.1 Program Improvements.

Several improvements can be made to the program that may improve kriging's ability to enhance resolution of digital images as well as improve the speed of the processing.

5.1.1 Model Estimation. The spherical model, exponential model, and interpolation methods were used to estimate the semi-variogram values within the kriging equations. The semi-variogram plots show for the lags of that used to make the estimations, a linear model could be used. This is why the linear interpolation was attempted. A linear model could be incorporated into the program to aid in this process.

5.2 Summary

Several things could be done to improve the speed of the processing as well as improving the results obtained from kriging. Faster processors and different software can be used to increase the speed and handle the data better. A more versatile structural analysis can be used to estimate the kriging equations and a varying neighborhood could be implemented in response to range fluctuations or limit krings use to only isotropic images. The fastest product that would produce high quality images should use universal kriging with no regression and incorporate the interpolation method for semi-variogram estimation.

Appendix A. *Image Sections*

The following is information on the image sections enhanced for this research. The data includes the image number, (the number used for all following tables, semi-variograms, and data files output from the program), information about the image (e.g., urban, countryside or water), and the column and row offsets input into the program. An image size of 40×40 was used in all sub-sampled images. In general the SPOT 1 image consisted of countryside with a small town, small streams, and river valleys. The SPOT 2 image was of the Washington DC area including the Mall area and Potomac river. Specifics of each image are listed with the following pixel data.

Table A.1. SPOT 1, Channel 2

SPOT 1	Description	Statistics	
Image Number		\bar{z}	s
Offset 000,210	Countryside	116.19	40.28
Offset 108,168	Countryside	97.60	21.74
Offset 365,370	Small Town	102.52	46.71
Offset 390,130	Countryside	74.00	38.65

Table A.2. SPOT 1, Channel 3

SPOT 1	Description	Statistics	
Image Number		\bar{z}	s
Offset 000,210	Countryside	102.22	38.78
Offset 108,168	Countryside	78.38	21.21
Offset 365,370	Small Town	90.94	44.79
Offset 390,130	Countryside	62.51	34.06

Table A.3. SPOT 2, Channel 2

SPOT 2	Description	Statistics	
Image Number		\bar{z}	s
Offset 090,250	Urban	61.88	59.83
Offset 100,130	Urban	89.03	60.72
Offset 100,470	Urban	124.64	67.87
Offset 100,570	Urban	139.42	53.20
Offset 150,100	Water	23.41	14.77
Offset 290,050	Urban	121.85	54.76
Offset 258,000	Urban	61.88	42.74

Table A.4. SPOT 2, Channel 3

SPOT 2	Description	Statistics	
Image Number		\bar{z}	s
Offset 090,250	Urban	67.35	61.37
Offset 100,130	Urban	99.22	61.92
Offset 100,470	Urban	127.33	68.32
Offset 100,570	Urban	139.12	55.98
Offset 150,100	Water	83.32	18.80
Offset 290,050	Urban	130.17	55.64
Offset 258,000	Urban	28.48	24.45

Appendix B. *Program Operation*

The test program was written in Turbo Pascal Version 6.0 to perform an analytical comparison between kriging and cubic convolution (current state of the art). It allows variations in trend analysis, model selection, neighborhood size, sub-sample size, and kriging method. Each selection is performed by setting a flag in the program.

B.1 Flags

Flags are used within the program to vary the test conditions.

B.1.1 Regression. To eliminate the regression, the following flag can be set:

regression = XXXXX;

where **XXXXX** will read "true" if regression will be used and "false" if regression will not be used.

For variations in the regression terms within the trend analysis, the following flag is set:

second_order = XXXXX;

where **XXXXX** will read "true" if second-order regression will be used and "false" if second-order regression will not be used. Second-order includes the X^2 and Y^2 terms into the regression equation to fit the polynomial to the data rather than a linear function.

B.1.2 Models. To vary the model to be used for the semi-variogram, the following flag is set:

model = X;

where **X** is set to "0" for no model (interpolation between data points is used for the kriging equations), set to "1" to use the spherical model, set to "2" for the square root model, and set to "3" for the exponential model.

B.1.3 Nugget Effect. To implement the nugget effect, the following flag is set:

nugget = XXXXX;

where **XXXXX** will read "true" if the nugget effect is to be used and "false" if it is not to be used.

B.1.4 Kriging. To vary the kriging method used within the program, the following flag is set:

kriging = X;

where **X** represents the type of kriging used. The flag is set to "0" if ordinary kriging is used and "1" if universal kriging is used.

B.2 Image Data

The program prompts the user to input the name of the image file used for a particular test. The program lists all available image files within the directory specified in the program. The directory specified within the program may be altered to allow the program to search any directory to accommodate any specific directory structure.

After the image file is selected, the program prompts for a size in width and height. At this point, the size of the image (width and height in pixels) section to be studied will be input at each prompt. Size was determined from viewing the image and selecting a proper section. Sections of more than 400 pixels are prohibited due to image file limitations.

The program also prompts for column and row offsets. This is the pixel point where the upper-right-hand corner of the selected section will start. Starting position, like the size, was determined from viewing the image and selecting the starting position of the proper section. The upper right hand corner of the original image is the "0,0" point.

The user must be careful not to position the test section off the original image or include sections of telemetry and calibration data. Then, the image section is sub-sampled to generate the test file to be kriged. The original image is saved to a file with an .ORI extension. This file will be used later to compare with the enhanced images.

B.3 Regression

The regression is performed using procedures included in the Quinn-Curtis Huge Virtual Array Toolbox. Procedure *HMultipleReg* uses least squares method to choose the best-fitting model which minimizes the sum of squares of the distances between the observed responses and predicted by the fitted model (22:196). The regression algorithm takes the following matrix form (22:196):

X - matrix of independent data values,

Y - vector of dependent variable values,
 B - vector of regression coefficients to solve for.

$$\begin{aligned}XB &= Y \\X^T X B &= X^T Y \\B &= (X^T X)^{-1} Y\end{aligned}$$

The vector B contains coefficients of the regression fit of the data. McGee states:

“An advantage of the least-squares polynomial regression technique is that it is capable of very closely modeling the trend . . . the trend is retained by the polynomial, and can be recombined with the kriged residuals.” (19:3-7)

Procedure *HStatAnalysis* performs statistical analysis of the regression results and outputs the residual vector (22:204). Regression output consists of mean, variance, standard deviation of the original data as well as the resulting residuals. The mean of the residuals should be approximately zero as a quick verification of the calculation. The semi-variogram procedure uses the residual vector supplied by the regression to performed the necessary calculations.

B.4 Semi-Variogram

Zero and ninety degree semi-variograms are calculated for use in developing a model for the kriging equations. The semi-variogram procedure takes advantage of the regularly grid structure of the digital image to simplify the calculations.

B.4.1 Calculations and Model Formulation. The variogram describes the variance of the difference of samples within the image and is calculated as:

$$\gamma^*(h) = \frac{1}{2n} \sum_{i=1}^n [z(x_i) - z(x_i + h)]^2$$

Each pixel is considered to be one lag (h) apart with calculations performed for half of the possible lags contained within the image section studied.

Once the semi-variogram is calculated, the sill (the ordinary variance of the image data) is calculated by the following:

$$s^2 = \frac{1}{n-1} \sum_{i=1}^n (z_i - \bar{z})^2$$

where

$$\bar{z} = \frac{1}{n} \sum_{i=1}^n (z_i)$$

B.4.2 Data and Plot Generation. GNUPLOT macro files are produced from the experimental zero and ninety degree semi-variograms and combined with a plot of the sill and the model if desired. The following is a typical macro file:

```
set term eepic
set output "k100-470s1c1.tex"
set size 1,1
set nokey
set xrange [0:10]
set yrange [0:5500]
set tics out
set xlabel "h"
set ylabel "$\gamma(h)$"
set title "Variogram (Offset 100,470; First Order)"
plot 3850, "k100-470.v00" w linesp, 295.447*sqrt(x) w line
```

When run with GNUPLOT, this macro will produce the \LaTeX file in Figure B.1.

The semi-variogram data and plots were used to determine the most accurate model to use, the level of anisotropy within the data, and any variations in the range of influence between various image sections. Any simplifying assumption that can be made with respect to the semi-variograms will shorten processing time and decrease programming complexity when this is included within the image processing software later (not performed for this research).

B.4.3 Output Files. The program produces three files:

1. File one contains zero degree semi-variogram data labeled as follows:

kXXX-YYY.v00

2. File two contains ninety degree semi-variogram data labeled as follows:

kXXX-YYY.v90

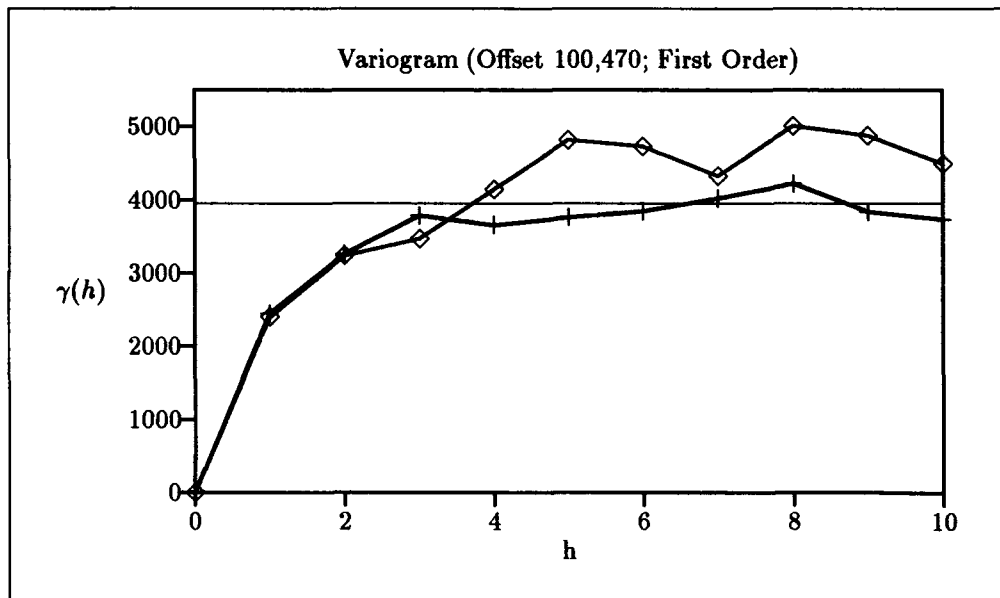


Figure B.1. GNUPLOT Example.

3. File three contains the GNUPLOT macro file labeled as follows:

kXXX-YYY.gnu

XXX represents the row and **YYY** the column offset value.

B.5 Kriging Equations

Once the semi-variogram calculations are completed, both ordinary and universal kriging matrices were generated using a 16-pixel neighborhood. Both methods are used to verify any differences between the two. Ordinary kriging is simpler to implement and is less processor intensive but universal kriging can handle any remaining local trend within the data.

B.5.1 Ordinary Kriging. The ordinary kriging matrix is generated using the chosen model to estimate the semi-variogram values for lag (h) between the pixels within the neighborhood. The

ordinary kriging matrix takes the following form:

$$\begin{bmatrix} 0 & 1 & 1 & \cdots & 1 \\ 1 & \gamma(h_{11}) & \gamma(h_{12}) & \cdots & \gamma(h_{1n}) \\ 1 & \gamma(h_{21}) & \gamma(h_{22}) & \cdots & \gamma(h_{2n}) \\ \vdots & \vdots & \vdots & \ddots & \vdots \\ 1 & \gamma(h_{n1}) & \gamma(h_{n2}) & \cdots & \gamma(h_{nn}) \end{bmatrix}$$

where $n = 16$.

To calculate h_{ij} , the distance between i and j are computed via the following algorithm:

$$h := \text{Sqrt}(\text{Sqr}((i \bmod \text{neighborhood}) - (j \bmod \text{neighborhood})) + \text{Sqr}((i \div \text{neighborhood}) - (j \div \text{neighborhood})))$$

The value for h is input into the model or interpolation and the result is $\gamma(h_{ij})$.

B.5.2 Universal Kriging. The universal kriging matrix is generated like that of the ordinary matrix with the exception of the inclusion of term representing the locations of the pixels within the neighborhood. To simplify the calculations and reduce the number of matrices, pixel one in the upper left hand corner of the neighborhood represents the "0,0" pixel or the control point of the neighborhood (Figure 3.1). The universal kriging matrix takes the following form:

$$\begin{bmatrix} 0 & 0 & 0 & 1 & 1 & \cdots & 1 \\ 0 & 0 & 0 & X_1 & X_2 & \cdots & X_n \\ 0 & 0 & 0 & Y_1 & Y_2 & \cdots & Y_n \\ 1 & X_1 & Y_1 & \gamma(h_{11}) & \gamma(h_{12}) & \cdots & \gamma(h_{1n}) \\ 1 & X_2 & Y_2 & \gamma(h_{21}) & \gamma(h_{22}) & \cdots & \gamma(h_{2n}) \\ \vdots & \vdots & \vdots & \vdots & \vdots & \ddots & \vdots \\ 1 & X_n & Y_n & \gamma(h_{n1}) & \gamma(h_{n2}) & \cdots & \gamma(h_{nn}) \end{bmatrix}$$

B.5.3 Right-Hand-Side. Three right-hand-side (RHS) terms were developed to correspond to the three pixel estimates required within the neighborhood. These RHS terms are designated *TOP*, *LEFT*, and *MIDDLE* and Figure 3.1 graphically displays the position of pixels used to create the RHS estimates. The RHS terms use the selected model to estimate the semi-variogram value of the lag from the estimated point to all points in the neighborhood ($\gamma(h_{np})$). A 16-pixel

neighborhood will result in a 17-term RHS vectors for ordinary kriging and 19-term RHS vectors for universal kriging. The following demonstrate the format for the RHS matrices:

- Ordinary kriging RHS

$$\begin{bmatrix} 1 \\ \gamma(h_{1p}) \\ \gamma(h_{2p}) \\ \vdots \\ \gamma(h_{np}) \end{bmatrix}$$

- Universal kriging RHS

$$\begin{bmatrix} 1 \\ X_p \\ Y_p \\ \gamma(h_{1p}) \\ \gamma(h_{2p}) \\ \vdots \\ \gamma(h_{np}) \end{bmatrix}$$

The three RHS terms are combined with their corresponding kriging matrices to make a system of equations in matrix form to solve for the weights in the estimator.

B.5.4 Solution. The matrices and vectors are feed to the Quinn-Curtis procedure *HGaussJordan* in the matrix form:

$$AX = B$$

where A is the square kriging matrix, X is the vector of weights, and B is the RHS vector. A matrix inversion of the matrix system takes place to solve for the weights.

Three inversions take place that solve for the weights at the estimate pixel locations and these weights with the neighborhood are moved throughout the image section to generate the kriged image.

B.6 Cubic Convolution

Cubic convolution is implemented as discussed in Chapter II for a direct comparison with the kriging techniques.

B.7 Recombination

The final step of the kriging process is the recombination of the polynomial equation with the kriged residuals. Both ordinary and universal kriging are compared to the original image to determine any difference in techniques.

B.8 Image Comparison

The image files generated previously are use in an analytical comparison between kriging and cubic convolution techniques. The files for kriging and cubic convolution are subtracted for the original file to generate subtracted images. These may be displayed as is but this was not performed for this research. The difference of all pixels is summed and a mean difference is calculated. A similar calculation is performed to compute the standard deviation of the data. Both the mean and standard deviation for kriging and cubic convolution are written to the display for collection.

Appendix C. *Semi-Variograms of Residuals*

The following are semi-variograms generated from image sections selected. The diamonds represent the 0° direction calculations and the plus signs represent the 90° direction calculations. This data is used to determine if the range of influence and anisotropy vary between differing image sections. Image sections from multiple channels of SPOT data were used to see if varying the observed wavelength causes any appreciable difference in the semi-variogram calculations. Similar sections of differing channels are included on the same pages for ease of comparison.

C.1 *Variograms*

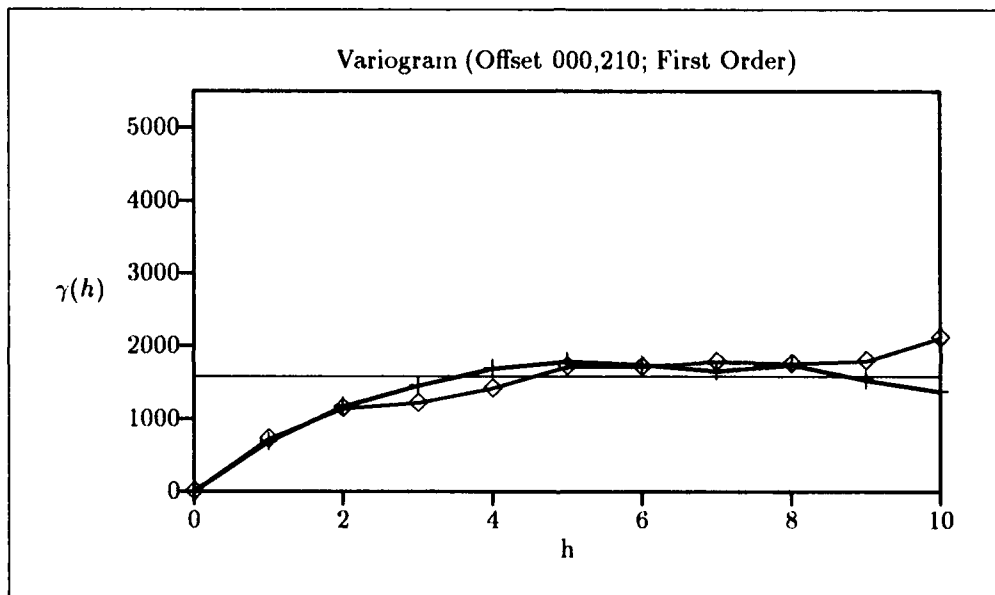


Figure C.1. SPOT 1 Channel 2.

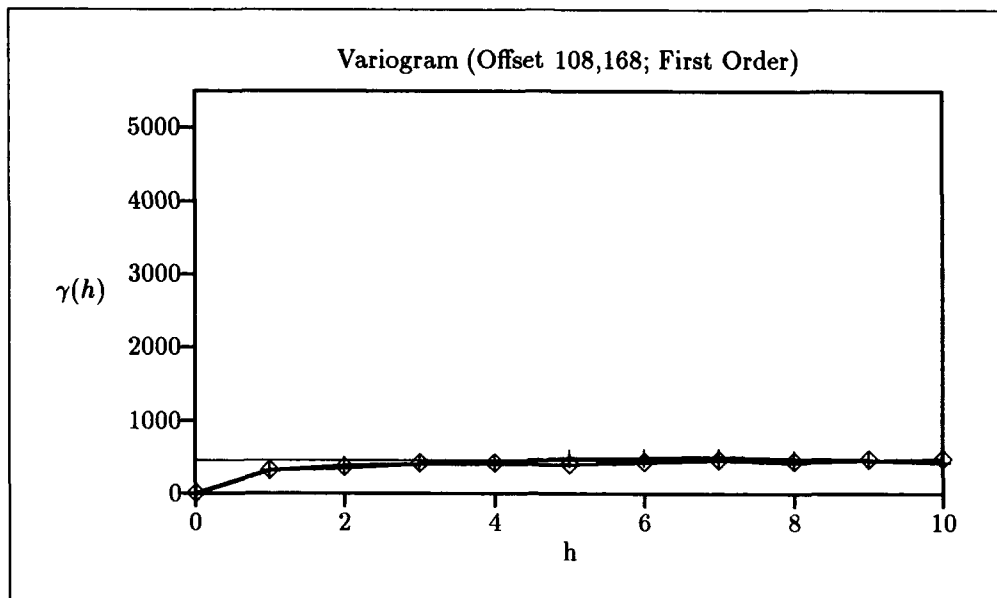


Figure C.2. SPOT 1 Channel 2.

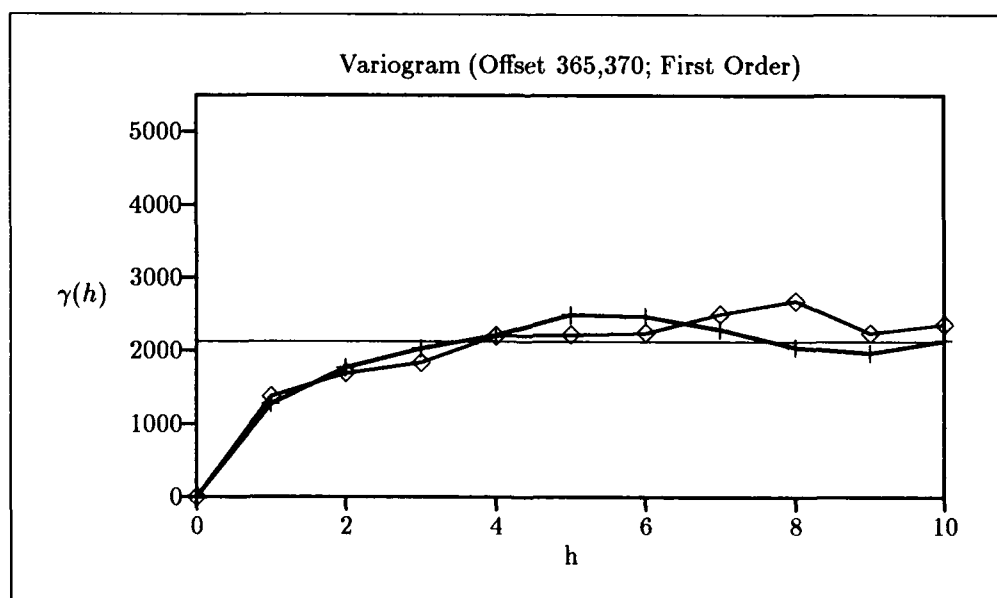


Figure C.3. SPOT 1 Channel 2.

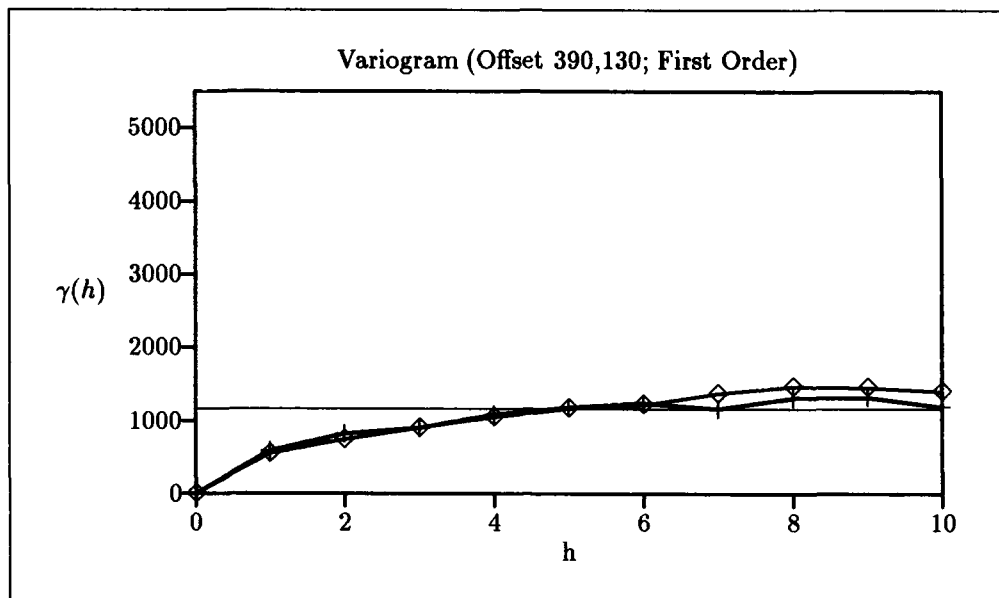


Figure C.4. SPOT 1 Channel 2.

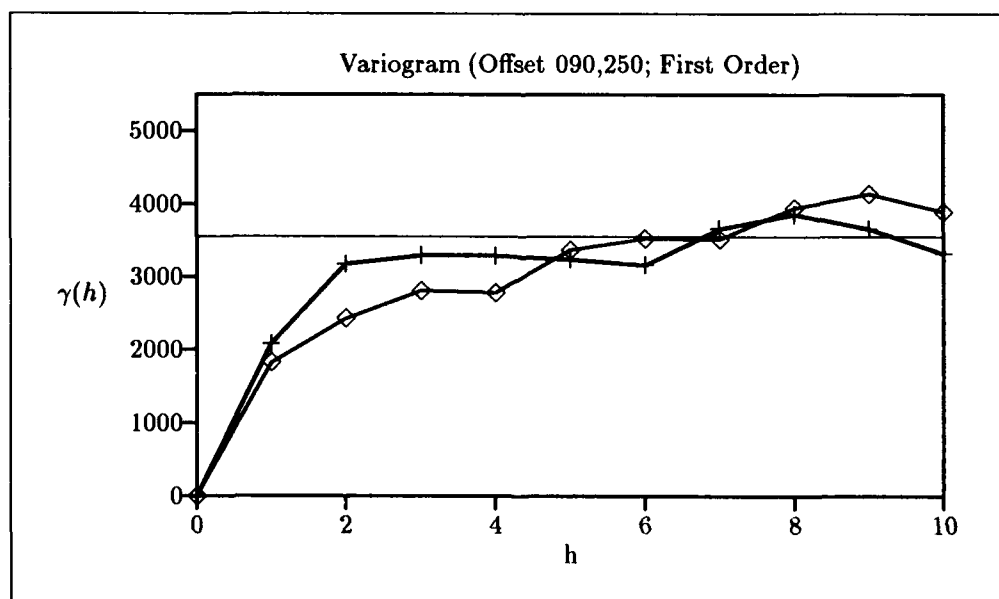


Figure C.5. SPOT 2 Channel 2.

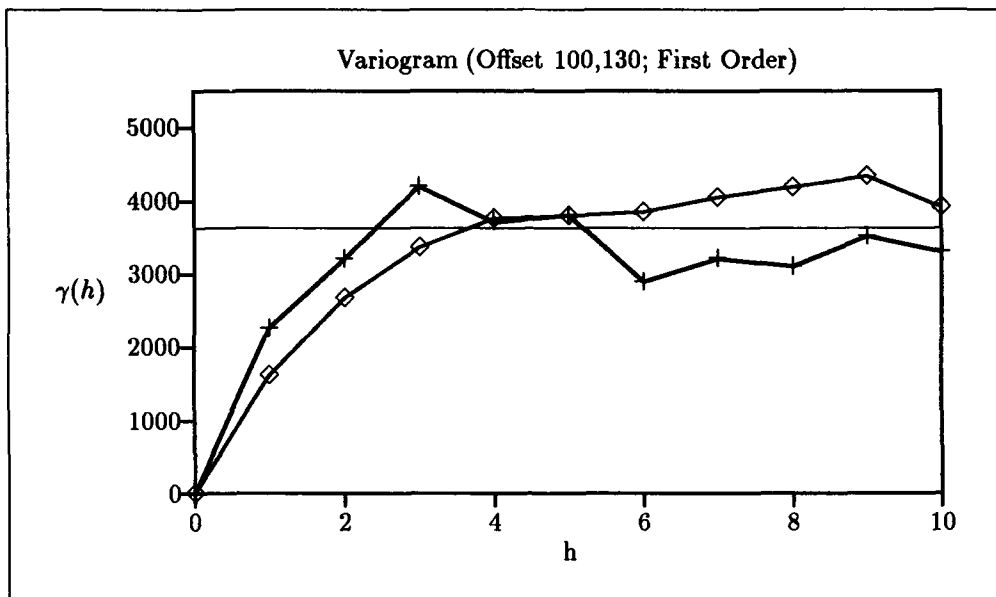


Figure C.6. SPOT 2 Channel 2.

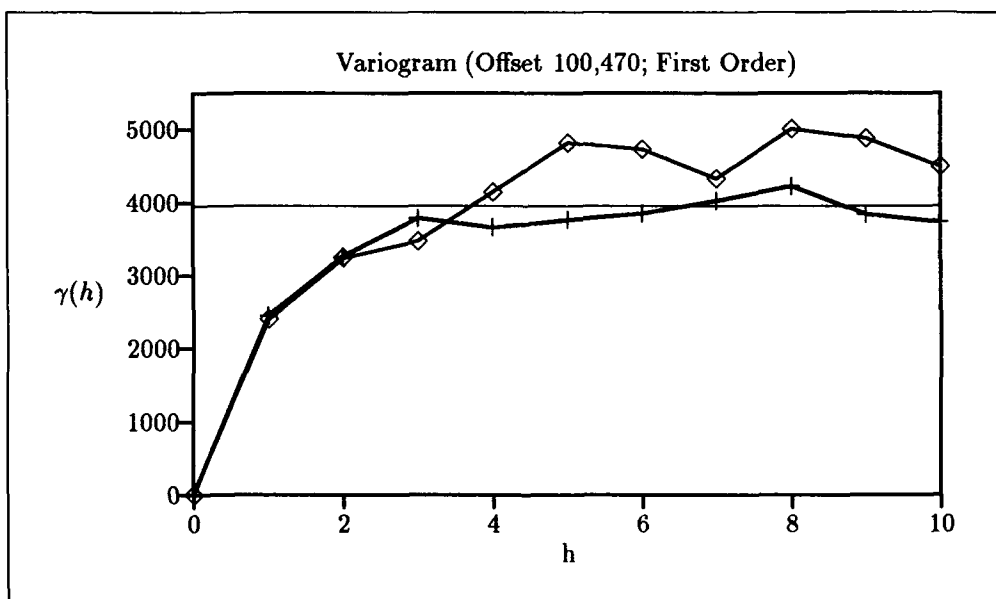


Figure C.7. SPOT 2 Channel 2.

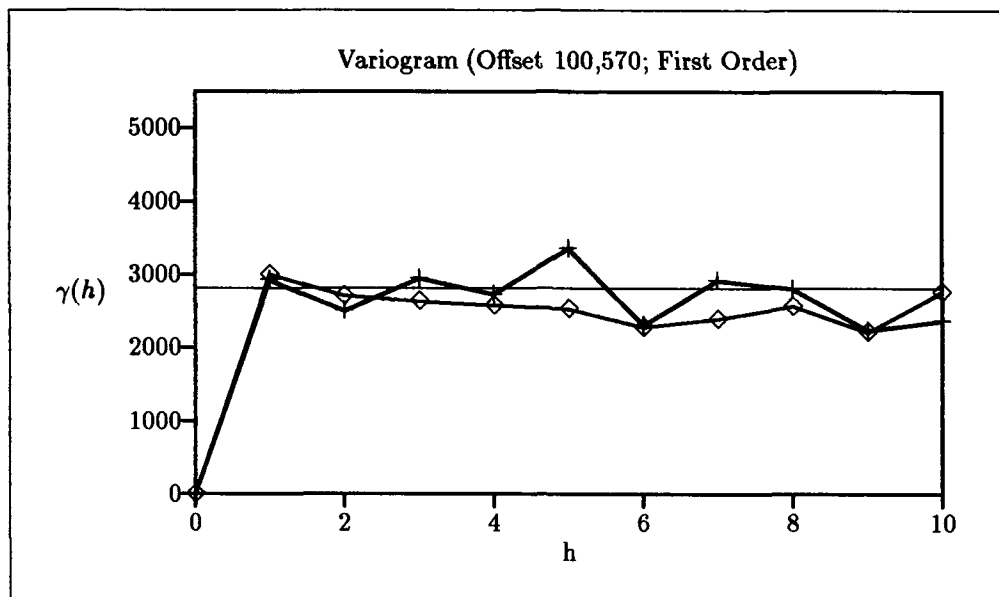


Figure C.8. SPOT 2 Channel 2.

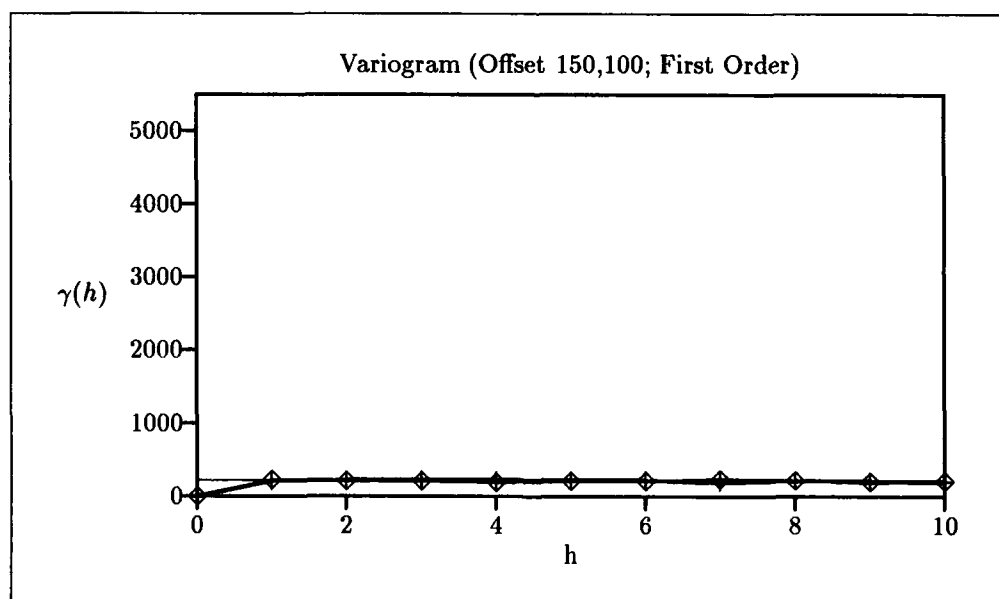


Figure C.9. SPOT 2 Channel 2.

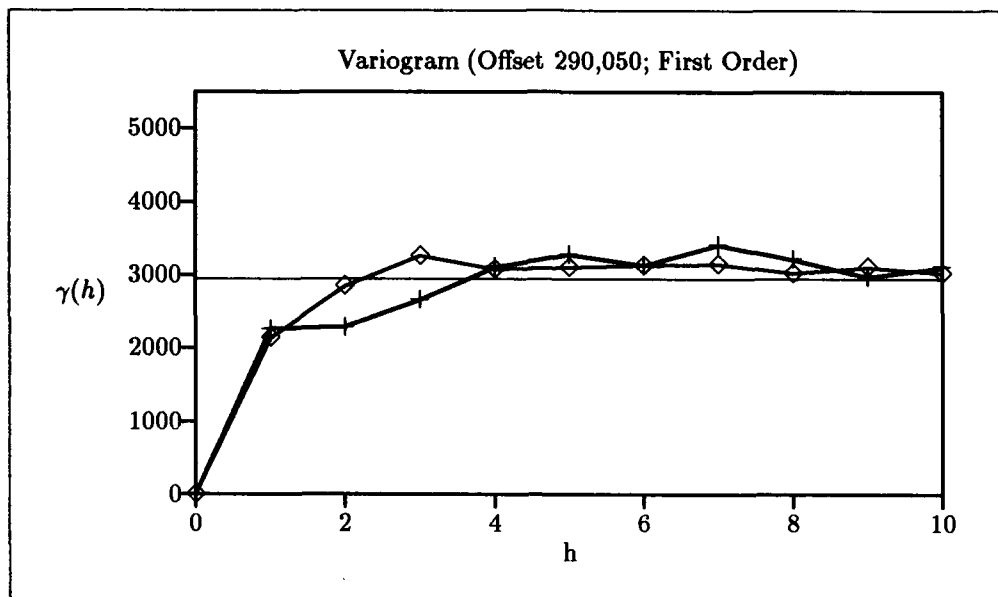


Figure C.10. SPOT 2 Channel 2.

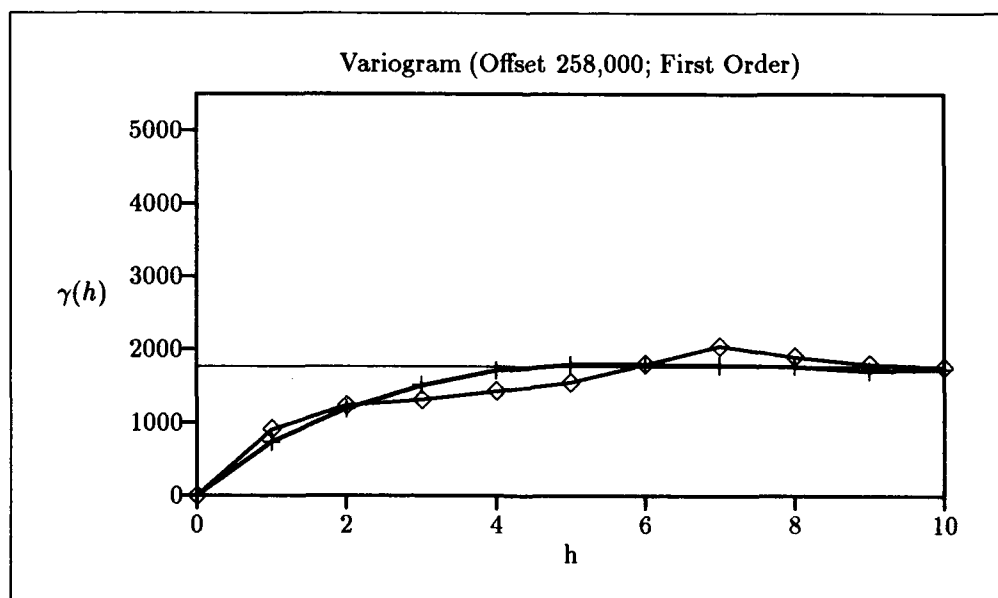


Figure C.11. SPOT 2 Channel 2.

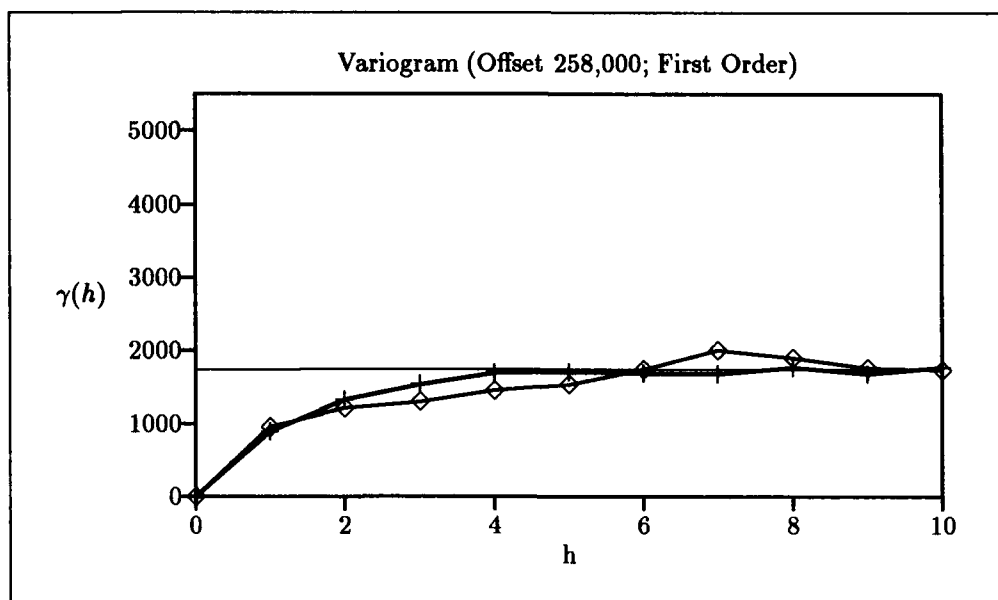


Figure C.12. SPOT 2 Channel 3.

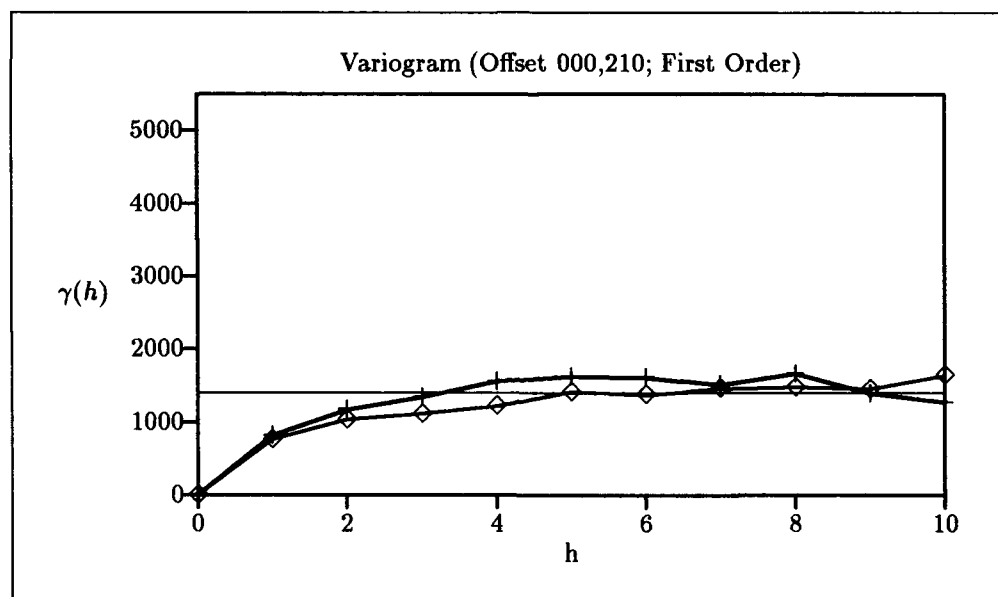


Figure C.13. SPOT 1 Channel 3.

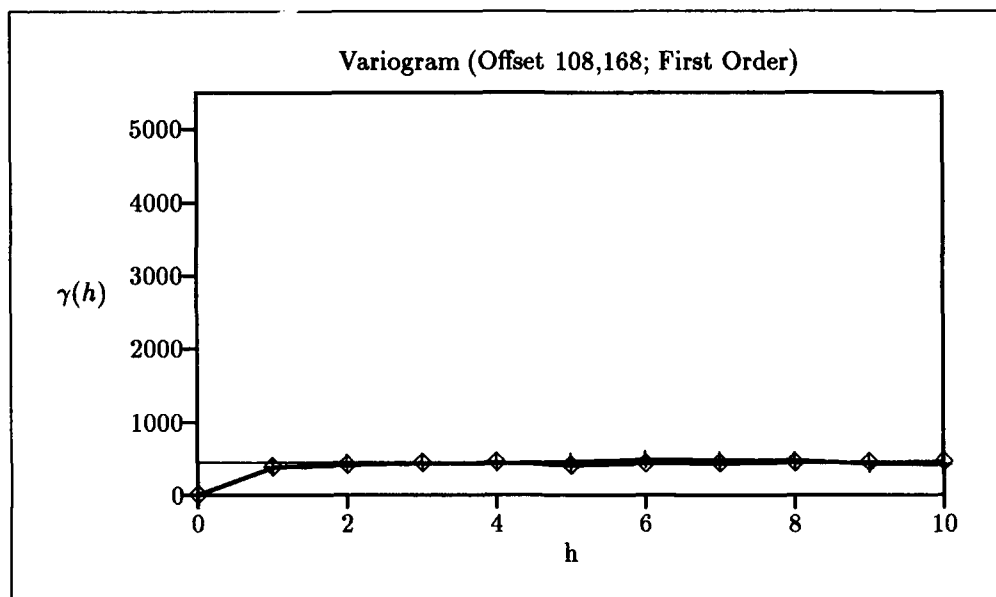


Figure C.14. SPOT 1 Channel 3.

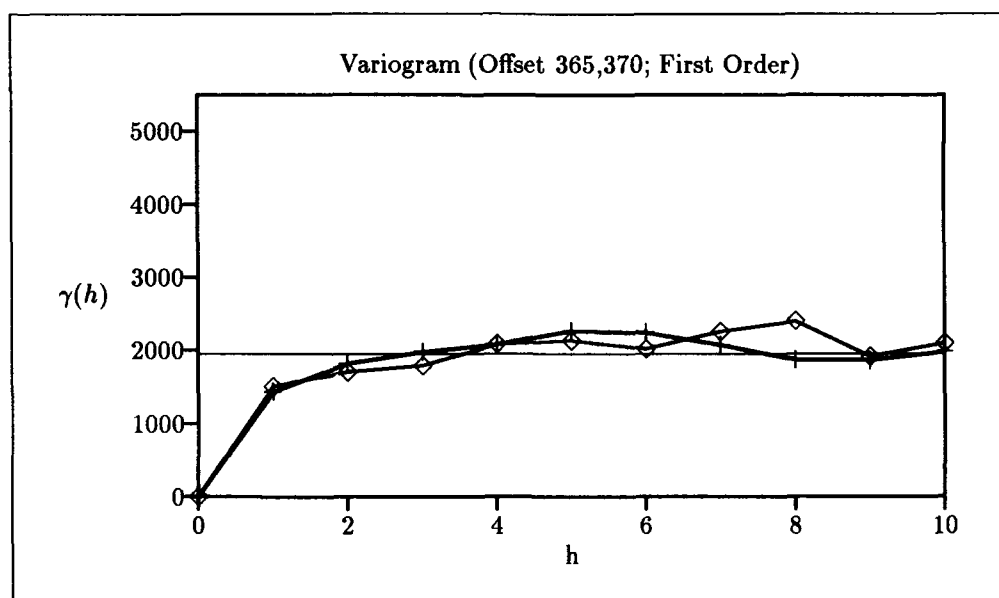


Figure C.15. SPOT 1 Channel 3.

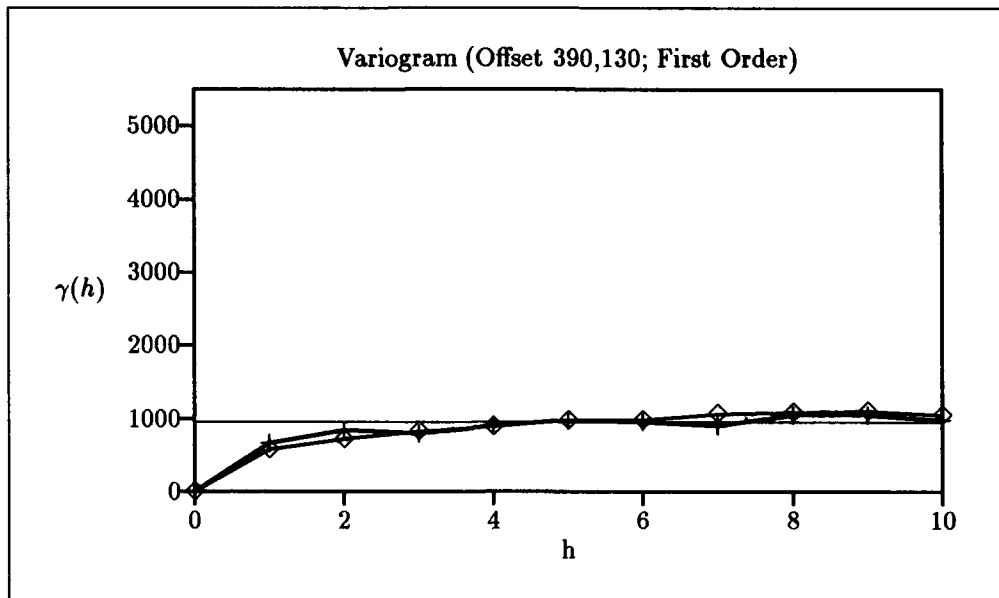


Figure C.16. SPOT 1 Channel 3.

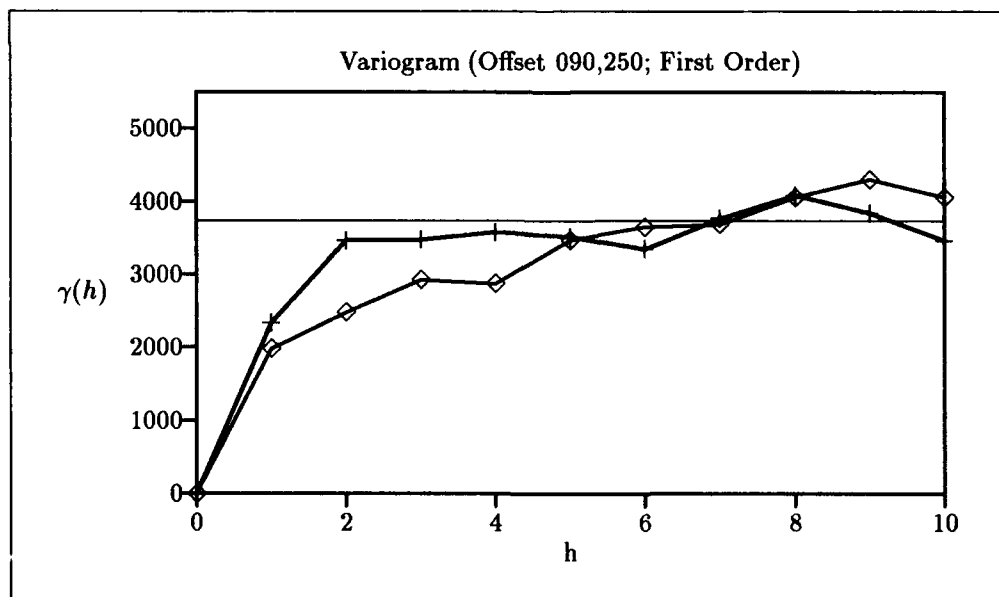


Figure C.17. SPOT 2 Channel 3.

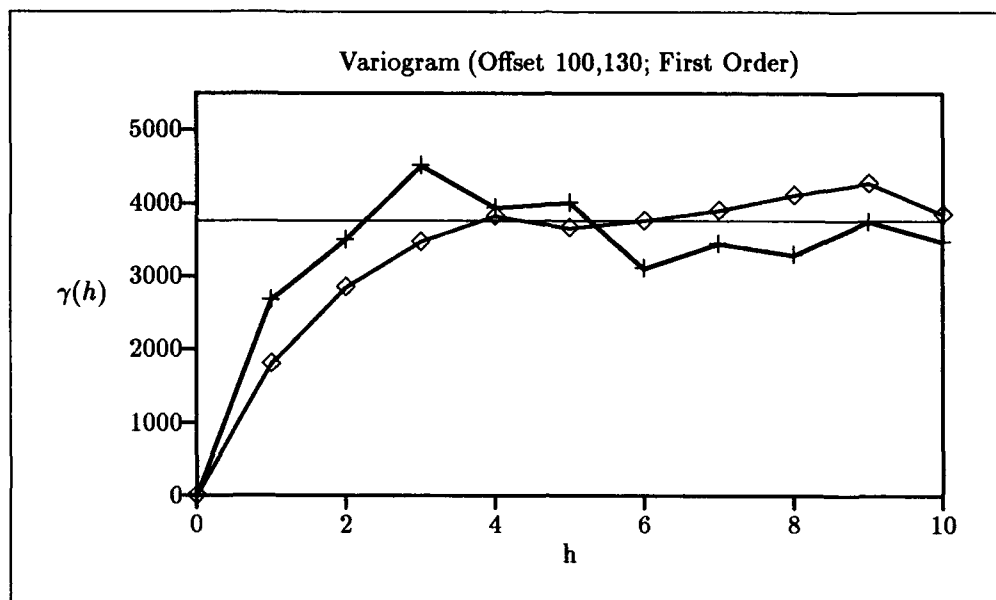


Figure C.18. SPOT 2 Channel 3.

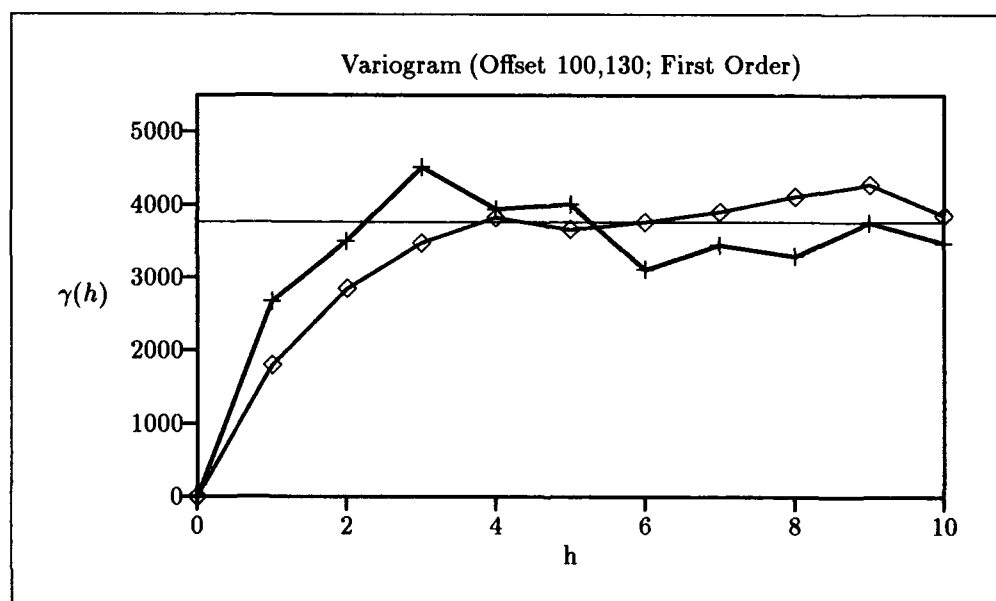


Figure C.19. SPOT 2 Channel 3.

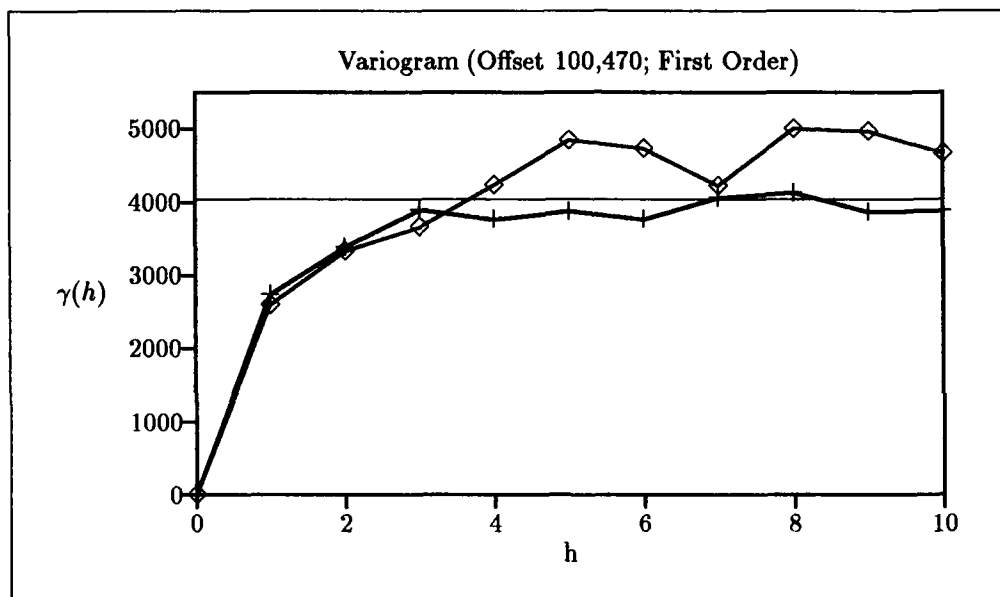


Figure C.20. SPOT 2 Channel 3.

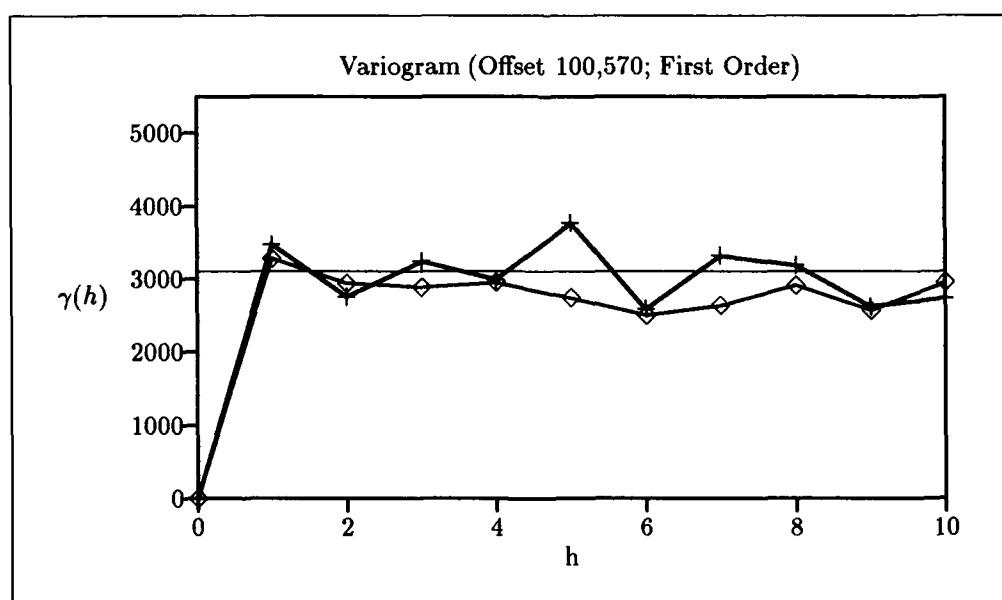


Figure C.21. SPOT 2 Channel 3.

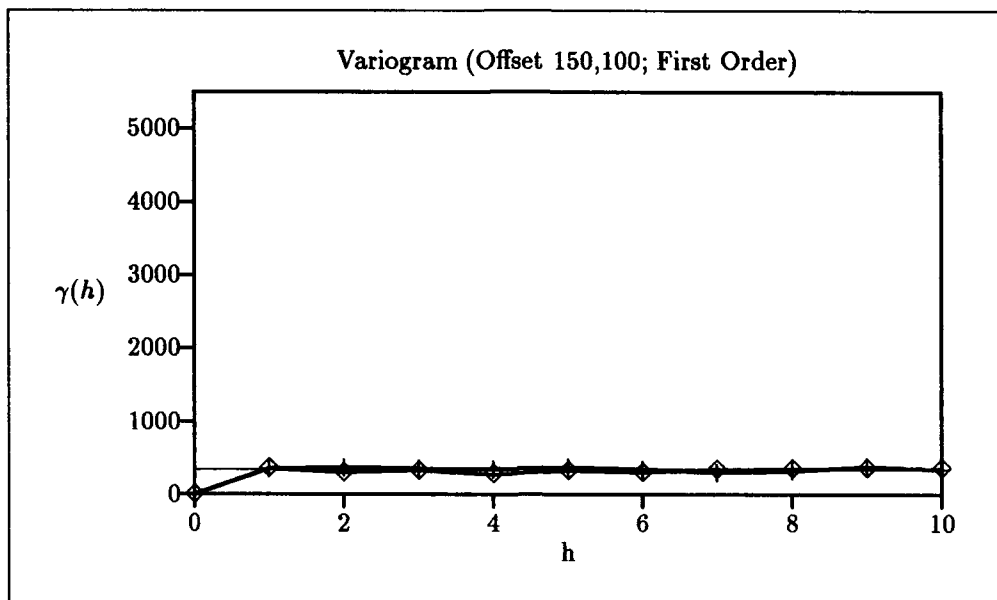


Figure C.22. SPOT 2 Channel 3.

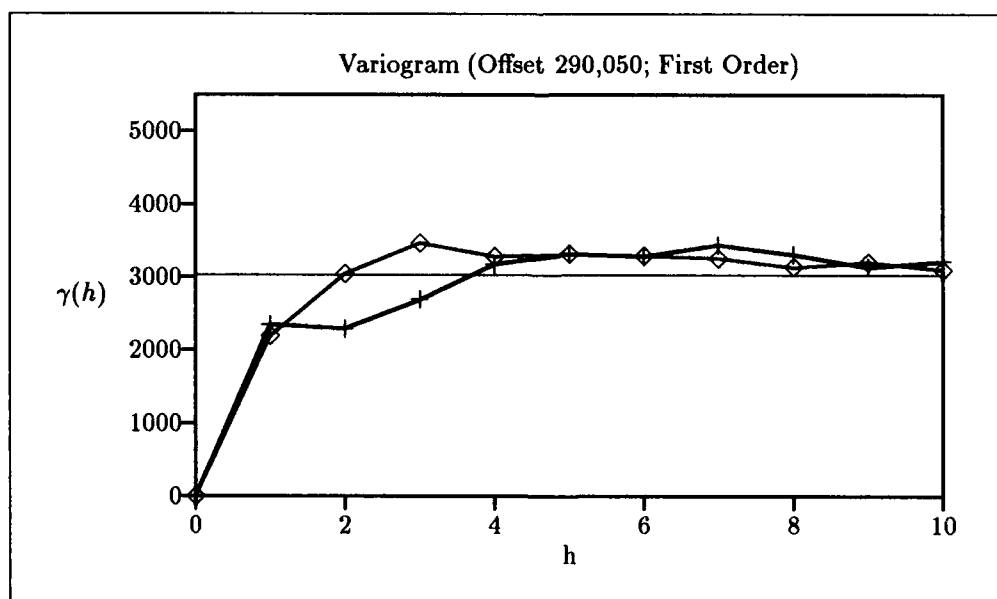


Figure C.23. SPOT 2 Channel 3.

C.2 Exponential Model

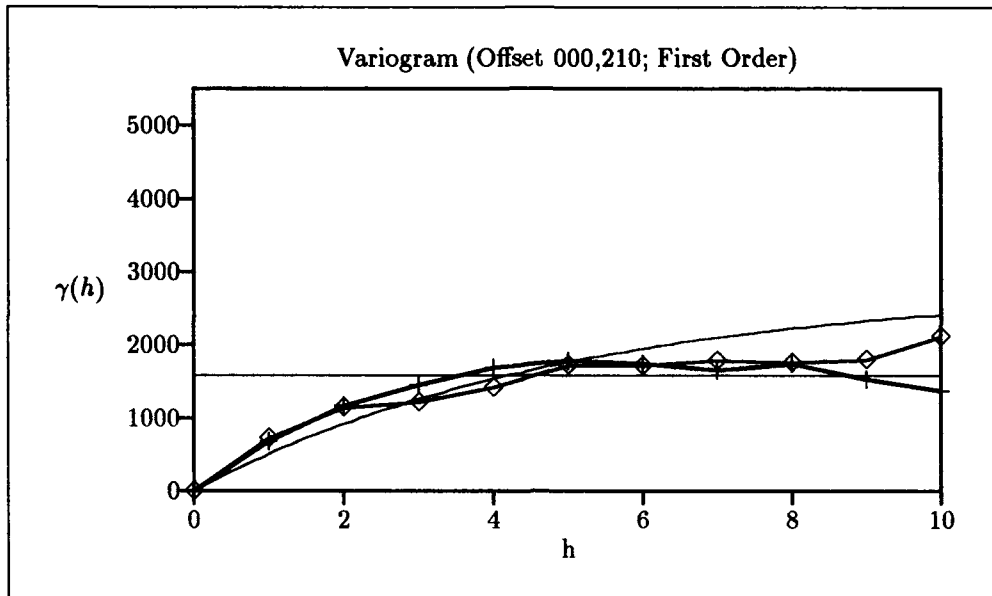


Figure C.24. SPOT 1 Channel 2.

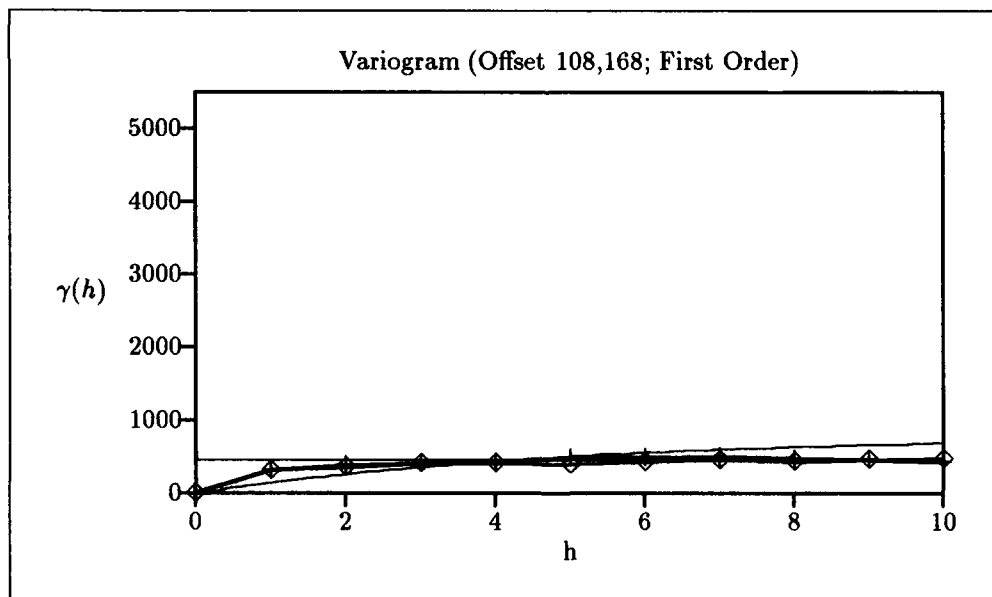


Figure C.25. SPOT 1 Channel 2.

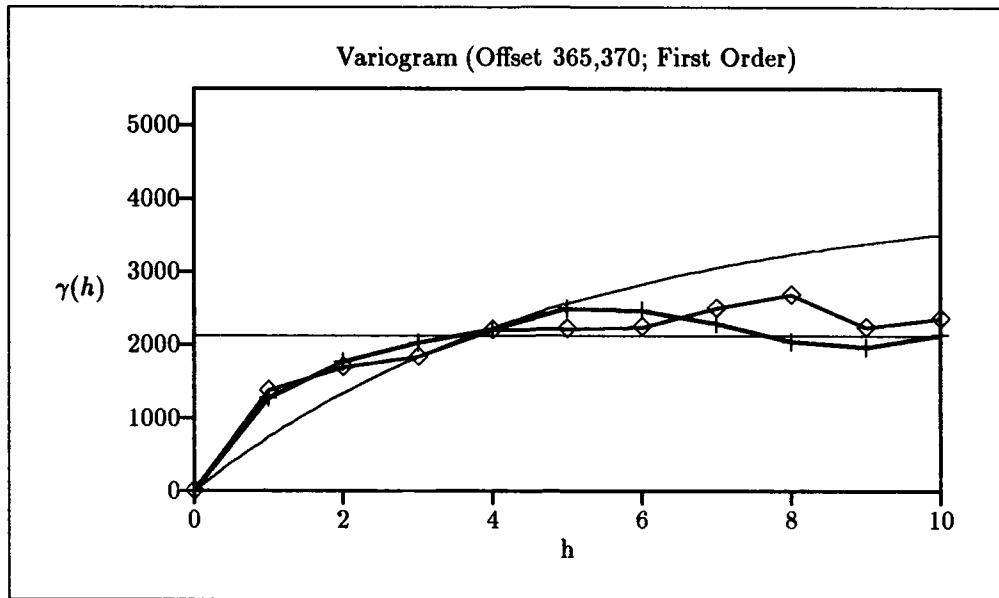


Figure C.26. SPOT 1 Channel 2.

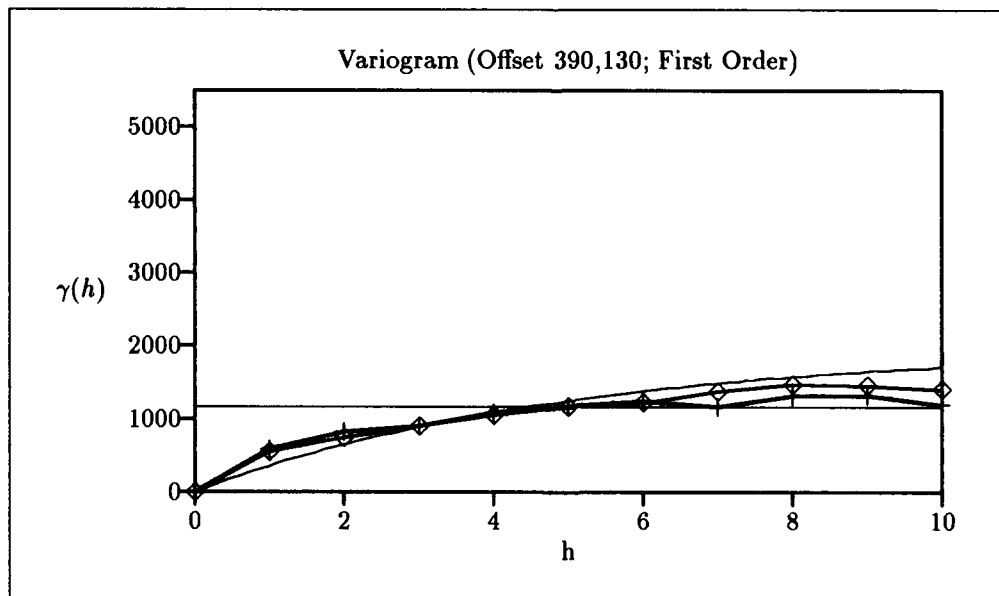


Figure C.27. SPOT 1 Channel 2.

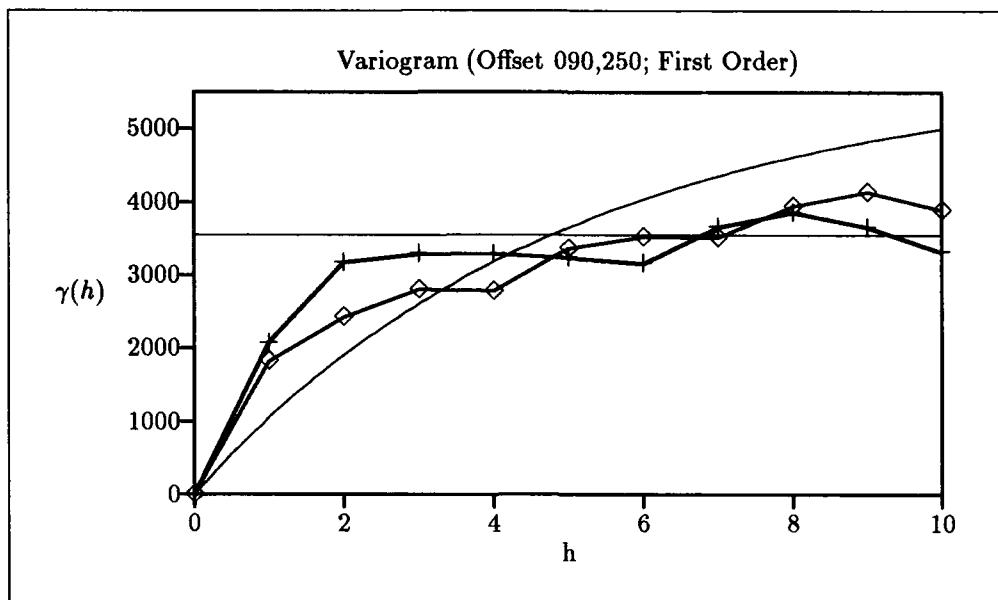


Figure C.28. SPOT 2 Channel 2.

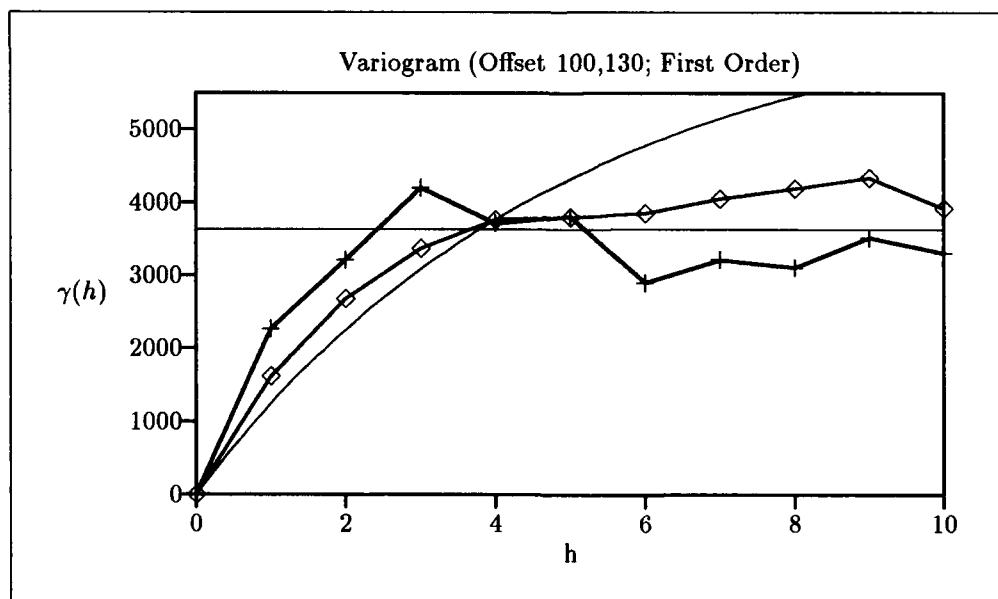


Figure C.29. SPOT 2 Channel 2.

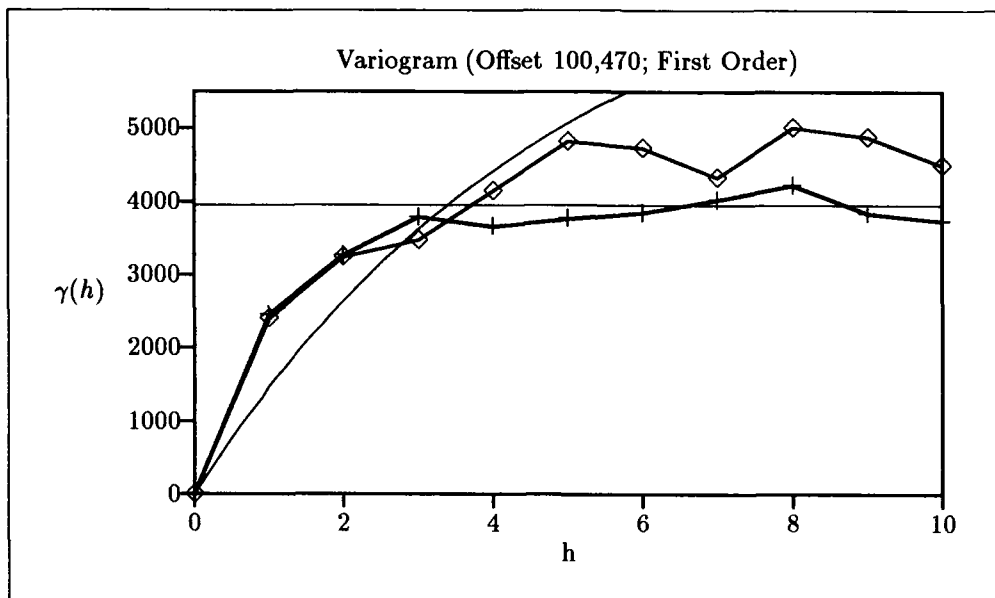


Figure C.30. SPOT 2 Channel 2.

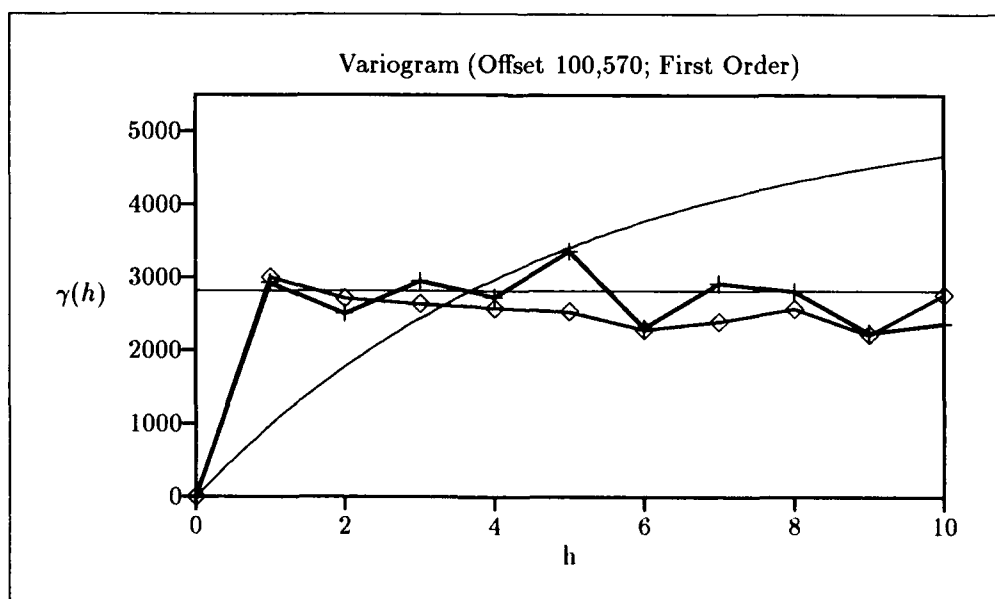


Figure C.31. SPOT 2 Channel 2.

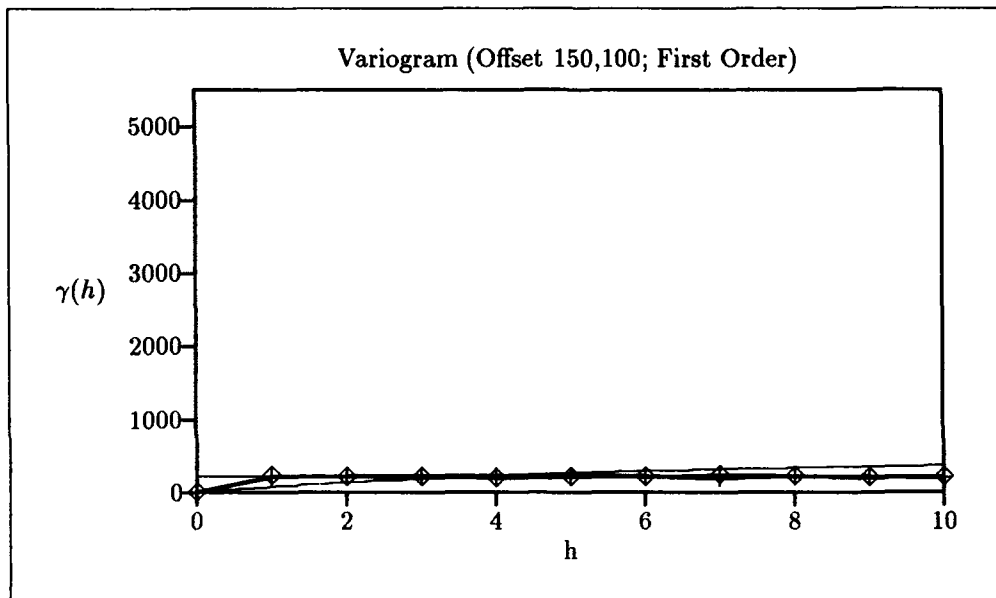


Figure C.32. SPOT 2 Channel 2.

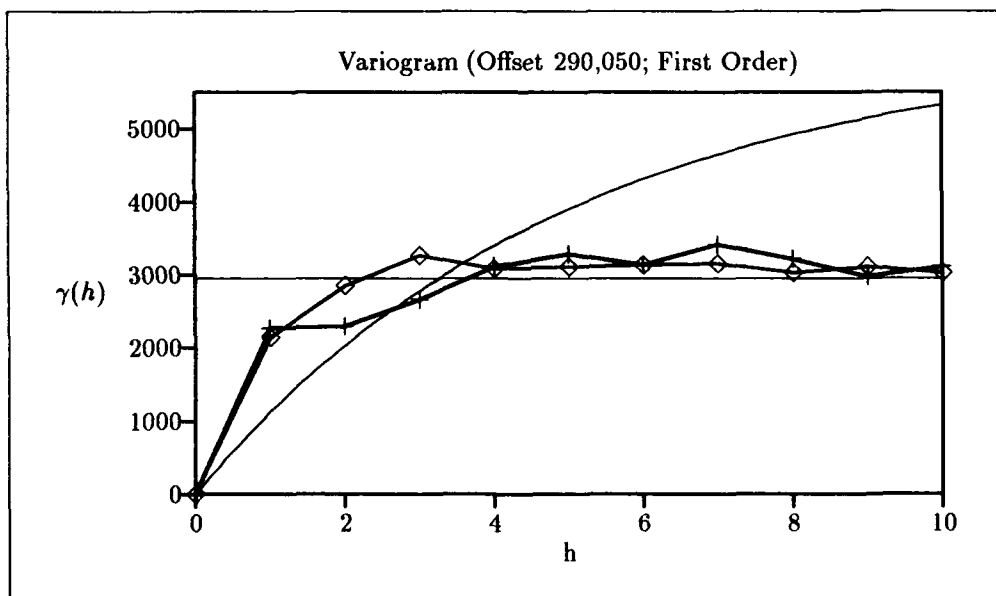


Figure C.33. SPOT 2 Channel 2.

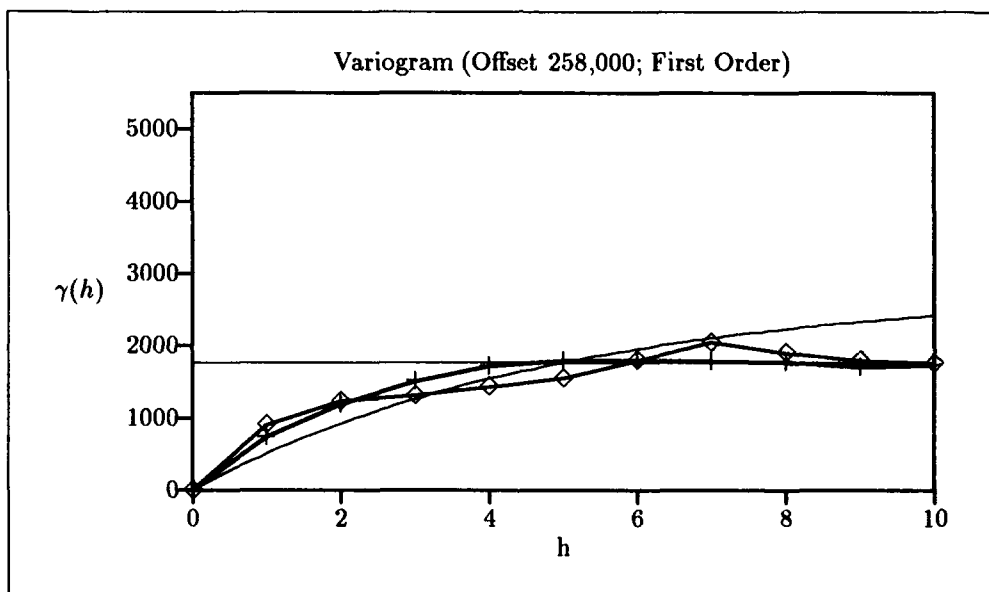


Figure C.34. SPOT 2 Channel 2.

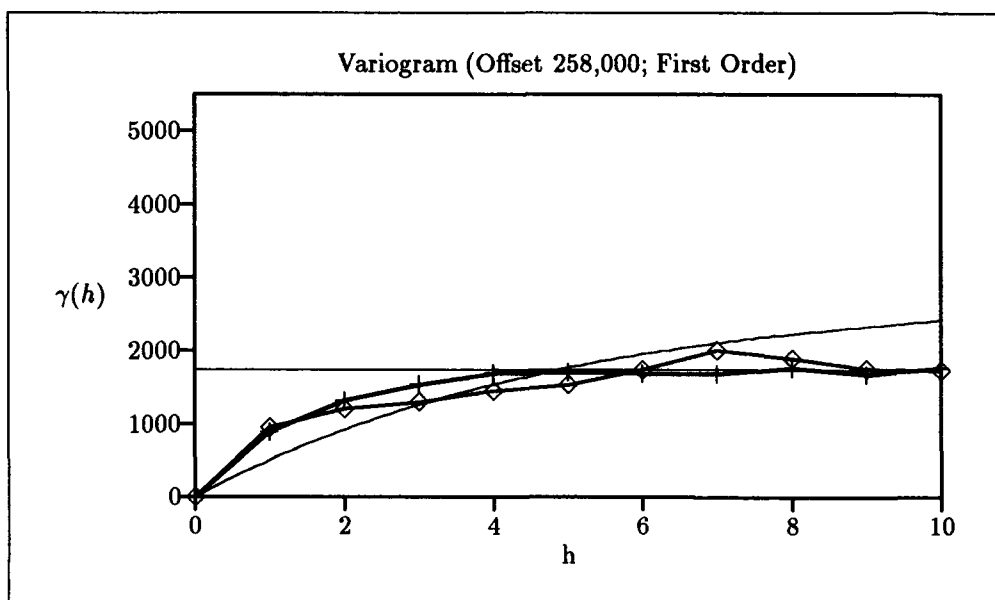


Figure C.35. SPOT 2 Channel 3.

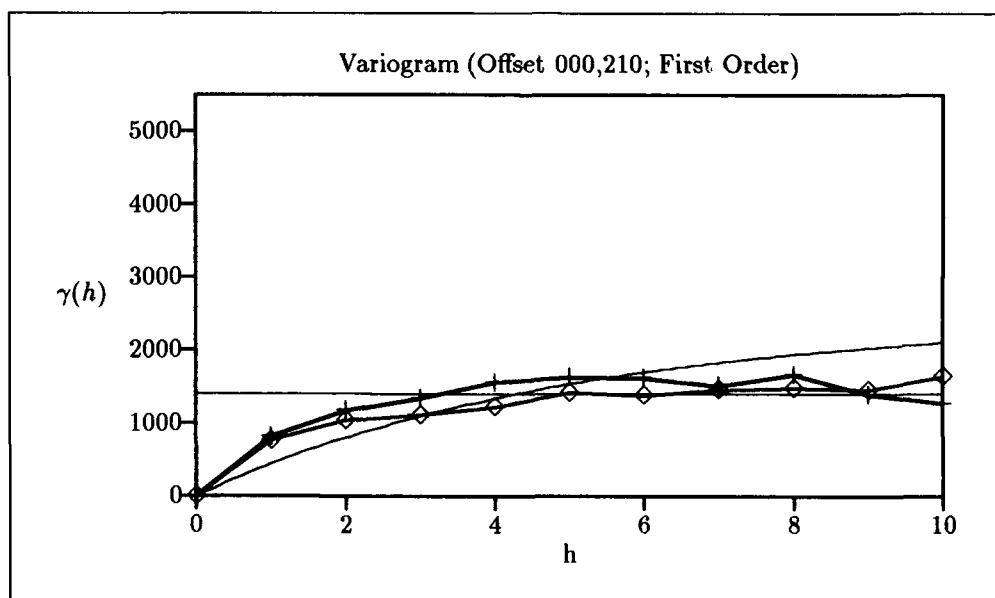


Figure C.36. SPOT 1 Channel 3.

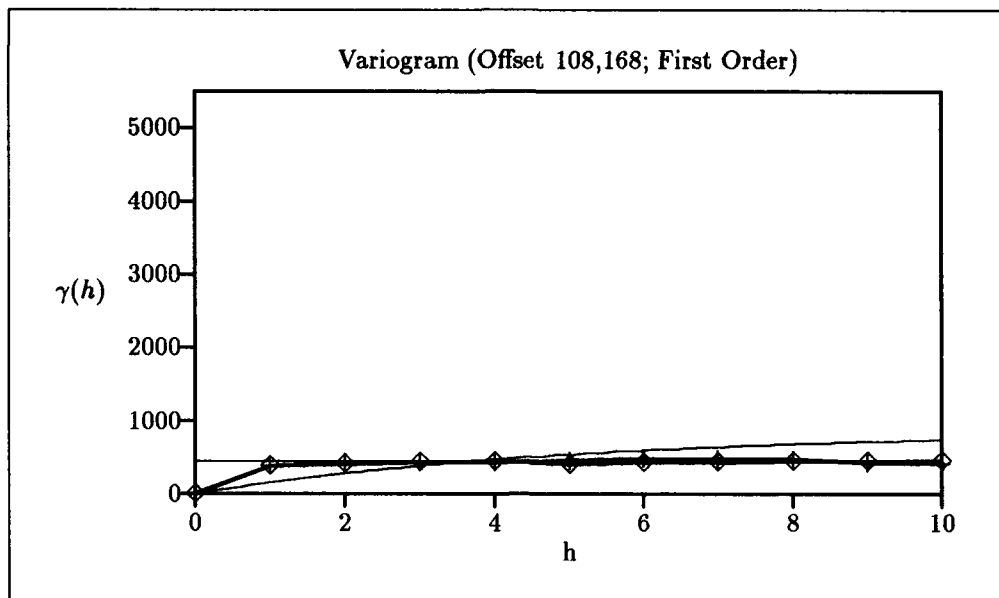


Figure C.37. SPOT 1 Channel 3.

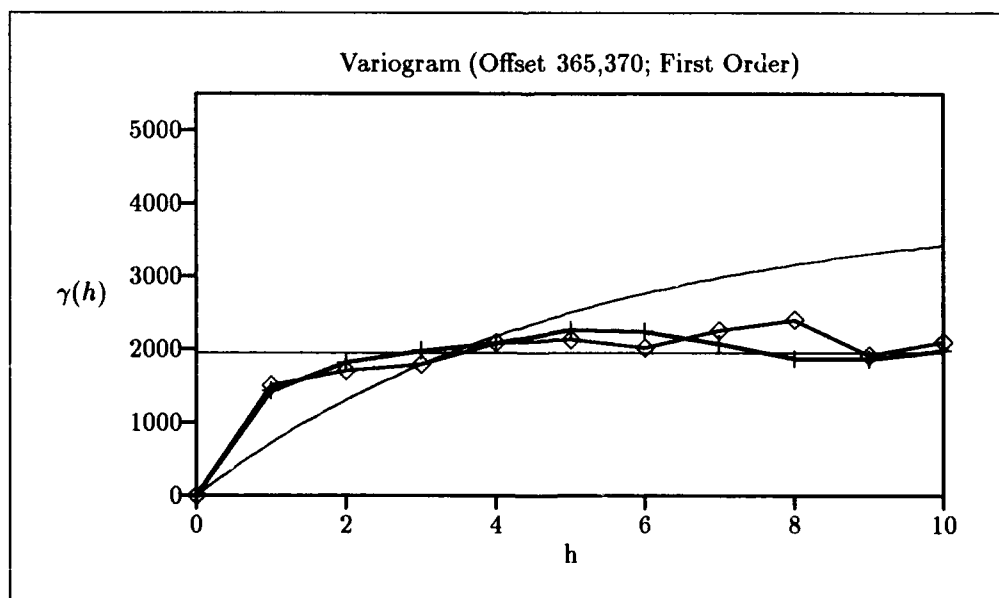


Figure C.38. SPOT 1 Channel 3.

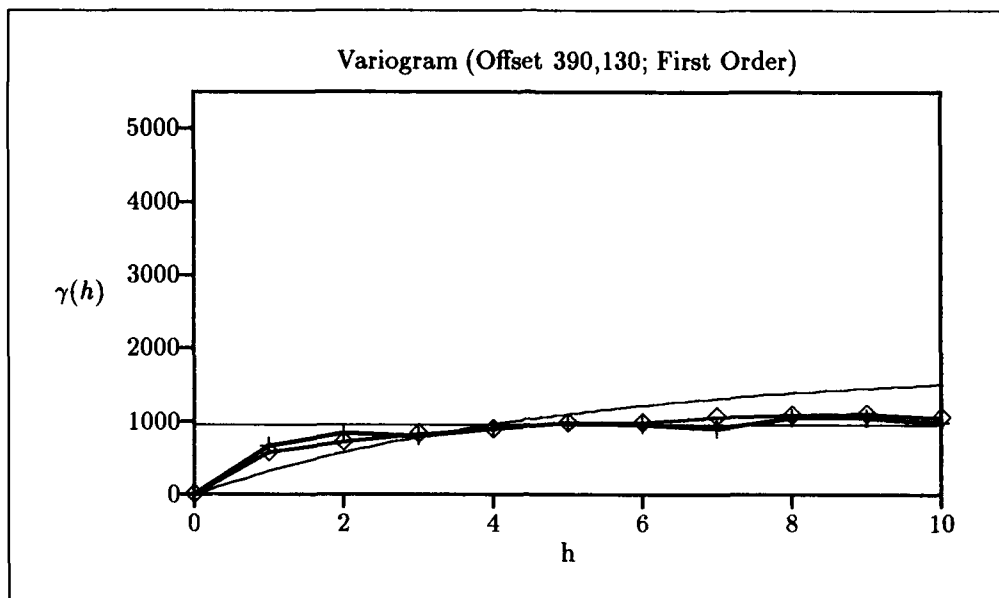


Figure C.39. SPOT 1 Channel 3.

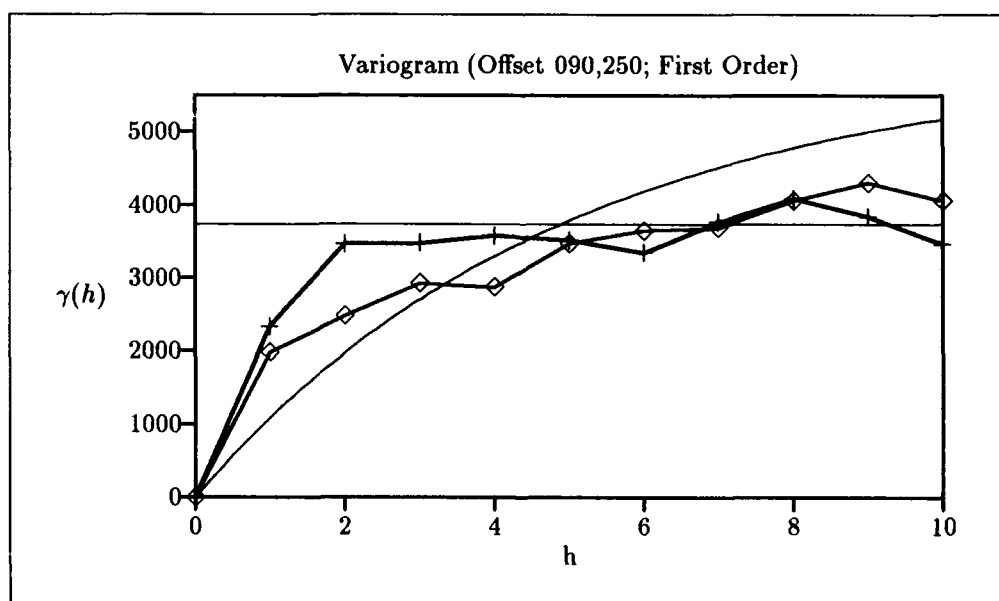


Figure C.40. SPOT 2 Channel 3.

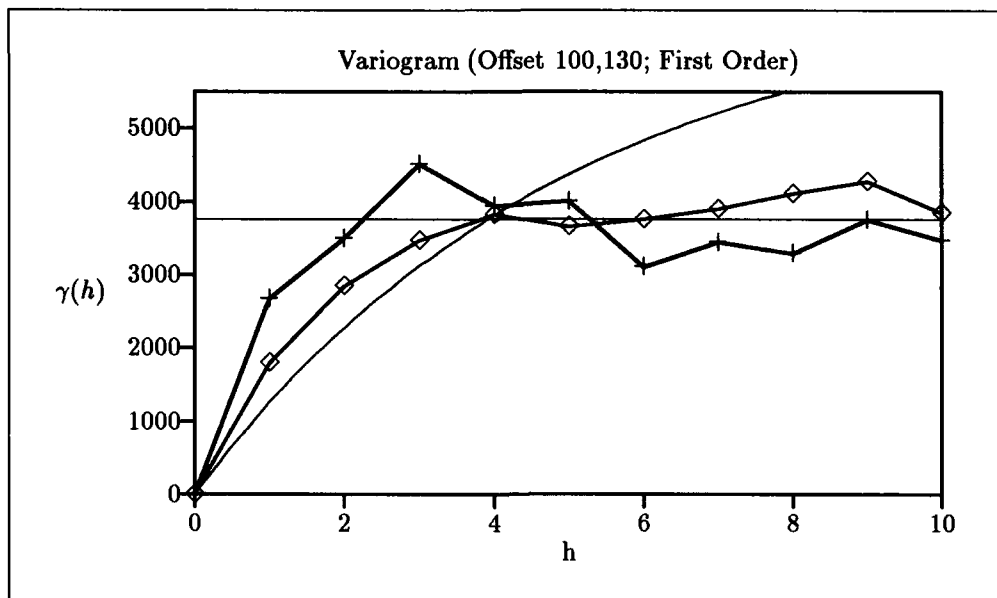


Figure C.41. SPOT 2 Channel 3.

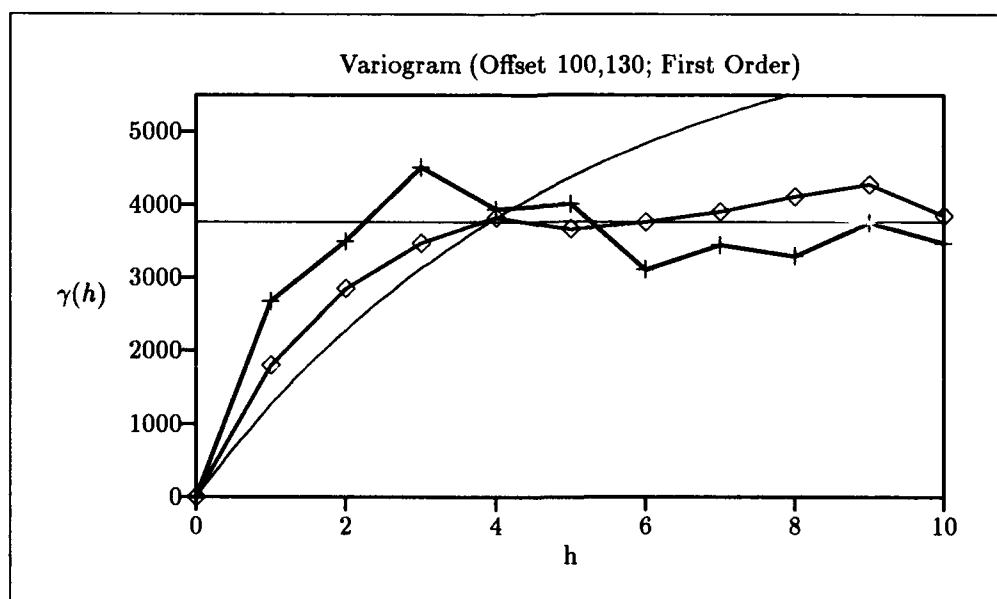


Figure C.42. SPOT 2 Channel 3.

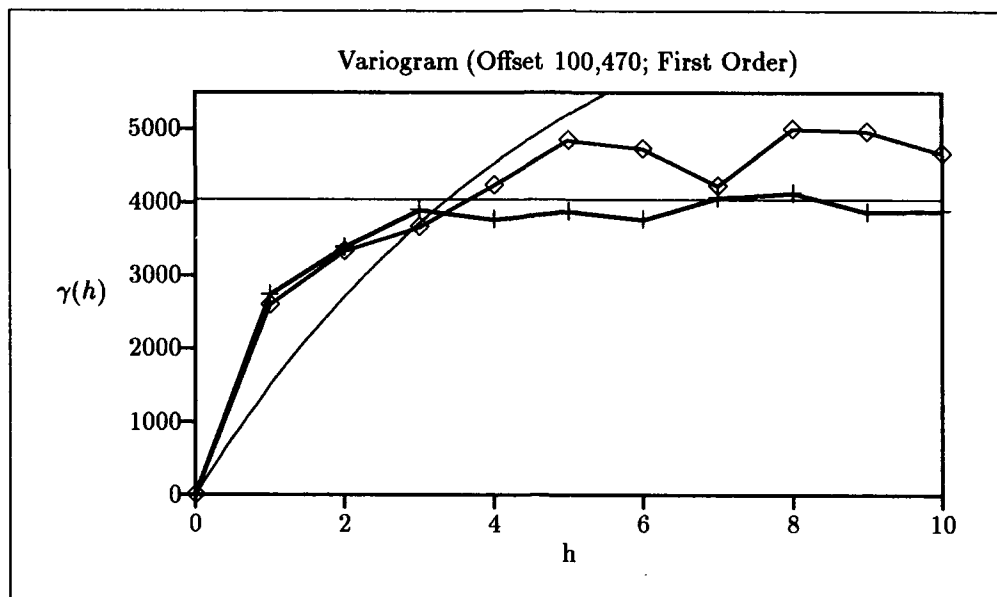


Figure C.43. SPOT 2 Channel 3.

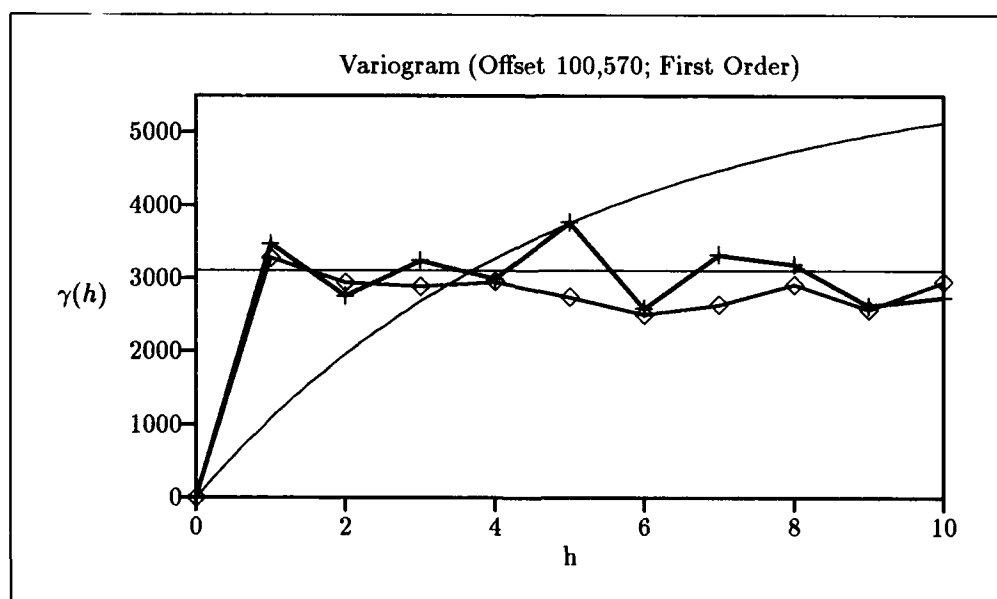


Figure C.44. SPOT 2 Channel 3.

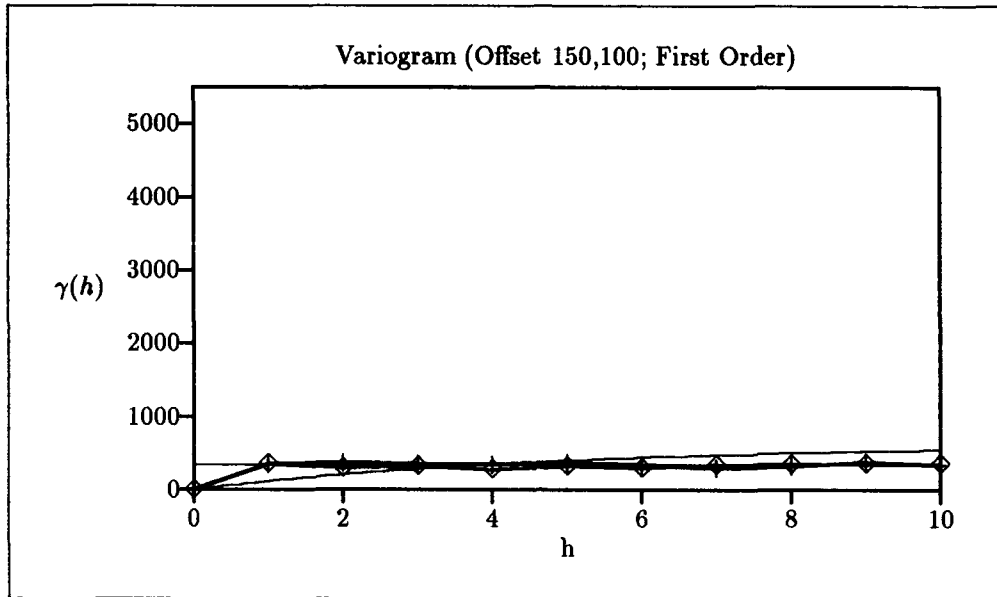


Figure C.45. SPOT 2 Channel 3.

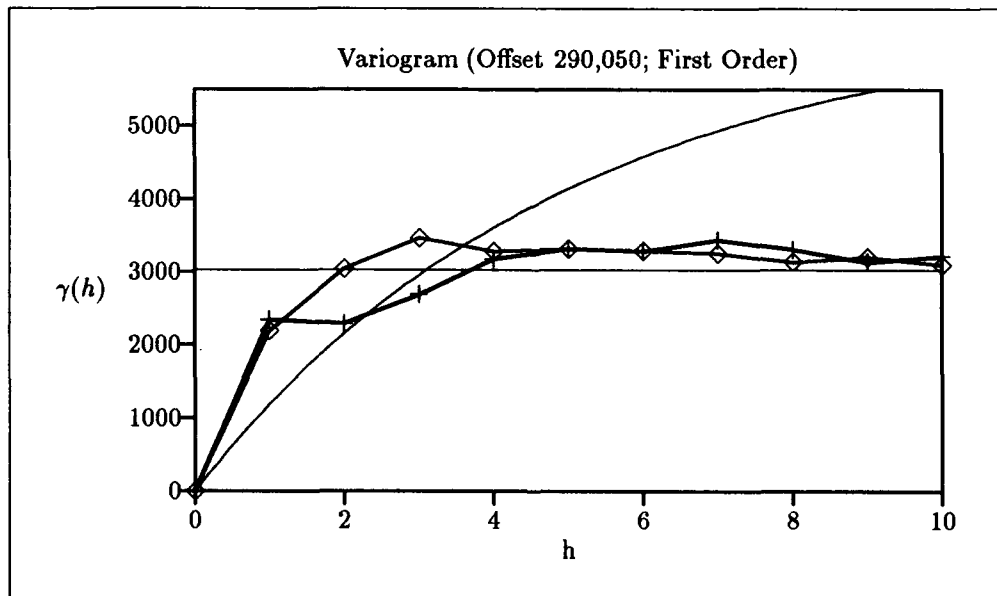


Figure C.46. SPOT 2 Channel 3.

C.3 Spherical Model

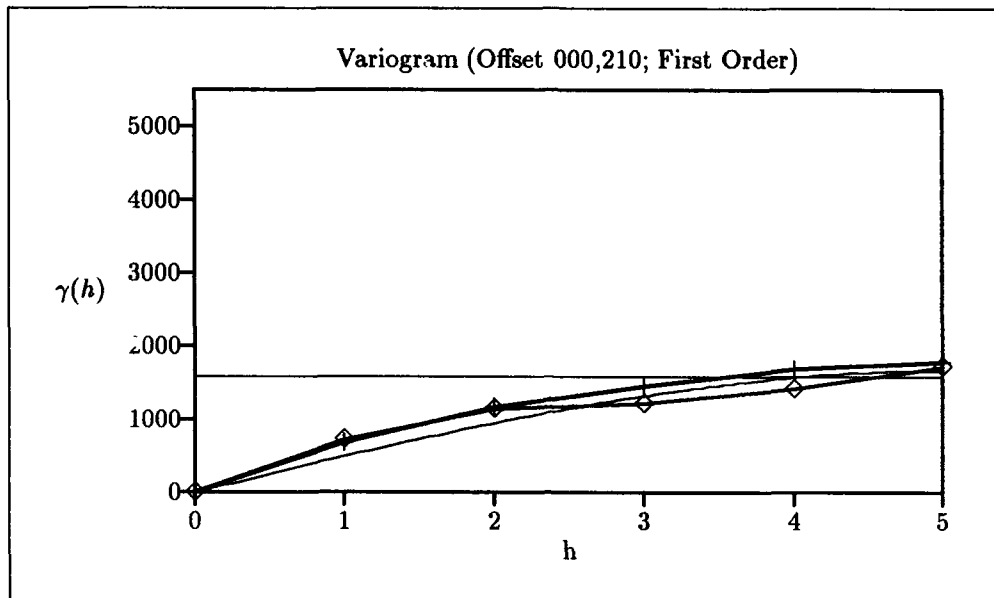


Figure C.47. SPOT 1 Channel 2.

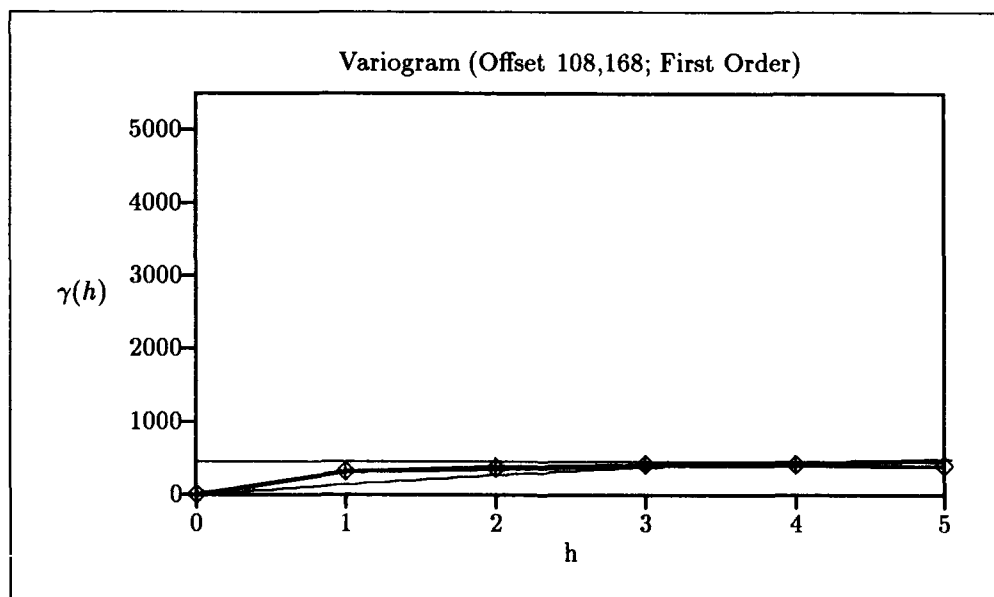


Figure C.48. SPOT 1 Channel 2.

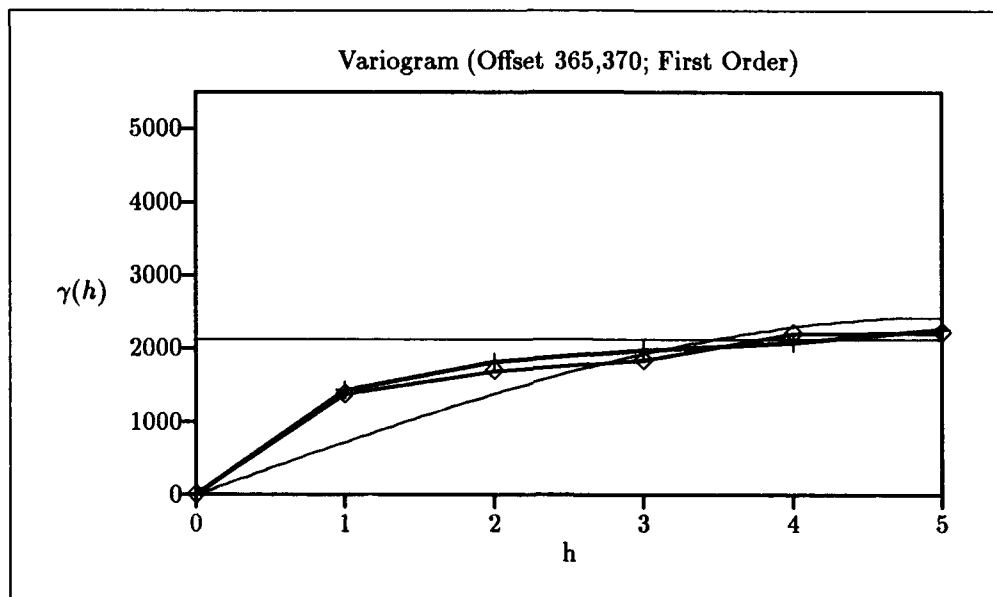


Figure C.49. SPOT 1 Channel 2.

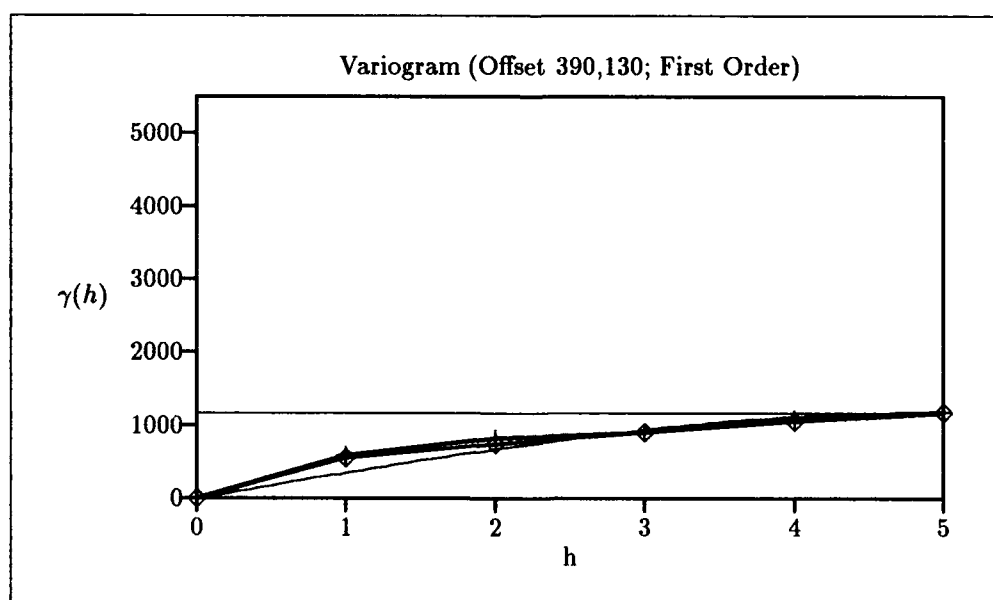


Figure C.50. SPOT 1 Channel 2.

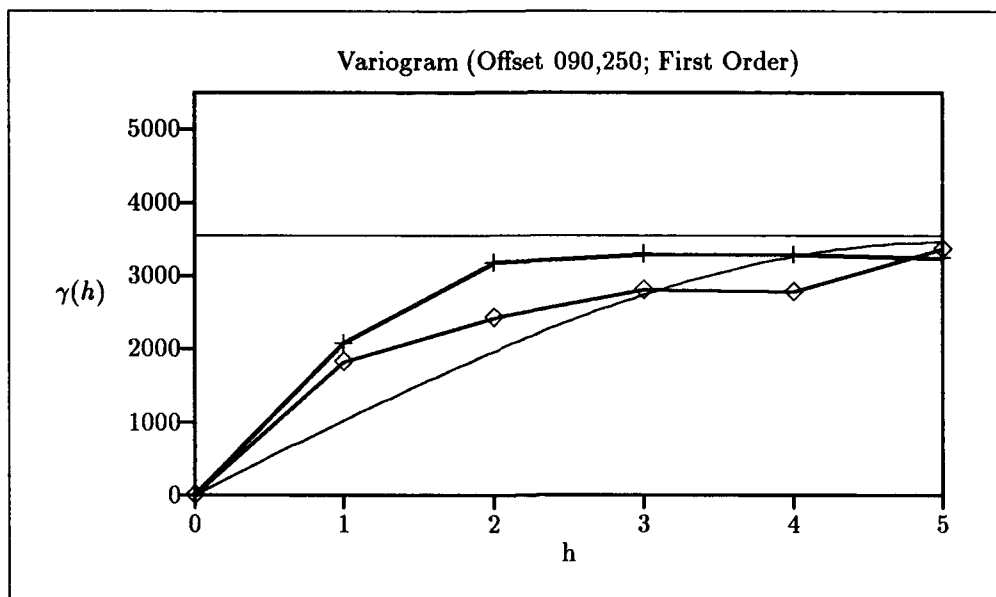


Figure C.51. SPOT 2 Channel 2.

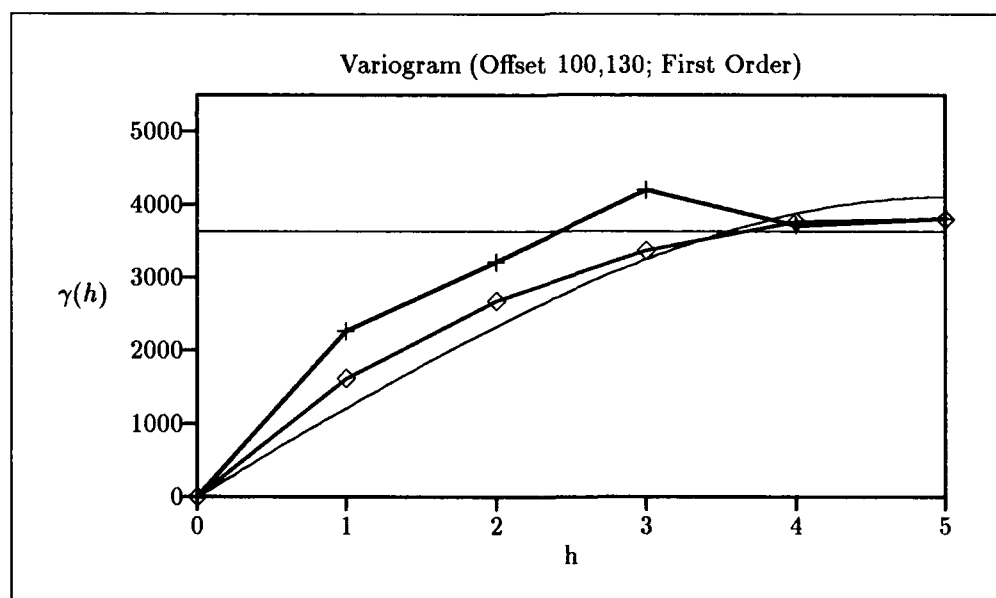


Figure C.52. SPOT 2 Channel 2.

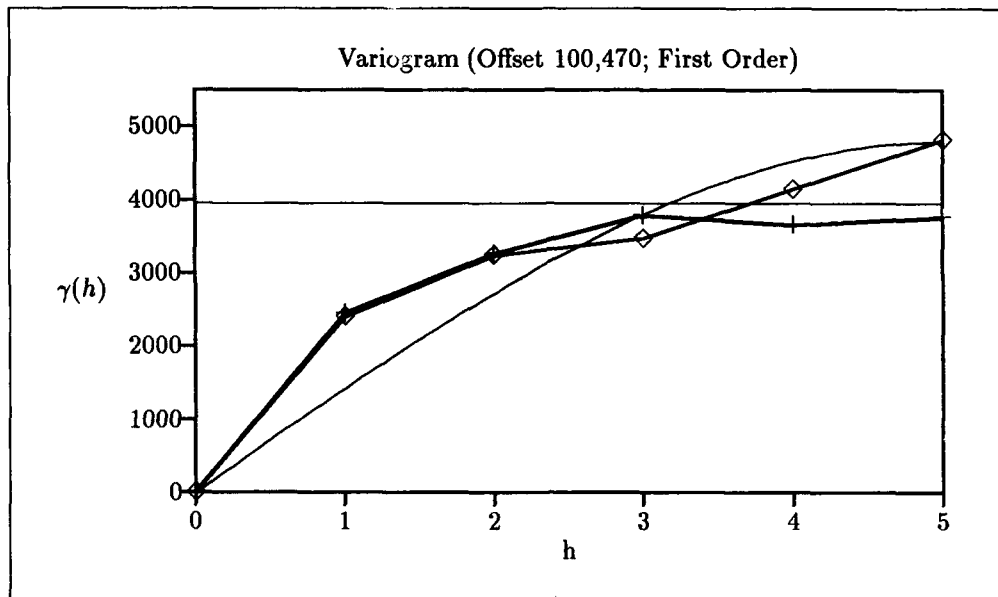


Figure C.53. SPOT 2 Channel 2.

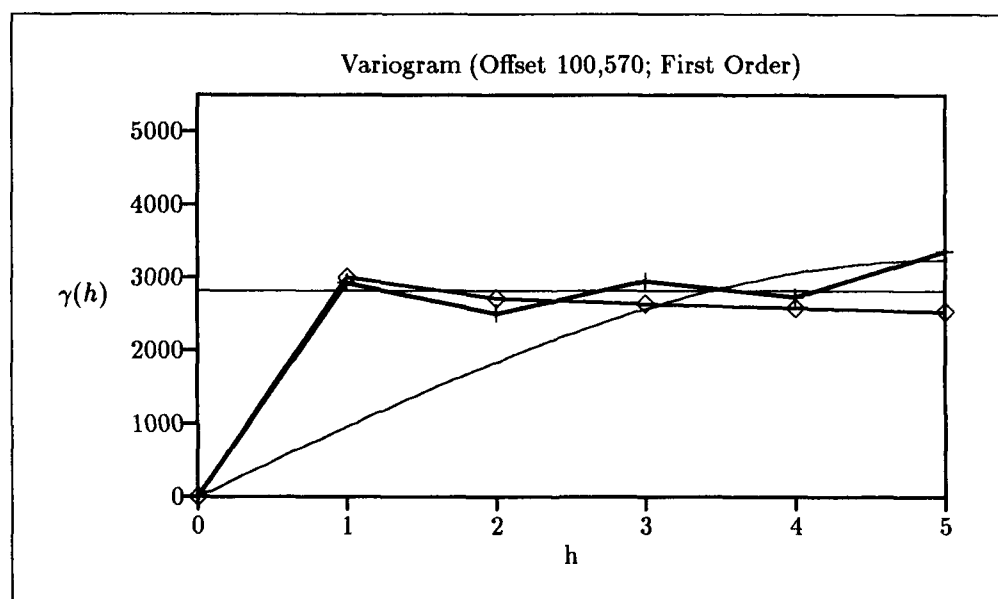


Figure C.54. SPOT 2 Channel 2.

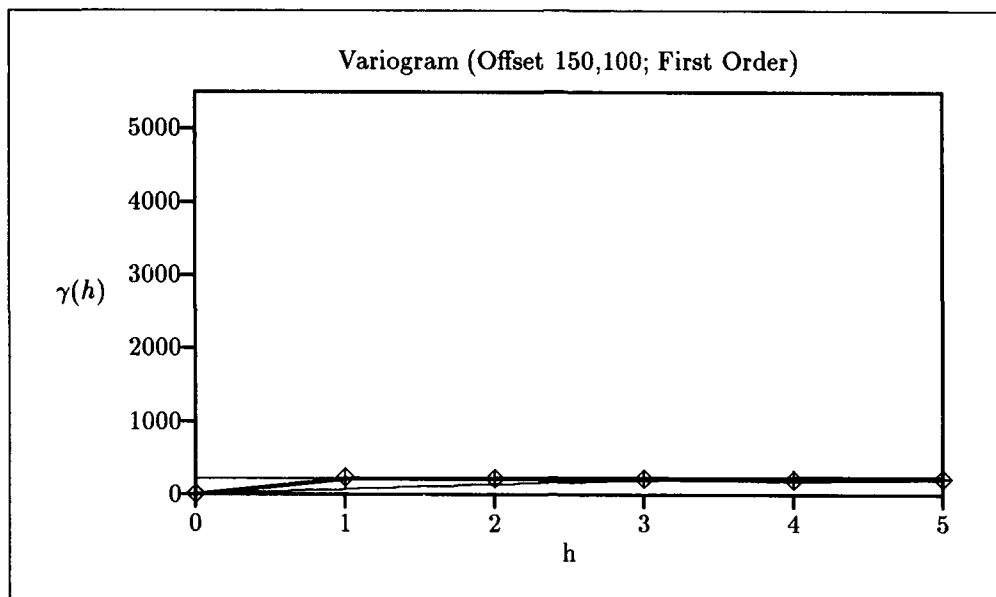


Figure C.55. SPOT 2 Channel 2.

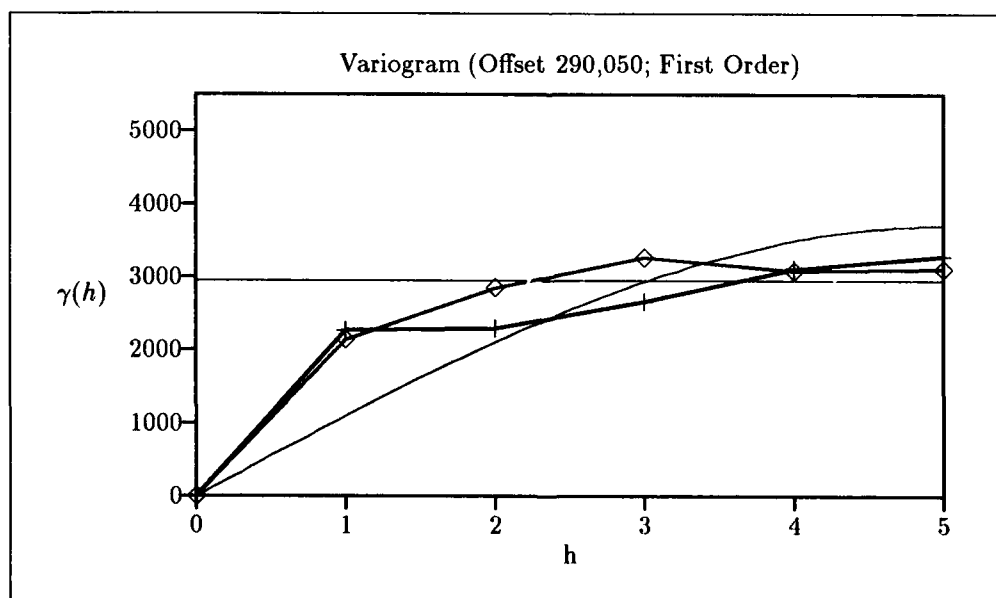


Figure C.56. SPOT 2 Channel 2.

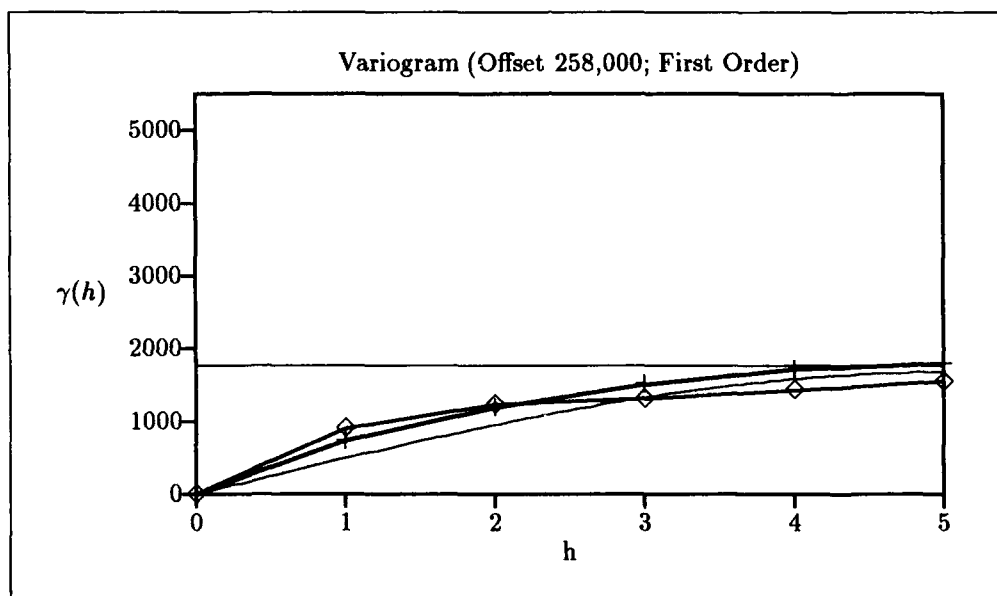


Figure C.57. SPOT 2 Channel 2.

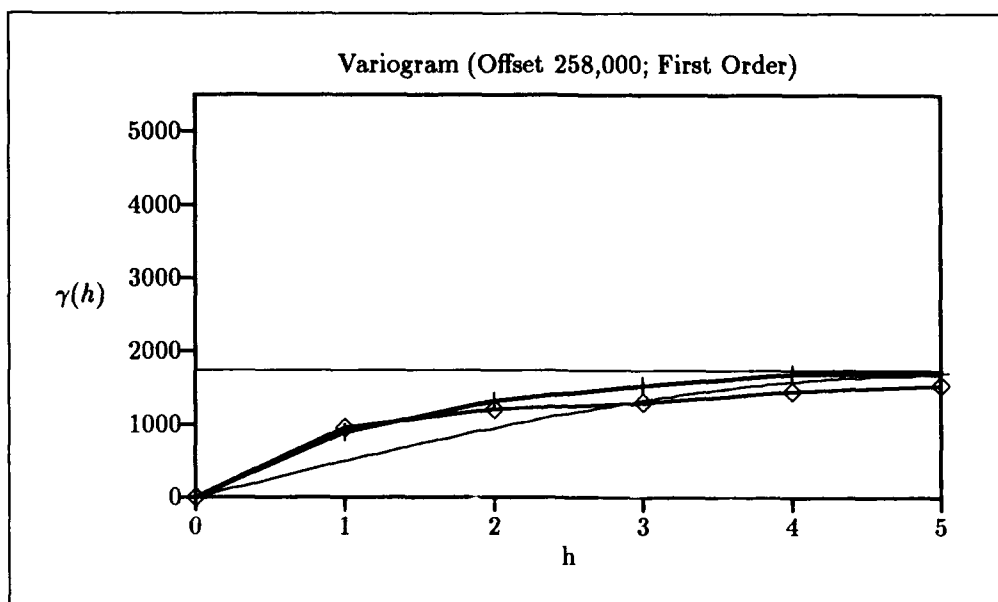


Figure C.58. SPOT 2 Channel 3.

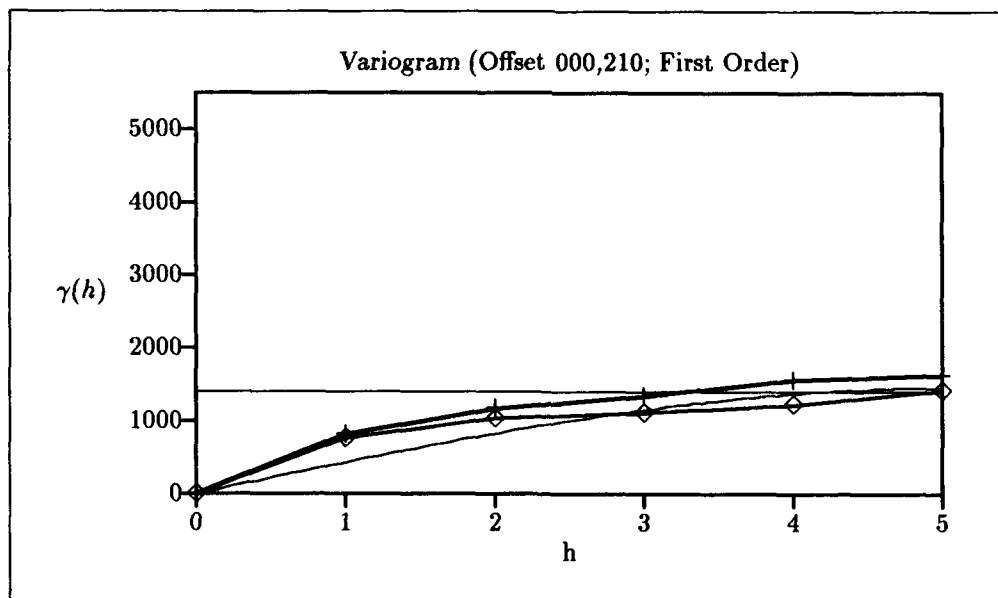


Figure C.59. SPOT 1 Channel 3.

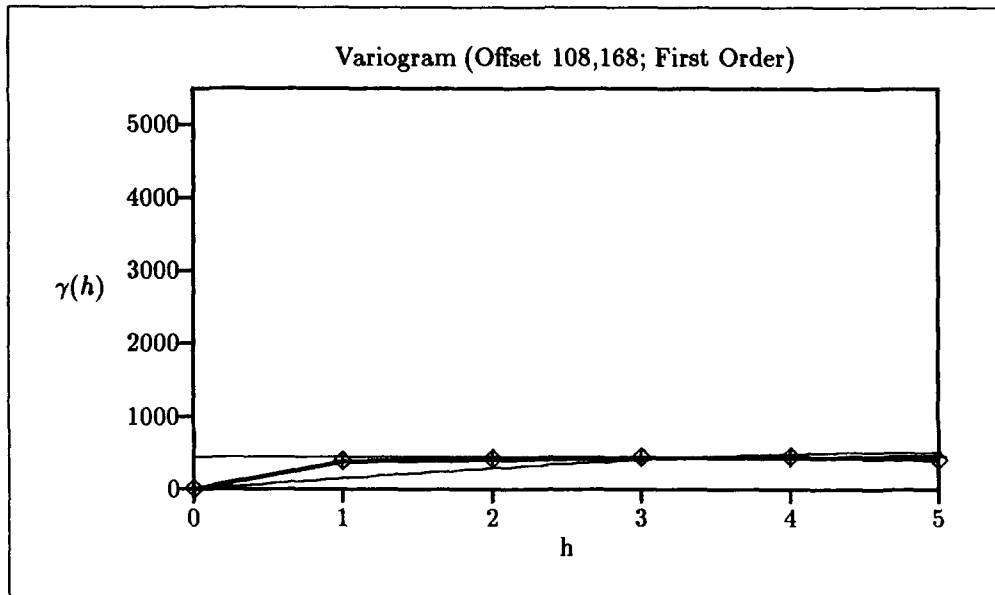


Figure C.60. SPOT 1 Channel 3.

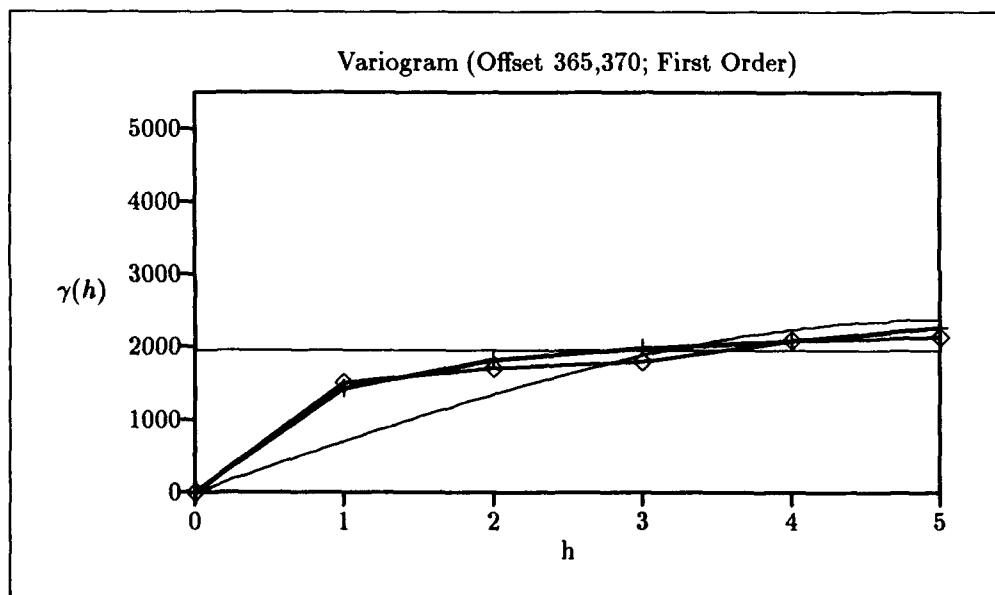


Figure C.61. SPOT 1 Channel 3.

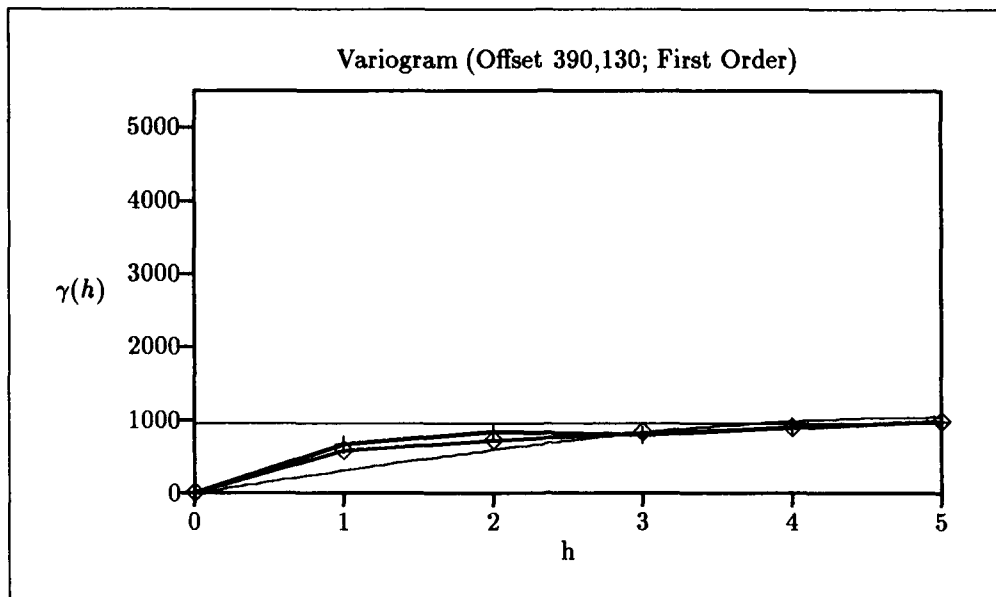


Figure C.62. SPOT 1 Channel 3.

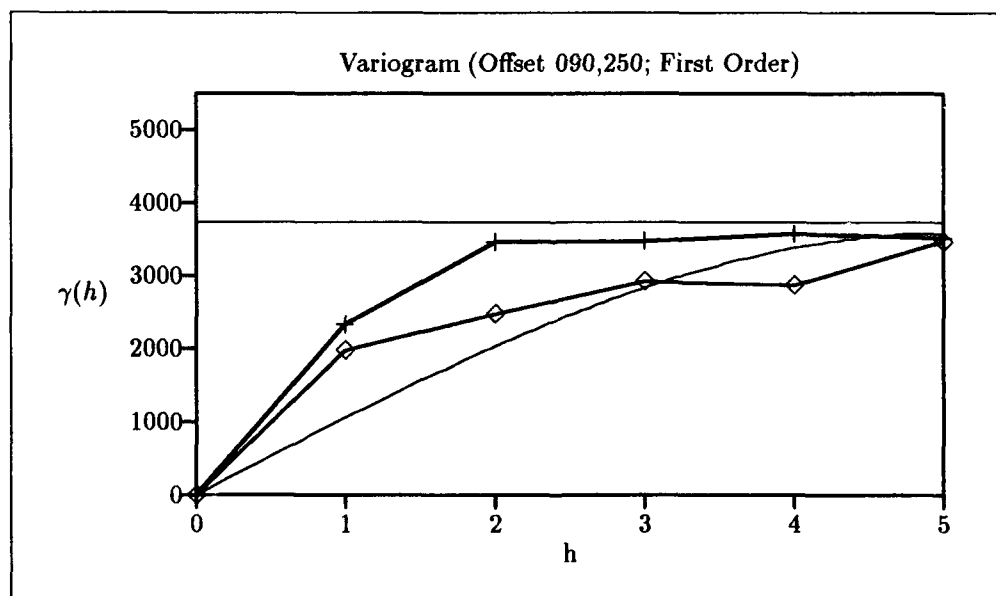


Figure C.63. SPOT 2 Channel 3.

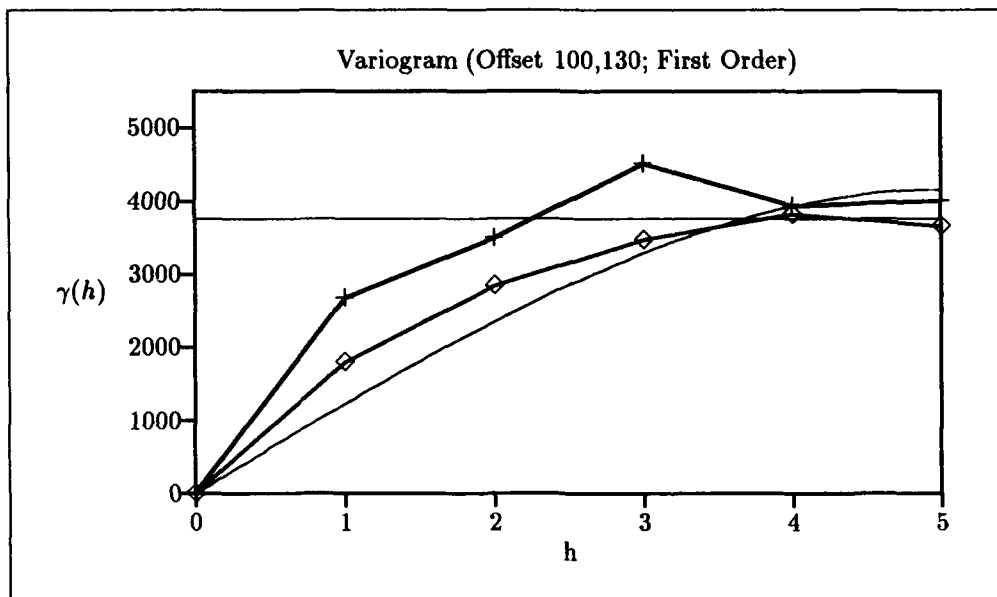


Figure C.64. SPOT 2 Channel 3.

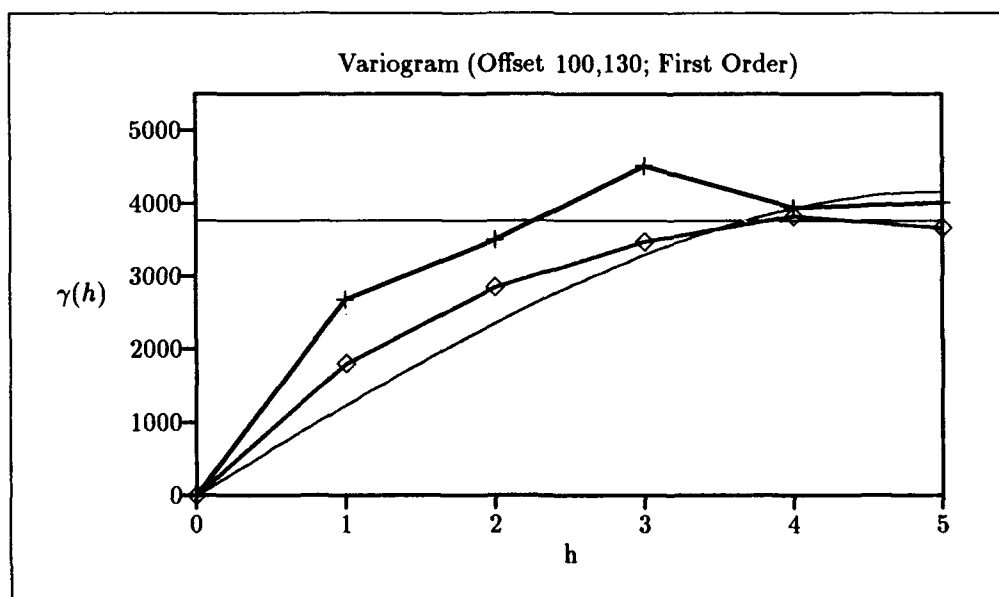


Figure C.65. SPOT 2 Channel 3.

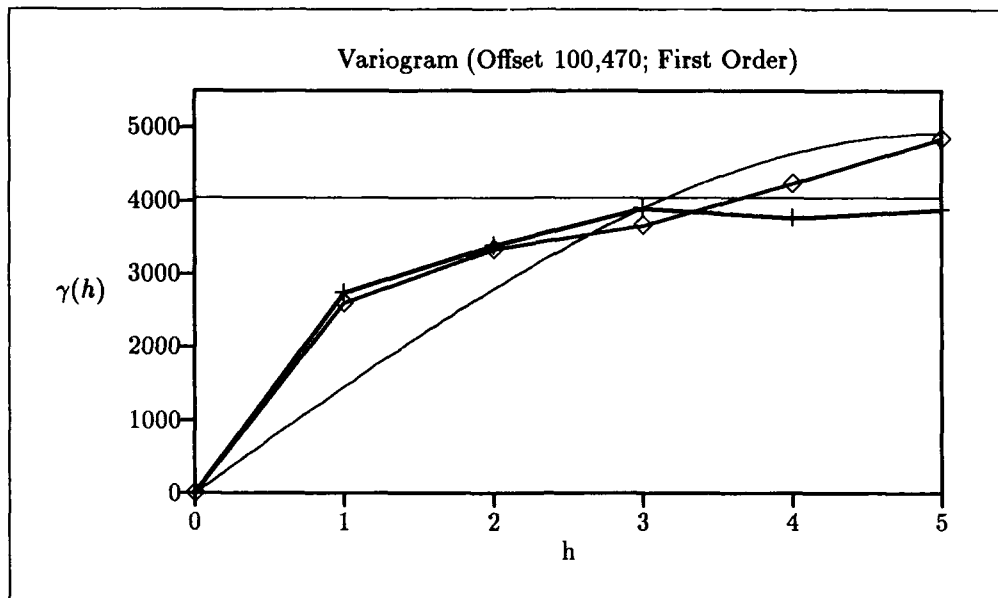


Figure C.66. SPOT 2 Channel 3.

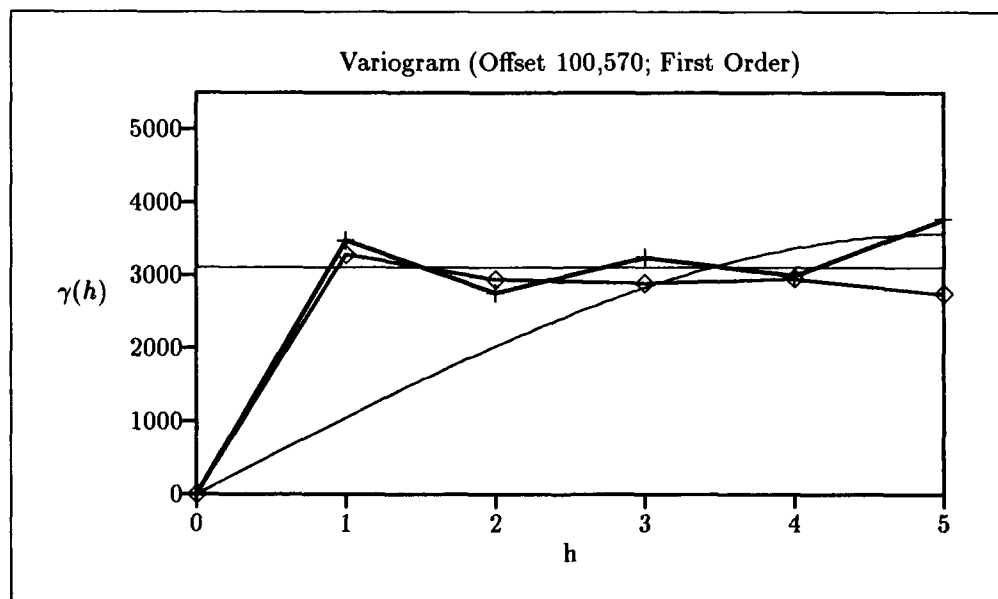


Figure C.67. SPOT 2 Channel 3.

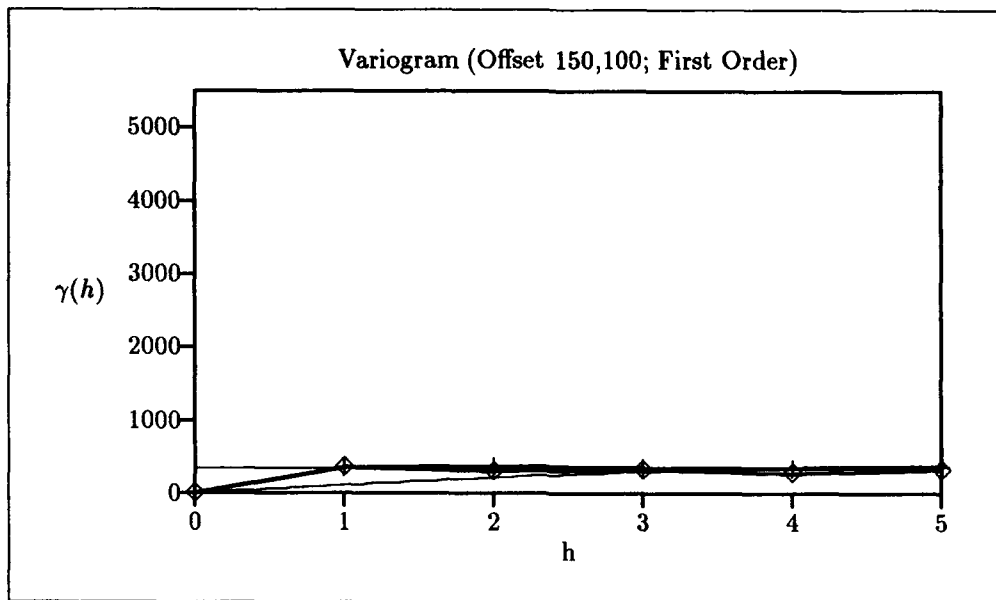


Figure C.68. SPOT 2 Channel 3.

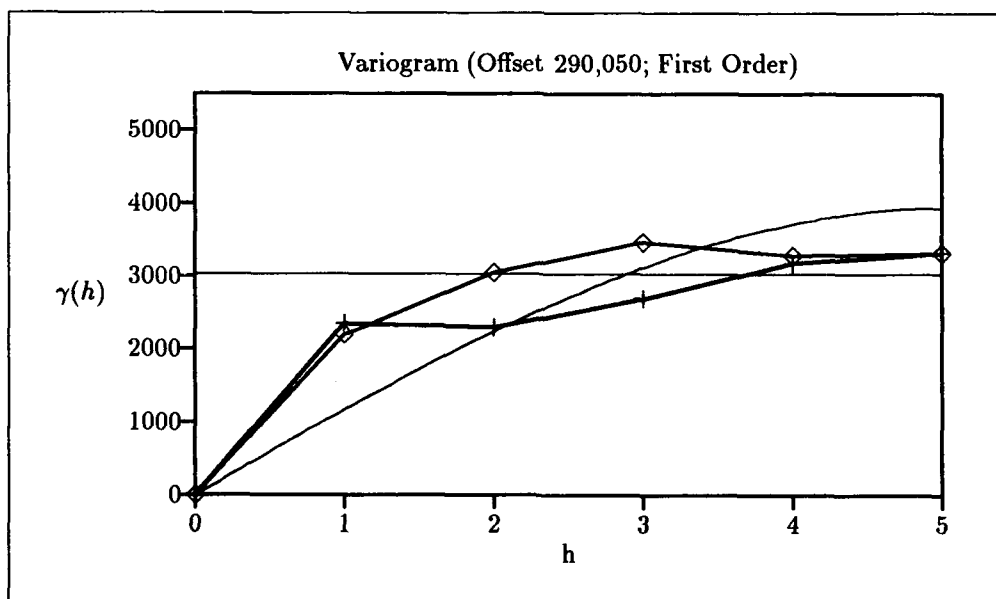


Figure C.69. SPOT 2 Channel 3.

C.4 Nugget (Exponential Model).

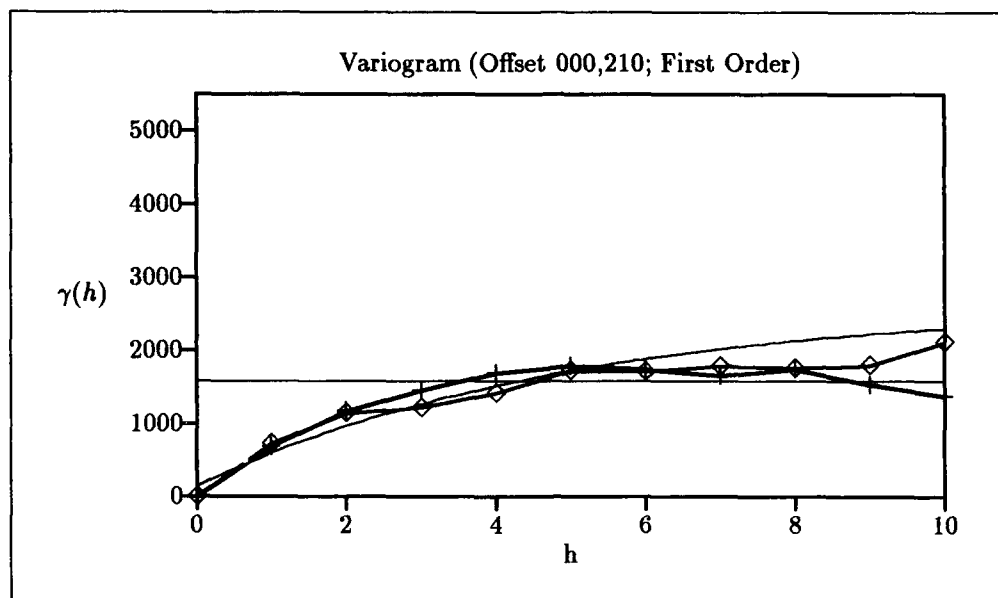


Figure C.70. SPOT 1 Channel 2.

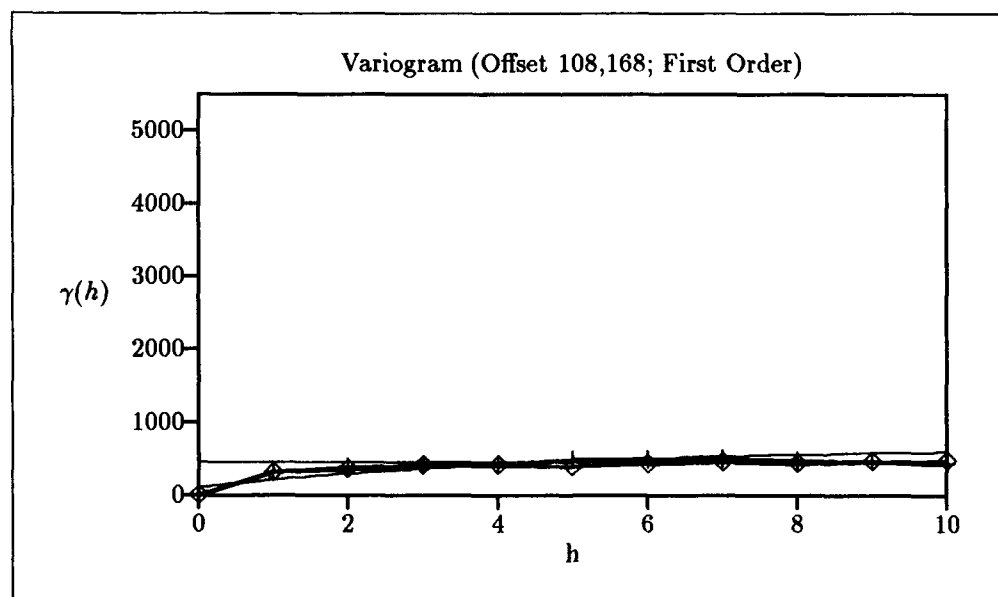


Figure C.71. SPOT 1 Channel 2.

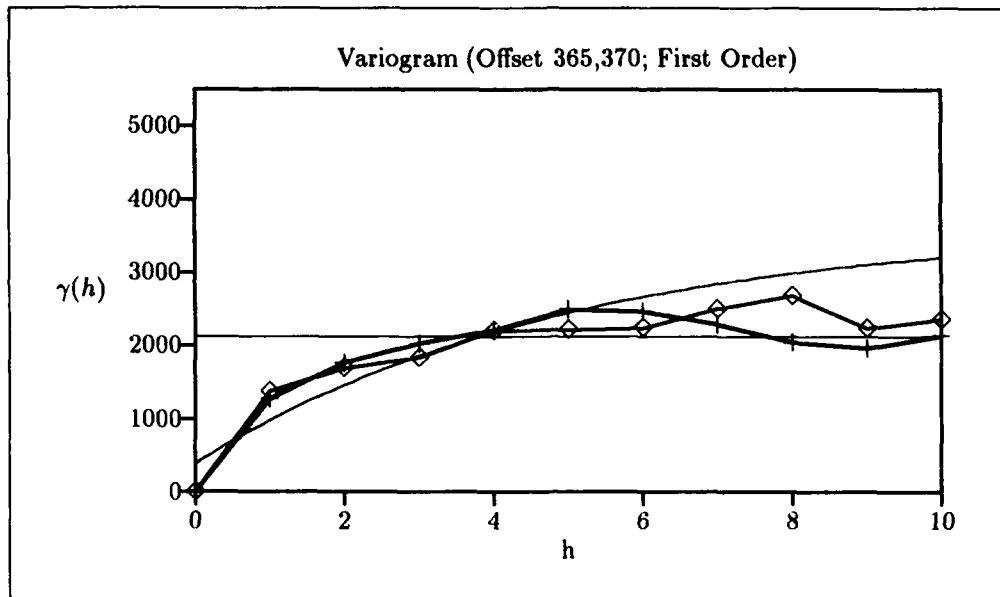


Figure C.72. SPOT 1 Channel 2.

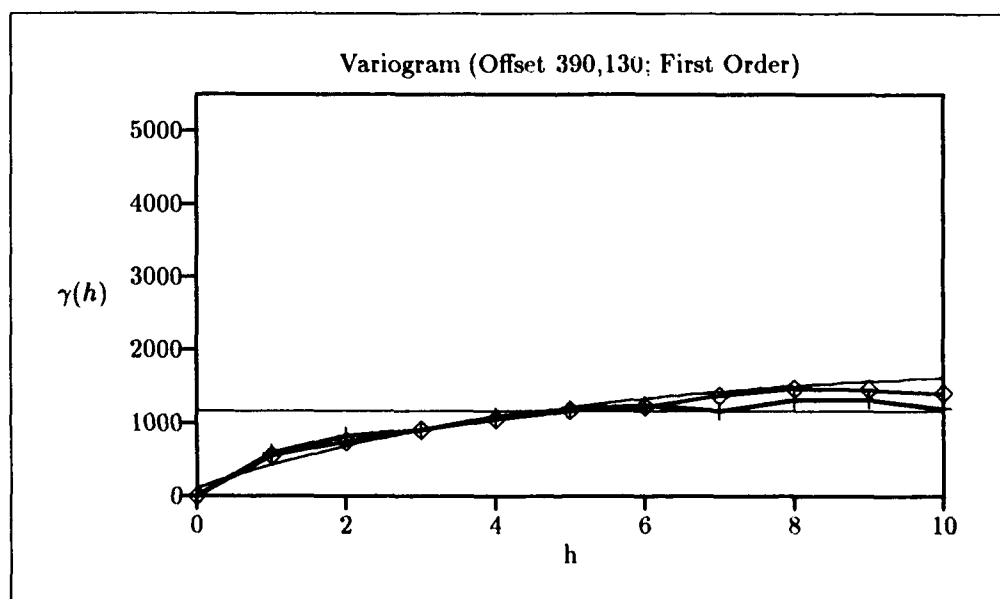


Figure C.73. SPOT 1 Channel 2.

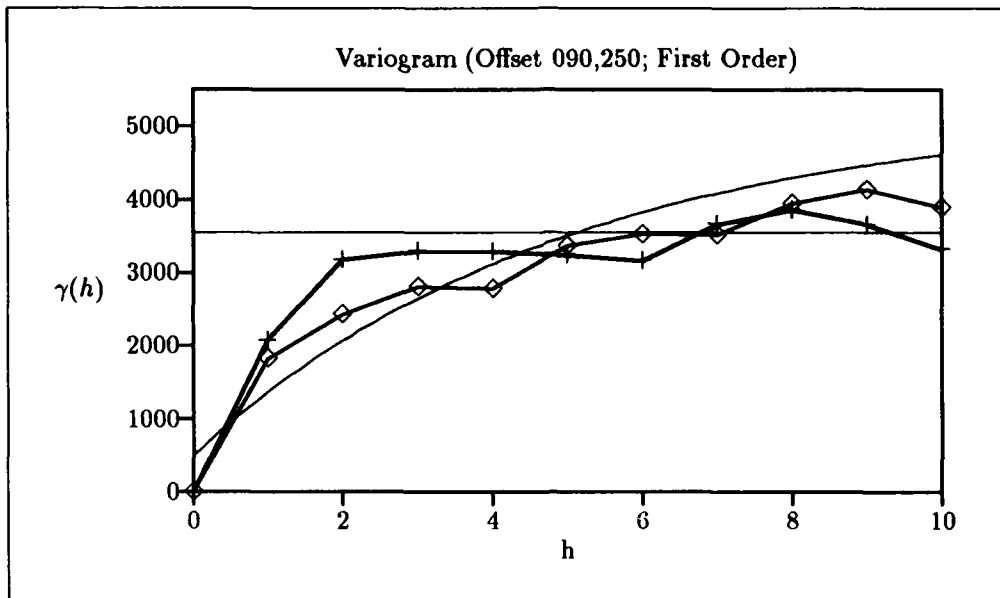


Figure C.74. SPOT 2 Channel 2.

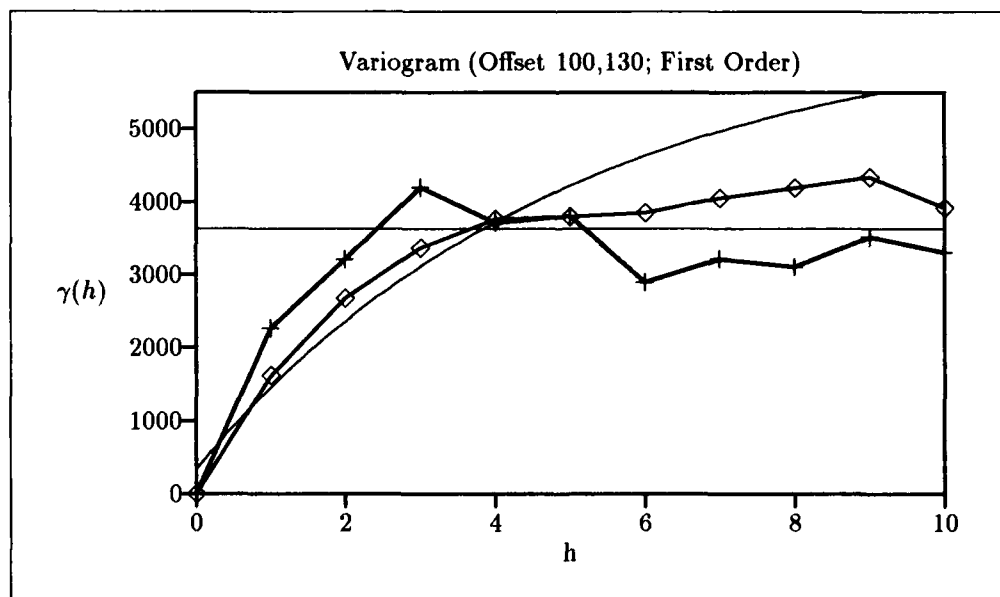


Figure C.75. SPOT 2 Channel 2.

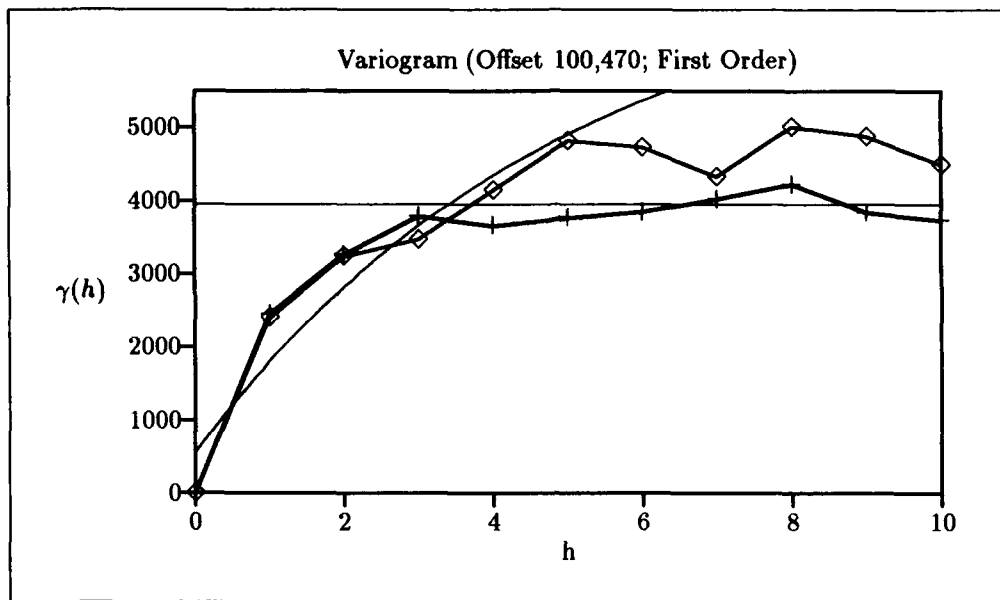


Figure C.76. SPOT 2 Channel 2.

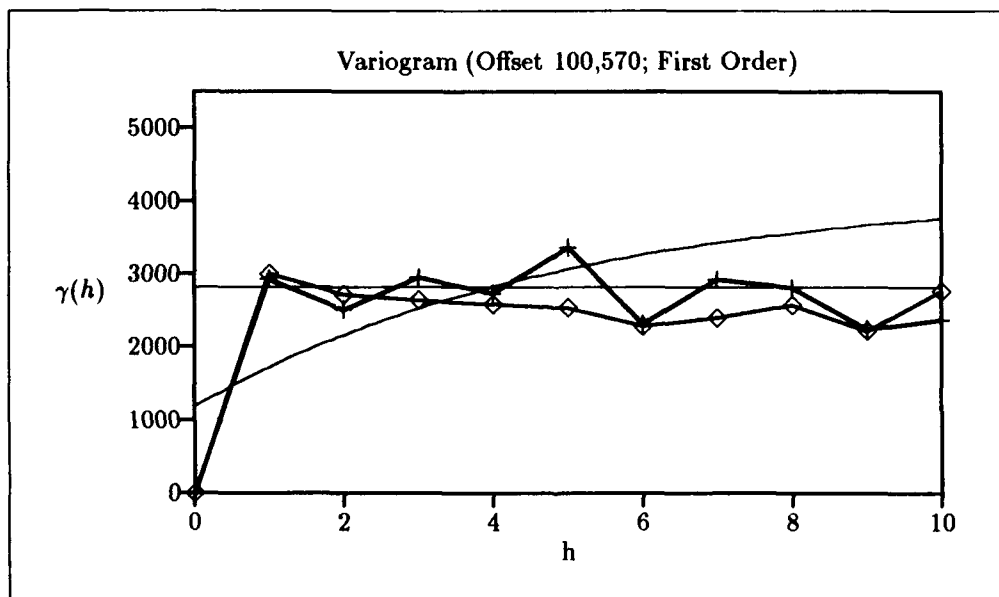


Figure C.77. SPOT 2 Channel 2.

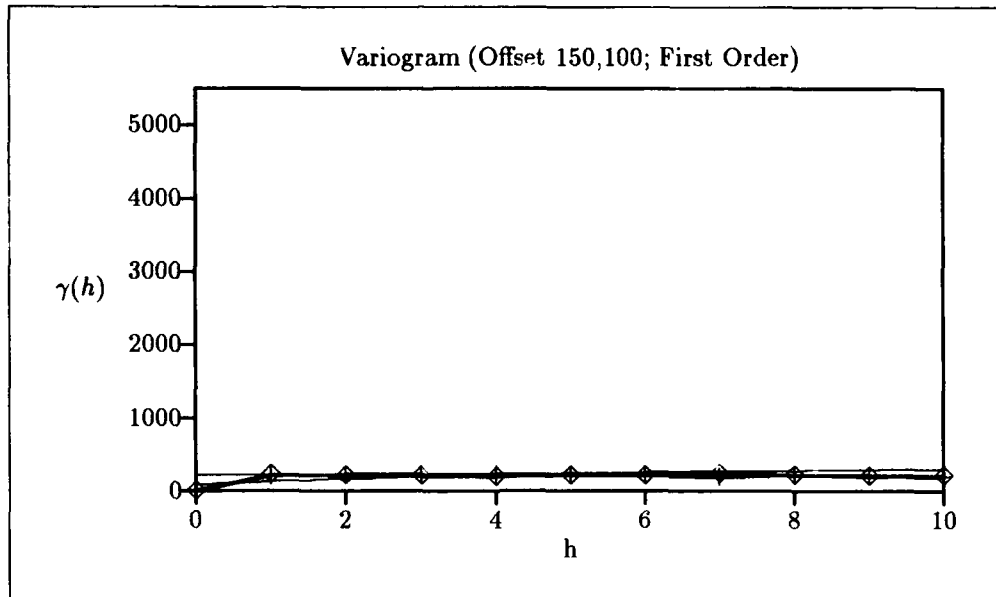


Figure C.78. SPOT 2 Channel 2.

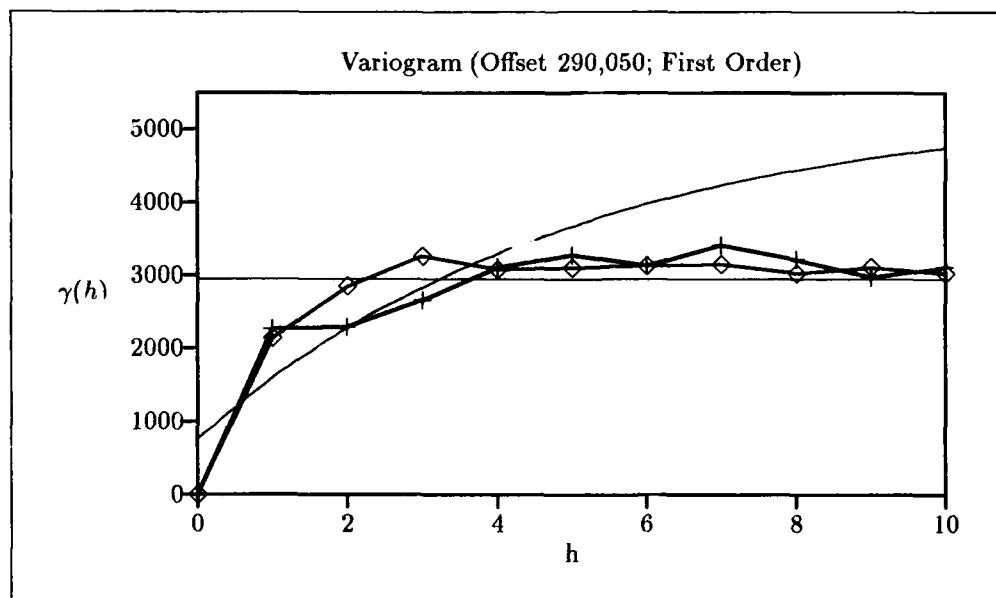


Figure C.79. SPOT 2 Channel 2.

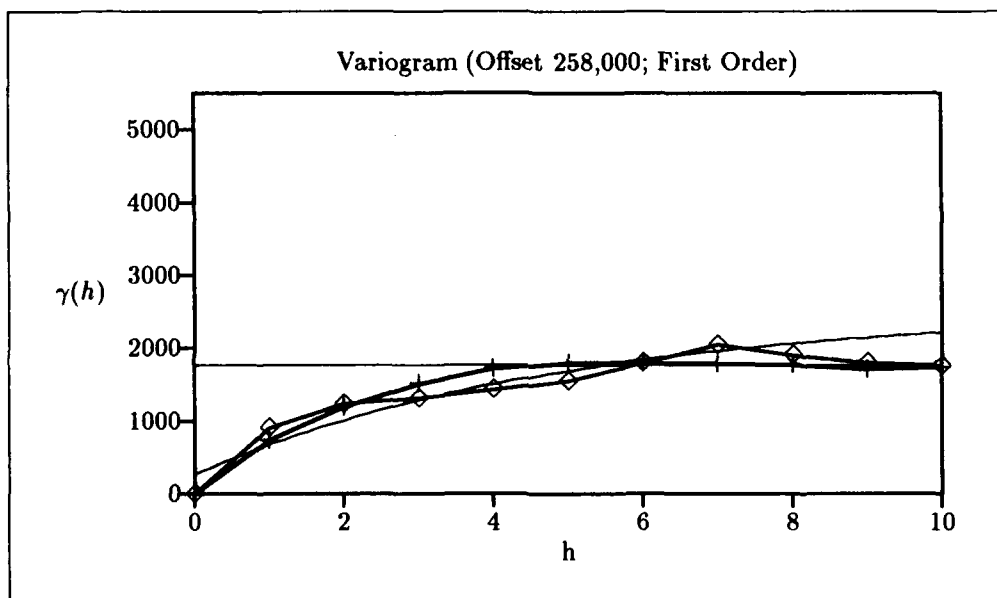


Figure C.80. SPOT 2 Channel 2.

C.5 Nugget (Spherical Model).

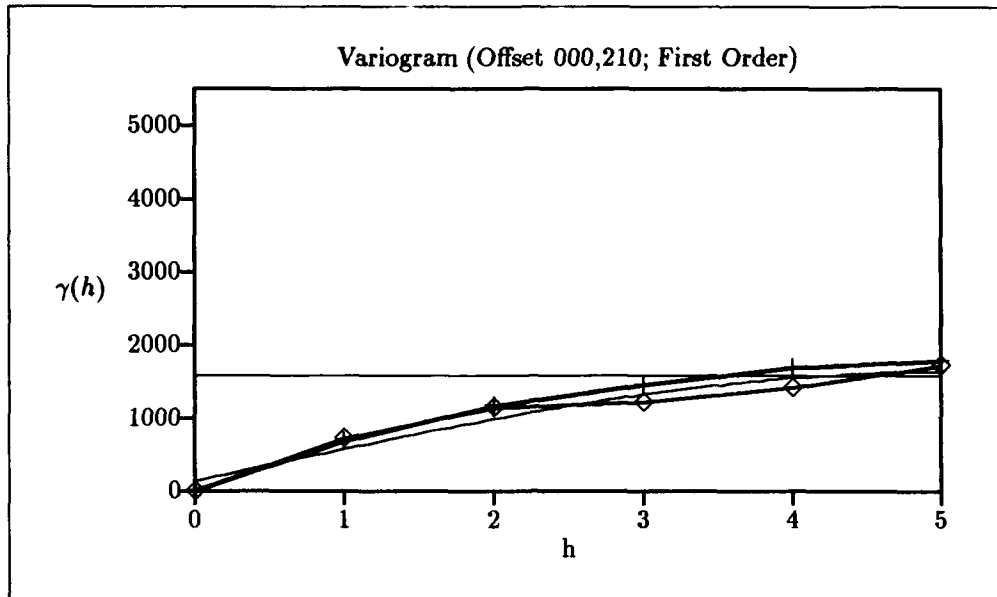


Figure C.81. SPOT 1 Channel 2.

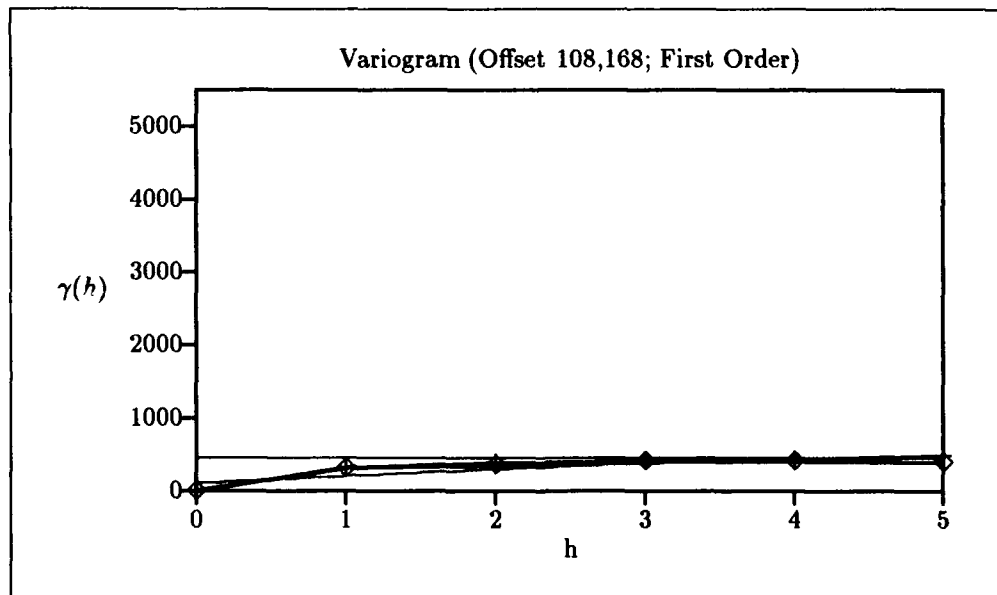


Figure C.82. SPOT 1 Channel 2.

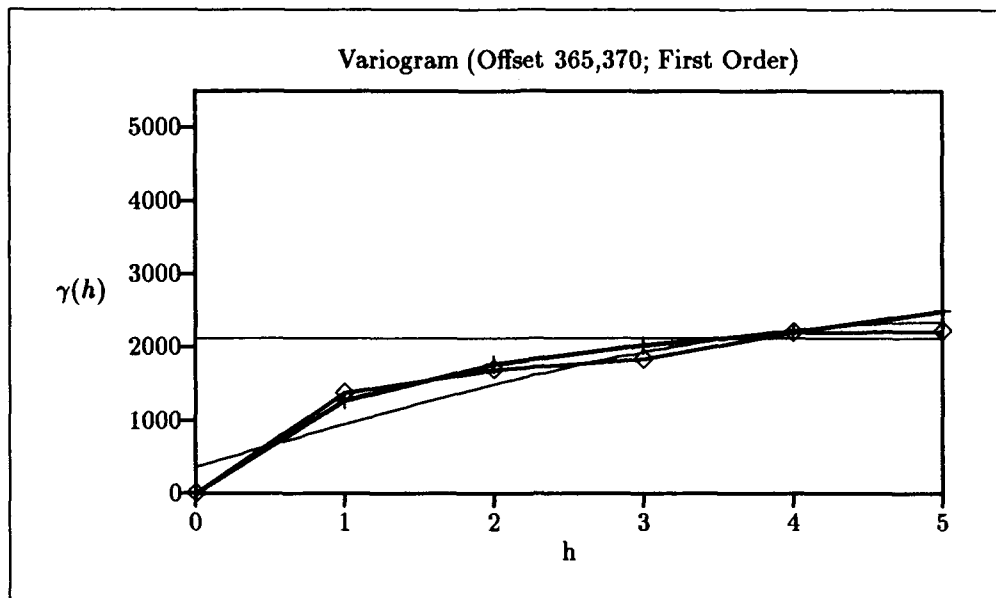


Figure C.83. SPOT 1 Channel 2.

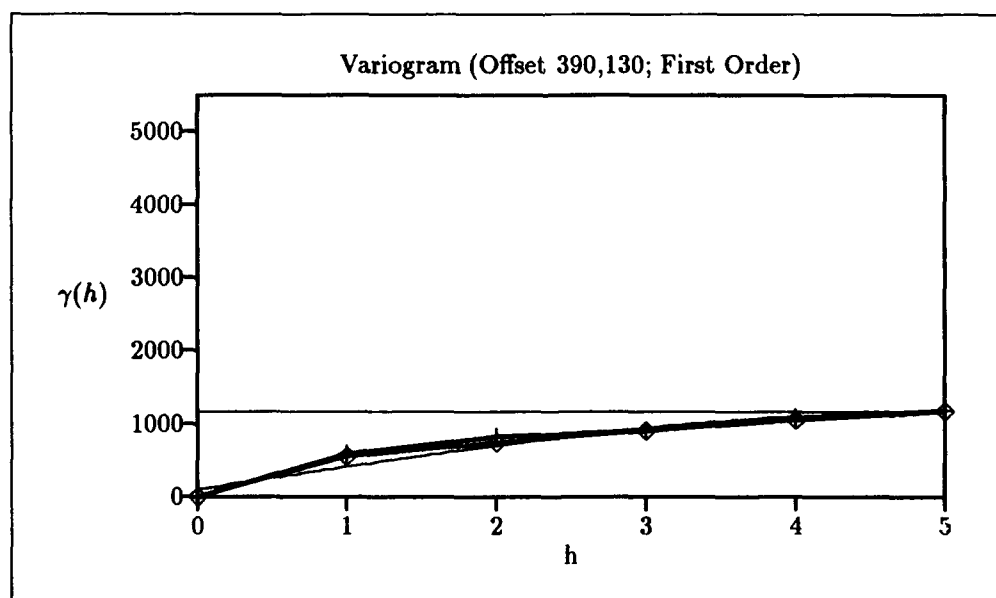


Figure C.84. SPOT 1 Channel 2.

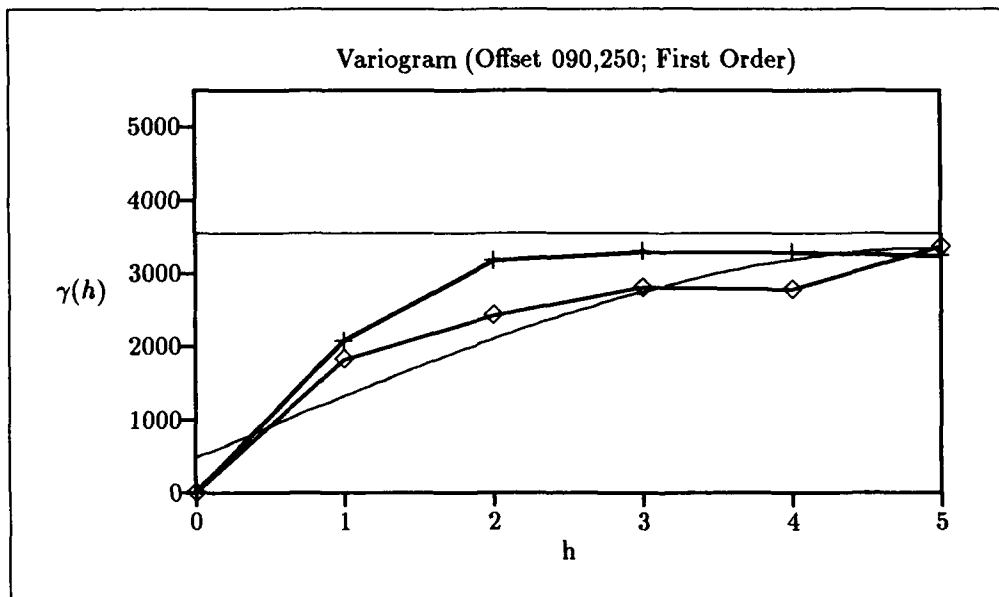


Figure C.85. SPOT 2 Channel 2.

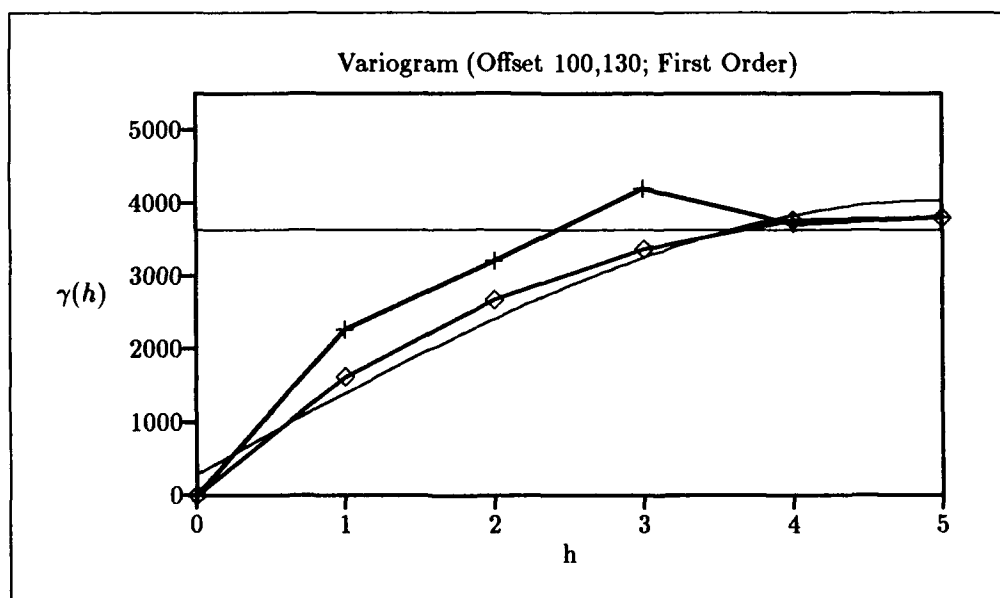


Figure C.86. SPOT 2 Channel 2.

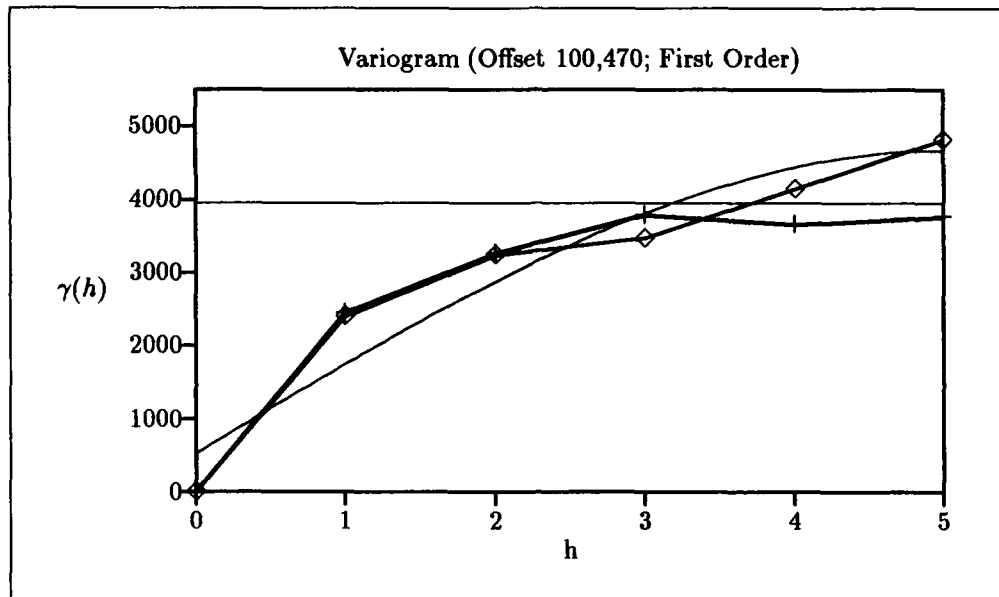


Figure C.87. SPOT 2 Channel 2.

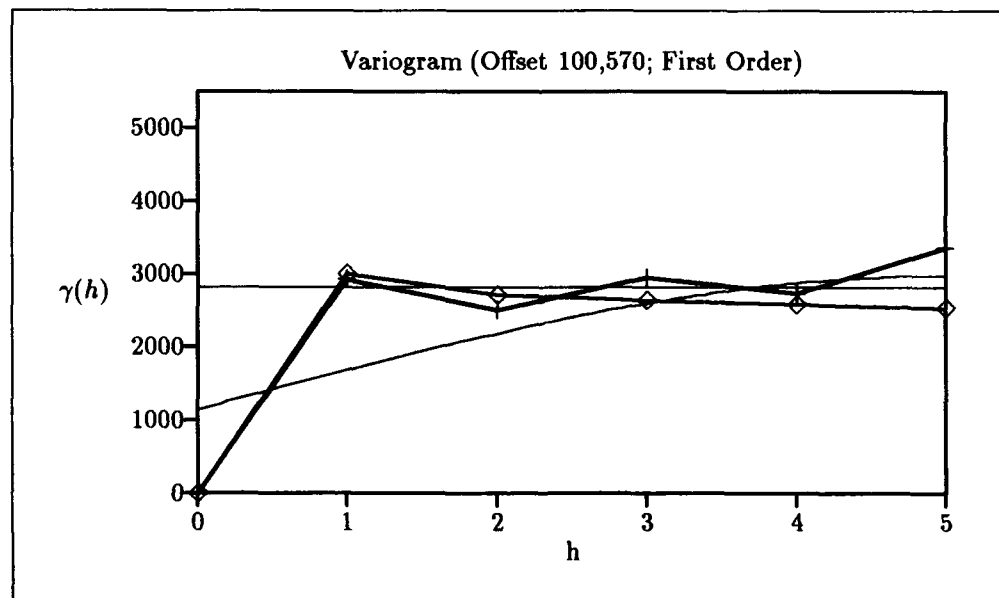


Figure C.88. SPOT 2 Channel 2.

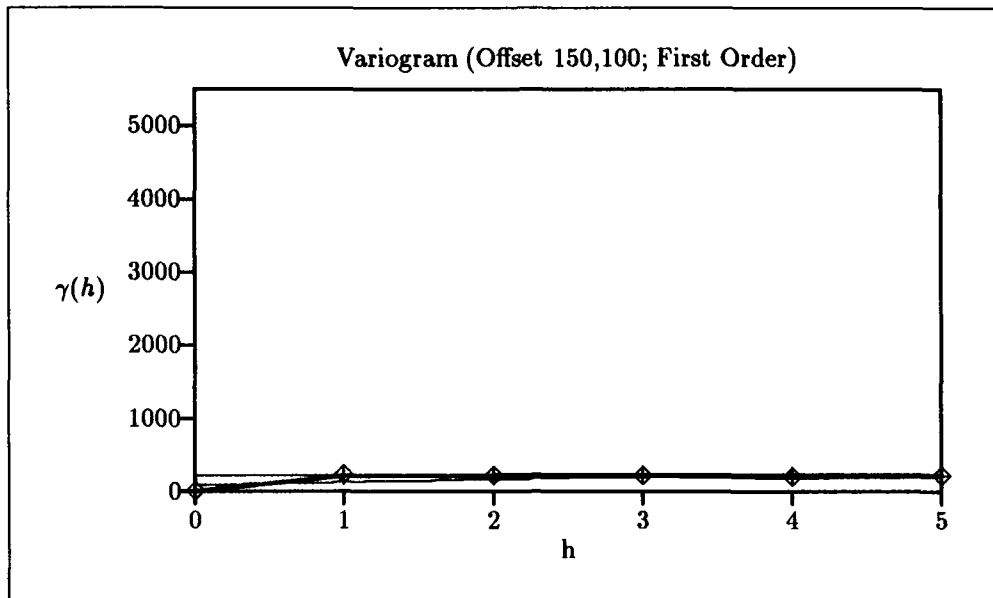


Figure C.89. SPOT 2 Channel 2.

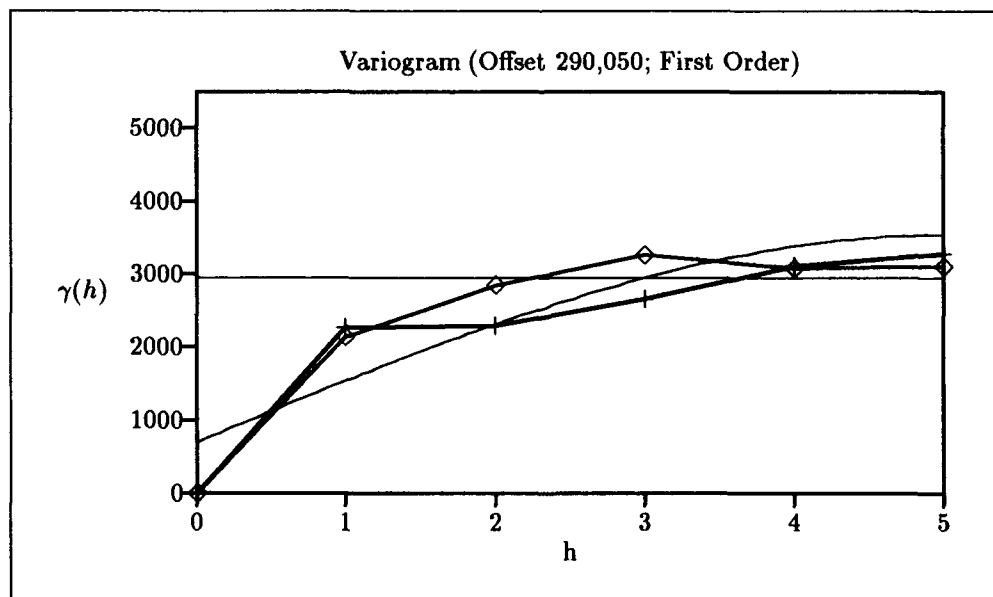


Figure C.90. SPOT 2 Channel 2.

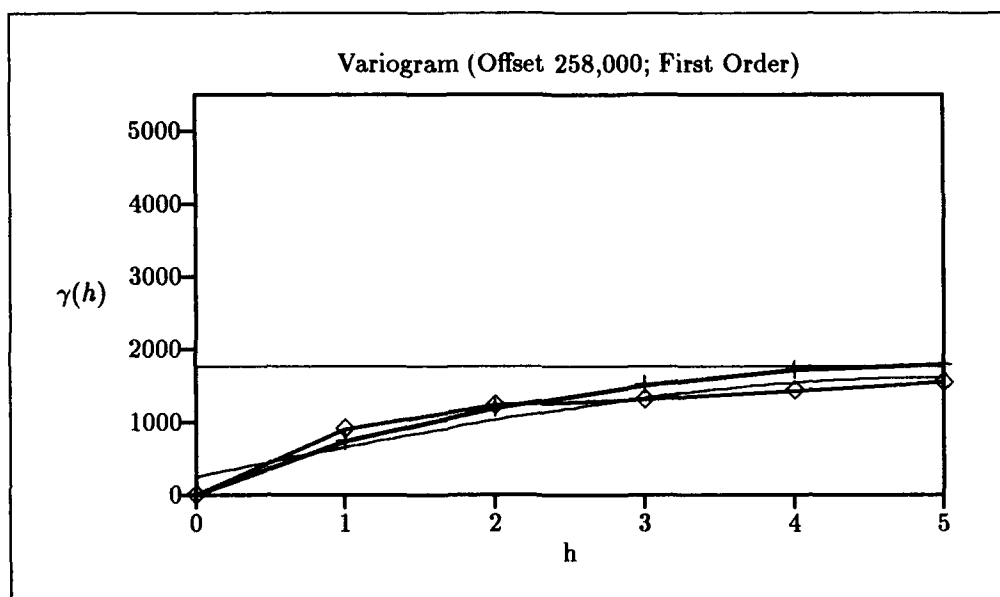


Figure C.91. SPOT 2 Channel 2.

Appendix D. Test Statistics (Mean and Standard Deviation)

The following is data generated in comparison of kriging and cubic convolution as well as the spherical and exponential models with interpolation method. Images were sub-sampled and data regenerated using all techniques. The reproduced image was then subtracted from the original data, a sample mean (\bar{x}) and standard deviation (s) of the difference was calculated for all pixels, and this data was compared between the two techniques.

D.1 Kriging and Cubic Convolution Comparison

If the tests statistics indicate that Kriging is the better of the two means or variances, a K will be entered in the table under the column Best, a C will be entered if Cubic convolution is best and a - if neither is considered best by the statistics.

Table D.1. Comparison Data of Kriging and Cubic Convolution, Channel 2.

SPOT 1	Kriging		Cubic Convolution		Test Statistics		Best	
Image Number	\bar{x}	s	\bar{x}	s	t	F_o	\bar{x}	s
Offset 000,210	16.34	17.27	16.64	17.94	.35	.93	-	-
Offset 108,168	11.15	8.77	12.35	9.78	2.68	.80	K	K
Offset 365,370	20.22	16.63	20.53	20.22	.34	.67	-	K
Offset 390,130	12.28	11.04	13.86	12.25	2.82	.81	K	K

Table D.2. Comparison Data of Kriging and Cubic Convolution, Channel 3.

SPOT 1	Kriging		Cubic Convolution		Test Statistics		Best	
Image Number	\bar{x}	s	\bar{x}	s	t	F_o	\bar{x}	s
Offset 000,210	19.09	19.31	19.43	19.9	.36	.93	-	-
Offset 108,168	12.75	9.59	14.3	10.36	3.23	.85	K	K
Offset 365,370	22.35	18.08	22.5	18.32	.17	.97	-	-
Offset 390,130	14.96	12.38	16.43	13.9	2.3	.78	K	K

Table D.3. Comparison Data of Kriging and Cubic Convolution, Channel 2.

SPOT 2	Kriging		Cubic Convolution		Test Statistics		Best	
Image Number	\bar{x}	s	\bar{x}	s	t	F_o	\bar{x}	s
Offset 090,250	18.95	19.25	19.56	19.14	.66	1.01	-	-
Offset 100,130	22.65	19.79	23.19	20.25	.56	.95	-	-
Offset 100,470	22.67	21.35	24.12	21.81	1.39	.95	-	-
Offset 100,570	34.01	27.96	35.83	30.75	1.28	.82	-	K
Offset 150,100	12.32	9.56	13.68	10.66	2.79	.80	K	K
Offset 290,050	27.37	26.66	28.27	28.65	.67	.87	-	-
Offset 258,000	15.98	12.94	16.5	13.9	.81	.87	-	-

Table D.4. Comparison Data of Kriging and Cubic Convolution, Channel 3.

SPOT 2	Kriging		Cubic Convolution		Test Statistics		Best	
Image Number	\bar{x}	s	\bar{x}	s	t	F_o	\bar{x}	s
Offset 090,250	20.62	20.3	21.45	20.34	.85	.99	-	-
Offset 100,130	25.13	21.36	25.91	21.51	.75	.98	-	-
Offset 100,470	24.19	22.84	25.61	23.33	1.28	.95	-	-
Offset 100,570	36.62	29.3	38.66	32.13	1.38	.83	-	K
Offset 150,100	16.11	14.19	18.12	15.95	2.77	.79	K	K
Offset 290,050	28.07	27.66	28.93	30.03	.62	.84	-	K
Offset 258,000	17.2	14.8	18.19	15.96	1.33	.85	-	-

D.2 Interpolation and Spherical Model Comparison

If the tests statistics indicate that interpolation is the better of the two means or variances, an I will be entered in the table under the column Best, a S will be entered if the Spherical model is best and a - if neither is considered best by the statistics.

Table D.5. Comparison Data of Interpolation and Spherical Model, Channel 2.

SPOT 1	Spherical Model		Interpolation		Test Statistics		Best	
Image Number	\bar{x}	s	\bar{x}	s	t	F_o	\bar{x}	s
Offset 000,210	16.32	17.25	16.34	17.27	.02	.99	-	-
Offset 108,168	11.08	8.72	11.15	8.77	.16	.98	-	-
Offset 365,370	20.38	16.67	20.22	16.63	-.20	1.0	-	-
Offset 390,130	12.75	10.92	12.28	11.04	-.89	.97	-	-

Table D.6. Comparison Data of Interpolation and Spherical Model, Channel 3.

SPOT 1	Spherical Model		Interpolation		Test Statistics		Best	
Image Number	\bar{x}	s	\bar{x}	s	t	F_o	\bar{x}	s
Offset 000,210	19.23	19.21	19.09	19.31	-.28	.95	-	-
Offset 108,168	12.67	9.56	12.75	9.59	.17	.99	-	-
Offset 365,370	22.56	17.9	22.35	18.08	-.24	.98	-	-
Offset 390,130	14.98	12.27	14.96	12.38	-.25	.98	-	-

Table D.7. Comparison Data of Interpolation and Spherical Model, Channel 2.

SPOT 2	Spherical Model		Interpolation		Test Statistics		Best	
Image Number	\bar{x}	s	\bar{x}	s	t	F_o	\bar{x}	s
Offset 090,250	19.69	19.01	18.95	19.25	-.81	.97	-	-
Offset 100,130	23.02	19.66	22.65	19.79	-.39	.98	-	-
Offset 100,470	23.32	21.31	22.67	21.35	-.63	.99	-	-
Offset 100,570	35.03	28.03	34.01	27.96	-.75	1.0	-	-
Offset 150,100	12.22	9.23	12.32	9.56	.22	.93	-	-
Offset 290,050	28.36	26.55	27.37	26.66	-.77	.99	-	-
Offset 258,000	16.19	12.9	15.98	12.94	-.34	.99	-	-

Table D.8. Comparison Data of Interpolation and Spherical Model, Channel 3.

SPOT 2	Interpolation		Spherical Model		Test Statistics		Best	
Image Number	\bar{x}	s	\bar{x}	s	t	F_o	\bar{x}	s
Offset 090,250	21.27	20.09	20.62	20.3	-.47	.92	-	-
Offset 100,130	25.5	21.24	25.13	21.36	-.36	.98	-	-
Offset 100,470	24.91	22.76	24.19	22.84	-.65	.99	-	-
Offset 100,570	37.76	29.23	36.62	29.3	-.81	.99	-	-
Offset 150,100	15.92	14.16	16.11	14.19	.27	.99	-	-
Offset 290,050	28.86	27.57	28.07	27.66	-.59	.99	-	-
Offset 258,000	17.43	14.74	17.2	14.8	-.32	.99	-	-

D.3 Interpolation and Exponential Model Comparison

If the tests statistics indicate that interpolation is the better of the two means or variances, an I will be entered in the table under the column Best, an E will be entered if the Exponential model is best and a - if neither is considered best by the statistics.

Table D.9. Comparison Data of Interpolation and Exponential Model, Channel 2.

SPOT 1	Exponential Mode		Interpolation		Test Statistics		Best	
Image Number	\bar{x}	s	\bar{x}	s	t	F_o	\bar{x}	s
Offset 000,210	16.34	17.26	16.34	17.27	0.0	.99	-	-
Offset 108,168	11.06	8.69	11.15	8.77	.21	.98	-	-
Offset 365,370	20.42	16.72	20.22	16.63	-.24	1.0	-	-
Offset 390,130	12.74	10.89	12.28	11.04	-.87	.97	-	-

Table D.10. Comparison Data of Interpolation and Exponential Model, Channel 3.

SPOT 1	Exponential Model		Interpolation		Test Statistics		Best	
Image Number	\bar{x}	s	\bar{x}	s	t	F_o	\bar{x}	s
Offset 000,210	19.25	19.21	19.09	19.31	-.17	.98	-	-
Offset 108,168	12.63	9.55	12.75	9.59	.26	.99	-	-
Offset 365,370	22.6	18	22.35	18.08	-.28	.99	-	-
Offset 390,130	14.96	12.24	14.96	12.38	0.0	.98	-	-

Table D.11. Comparison Data of Interpolation and Exponential Model, Channel 2.

SPOT 2	Exponential Model		Interpolation		Test Statistics		Best	
Image Number	\bar{x}	s	\bar{x}	s	t	F_o	\bar{x}	s
Offset 090,250	19.76	19.09	18.95	19.25	-.87	.98	-	-
Offset 100,130	23.11	19.66	22.65	19.79	-.48	.98	-	-
Offset 100,470	23.4	21.35	22.67	21.35	-.71	1.0	-	-
Offset 100,570	35.04	27.99	34.01	27.96	-.77	1.0	-	-
Offset 150,100	12.19	9.19	12.32	9.56	.28	.92	-	-
Offset 290,050	28.43	26.51	27.37	26.66	-.83	.98	-	-
Offset 258,000	16.23	12.91	15.98	12.94	-.40	.99	-	-

Table D.12. Comparison Data of Interpolation and Exponential Model, Channel 3.

SPOT 2	Exponential Model		Interpolation		Test Statistics		Best	
Image Number	\bar{x}	s	\bar{x}	s	t	F_o	\bar{x}	s
Offset 090,250	21.36	20.12	20.62	20.3	-.76	.98	-	-
Offset 100,130	25.57	21.25	25.13	21.36	-.43	.98	-	-
Offset 100,470	25	22.78	24.19	22.84	-.73	.99	-	-
Offset 100,570	37.78	29.19	36.62	29.3	-.82	.99	-	-
Offset 150,100	15.86	14.18	16.11	14.19	.36	.99	-	-
Offset 290,050	28.95	27.48	28.07	27.66	-.66	.99	-	-
Offset 258,000	17.48	14.73	17.2	14.8	-.39	.99	-	-

D.4 Non-Nugget and Nugget Comparison

D.4.1 *Spherical Model.* If the tests statistics indicate that non-nugget is the better of the two means or variances, an NN will be entered in the table under the column Best, a N will be entered if the Exponential model is best and a - if neither is considered bets by the statistics.

Table D.13. Comparison Data of Non-Nugget and Nugget, Channel 2, Spherical Model.

SPOT 1	Non-Nugget		Nugget		Test Statistics		Best	
Image Number	\bar{x}	s	\bar{x}	s	t	F_o	\bar{x}	s
Offset 000,210	16.32	17.25	16.83	17.64	.60	.95	-	-
Offset 108,168	11.08	8.72	11.04	8.58	-.09	1.0	-	-
Offset 365,370	20.38	16.67	22.12	17.89	2.09	.87	NN	-
Offset 390,130	12.75	10.92	13.11	10.75	.69	1.0	-	-

Table D.14. Comparison Data of Non-Nugget and Nugget, Channel 2, Spherical Model.

SPOT 2	Nugget		Non-Nugget		Test Statistics		Best	
Image Number	\bar{x}	s	\bar{x}	s	t	F_o	\bar{x}	s
Offset 090,250	19.69	19.01	22.59	20.45	3.06	.86	NN	-
Offset 100,130	23.02	19.66	24.46	19.96	1.51	.97	-	-
Offset 100,470	23.32	21.31	25.69	22.02	2.27	.93	NN	-
Offset 100,570	35.03	28.03	39.15	29.44	2.99	.90	NN	-
Offset 150,100	12.22	9.23	11.65	8.19	-1.36	1.27	-	N
Offset 290,050	28.36	26.55	31.5	26.96	2.44	.96	NN	-
Offset 258,000	16.19	12.9	17.63	13.54	2.27	.91	-	-

D.5 Non-Nugget and Nugget Comparison

Table D.15. Comparison Data of Non-Nugget and Nugget, Channel 2, Exponential Model.

SPOT 1	Non-Nugget		Nugget		Test Statistics		Best	
Image Number	\bar{x}	s	\bar{x}	s	t	F_o	\bar{x}	s
Offset 000,210	16.34	17.26	16.9	17.7	.66	.95	-	-
Offset 108,168	11.06	8.69	11.05	8.5	-.02	1.03	-	-
Offset 365,370	20.42	16.72	22.28	18	2.22	.86	NN	-
Offset 390,130	12.74	10.89	13.14	10.73	.77	1.03	-	-

Table D.16. Comparison Data of Non-Nugget and Nugget, Channel 2, Exponential Model.

SPOT 2	Non-Nugget		Nugget		Test Statistics		Best	
Image Number	\bar{x}	s	\bar{x}	s	t	F_o	\bar{x}	s
Offset 090,250	19.76	19.09	22.97	20.54	3.37	.86	NN	-
Offset 100,130	23.11	19.66	24.88	19.98	1.85	.96	-	-
Offset 100,470	23.4	21.35	25.92	22.07	2.42	.93	NN	-
Offset 100,570	35.04	27.99	39.23	29.53	3.03	.89	NN	-
Offset 150,100	12.19	9.19	11.63	8.16	-1.34	1.26	-	N
Offset 290,050	28.43	26.51	31.81	27.03	2.62	.96	NN	-
Offset 258,000	16.23	12.91	17.82	13.65	2.49	.89	NN	-

D.5.1 Exponential Model. Appendix E. Program

E.1 Program Listing

The following is the Pascal code used in thesis research.

```
Uses CRT,Misc,TP030,
      Support,
      MinMax,
      hmulreg,
      hmatmath,
      matasc,
      stats,
      leq,
      Printer;

type
  line = array [0..799] of byte;

const
  regression = false;
  second_order = false;
  model = 0; {0=None,1=Spherical,2=Square Root,3=Exponential}
  nugget = false;
  neighborhood = 4;
  kriging = 1; {0=Simple,1=Universal}
  sub_sample = 2;
  latex = true;
  debug = false;

var
  pixel_c,pixel_k      : double;
  pixel_o,
  num_iv,dim,start     : byte;
  result,r1,r2,
  rdim,cdim            : integer;
  rows,cols,
  h,i,j               : longint;
  max_lag,range        : word;
  col_offset,row_offset,
  k,kh,pixels,n        : longint;
  mean_res,std_res,var_res,
  mean,sumx,
  std_dev,variance,
  gc,nug,
  d,det,cond,maxerr,
  dif_c,dif_k,
  bias_c,bias_k,
  sum_c,sum_c2,sum_k,sum_k2,
  mean_c,mean_k,
  stdv_c,stdv_k,
  z_value              : double;
  cpix,kpix,
  reg                  : double;
```

```

c                : array [0..4] of double;
gamma0,gamma90   : array [0..200] of double;
cn,kn,
wM,wT,wL        : array [0..neighborhood-1,0..neighborhood-1] of double;
dist,
pixel,
data,coef,zest,resid,
gamma,gcoef,res,
AMat,AMatInv,
TRHS,MRHS,LRHS,
TSol,MSol,LSol,
KSol,CSol       : ARRDESP;
rst             : regstats;
fni,fno        : string;
buffer         : line;
fi             : file of line;
fo             : text;
fbo,fbf,fbk    : file of byte;
si,sj,di,dj,mi,mj : integer;

Function Variogram(dist : double) : double;
var
  lower,upper : byte;
begin
  case model of
    0 : begin
      if Trunc(dist) = dist then
        Variogram := gamma0[Trunc(dist)]
      else
        begin
          lower := Trunc(dist);
          upper := lower + 1;
          Variogram := gamma0[lower]
            + (gamma0[upper] - gamma0[lower])*(dist - lower);
        end; {else}
      end; {No Model}
    1 : begin
      Variogram := gc*(1.5-0.5*Sqr(dist/range))*(dist/range) + nug;
      end; {Spherical Model}
    2 : begin
      Variogram := gc*sqrt(dist) + nug;
      end; {Square Root Model}
    3 : begin
      Variogram := gc*(1-exp(-dist/range)) + nug;
      end; {Exponential Model}
  end; {case}
end; {Function Variogram}

BEGIN

{ Input image }
ClrScr;
fni := Select_File('Image','\IMAGES\DATA\*..*','SPOT1.CH1',1,1,15,5);
Assign(fi,'\IMAGES\DATA\'+fni);
Reset(fi);
GotoXY(1,8);

```

```

{ Initialize regression }
Write('Image width? ');
Read(cols);
Write('Image height? ');
Read(rows);
pixels := rows * cols;
pixel := HVectDef(pixels);
Write('Column offset? ');
Read(col_offset);
Write('Row offset? ');
Read(row_offset);
fno := 'K' + ThreeDigit(row_offset)
      + '-' + ThreeDigit(col_offset);
Write('Reading image... ');
k := 0;
for i := 0 to rows-1 do
  begin
    Seek(fi,row_offset+sub_sample*i);
    Read(fi,buffer);
    Mark_Time;
    for j := 0 to cols-1 do
      begin
        HVectWrtEl(pixel,k,buffer[col_offset+sub_sample*j],result);
        k := k + 1;
      end; {for j}
    end; {for i}
  Writeln;
  if debug then
    HMatSaveASC(pixel,fno+'.pix',9,3,result);
  mean := HVectMean(pixel,v_col,0,sumx);
  std_dev := HVectStDev(pixel,v_col,0,mean,variance);
  Writeln('Original Image');
  Writeln(' Mean      = ',mean:7:2);
  Writeln(' St Dev    = ',std_dev:7:2);
  Writeln(' Variance = ',variance:7:2);
  if sub_sample > 1 then
    begin
      Write('Writing original file before subsampling...');
      Seek(fi,row_offset);
      Assign(fbo,fno+'.ORI');
      Rewrite(fbo);
      for i := 0 to (sub_sample*rows)-1 do
        begin
          Mark_Time;
          Read(fi,buffer);
          for j := 0 to (sub_sample*cols)-1 do
            Write(fbo,buffer[col_offset+j]);
          end; {for i}
        Close(fbo);
      end; {if}
    Close(fi);
  if regression then
    begin
      if second_order then
        num_iv := 4
      else

```

```

    num_iv := 2;
    data := HMatDef(pixels,num_iv);
    zest := HVectDef(pixels);
    resid := HVectDef(pixels);
    coef := HVectDef(num_iv+1);
{ Initialize X independent variable }
    k := 0;
    Mark_Time;
    for i := 0 to rows-1 do
        for j := 0 to cols-1 do
            begin
                HMatWrtEl(data,k,0,j,result);
                k := k + 1;
            end; {for j}
{ Initialize Y independent variable }
    k := 0;
    Mark_Time;
    for i := 0 to rows-1 do
        for j := 0 to cols-1 do
            begin
                HMatWrtEl(data,k,1,i,result);
                k := k + 1;
            end; {for j}
    if second_order then
        begin
            { Initialize X^2 independent variable }
            k := 0;
            Mark_Time;
            for i := 0 to rows-1 do
                for j := 0 to cols-1 do
                    begin
                        HMatWrtEl(data,k,2,Sqr(j),result);
                        k := k + 1;
                    end; {for j}
            { Initialize Y^2 independent variable }
            k := 0;
            Mark_Time;
            for i := 0 to rows-1 do
                for j := 0 to cols-1 do
                    begin
                        HMatWrtEl(data,k,3,Sqr(i),result);
                        k := k + 1;
                    end; {for j}
            end; {if second_order}
        Writeln;
        if second_order then
            Write('Calculating second-order regression...')
        else
            Write('Calculating first-order regression...');
        HMultipleReg(data,pixel,coef,nil,TRUE,nil,result);
        for i := 0 to num_iv do
            c[i] := HVectReadEl(coef,i,result);
        Writeln;
        Write('Calculating residuals...');
        HStatAnalysis(data,pixel,coef,nil,nil,0.95,nil,resid,zest,rst);
        mean_res := HVectMean(resid,v_col,0,sumx);

```

```

std_res := HvectStDev(resid,v_col,0,mean_res,var_res);
Writeln;
Writeln('Residuals');
Writeln(' Mean      = ',mean_res:7:2);
Writeln(' St Dev    = ',std_res:7:2);
Writeln(' Variance = ',var_res:7:2);
end {if regression}
else
begin
Writeln;
end; {else no regression}
max_lag := IMin(cols div 2,rows div 2);
range := 5;
{ Zero degree variogram }
Write('Calculating zero degree variogram...');
gamma0[0] := 0;
for h := 1 to max_lag do
begin
Mark_Time;
n := 0;
gamma0[h] := 0;
for i := 0 to rows-1 do
for j := 0 to (cols - h - 1) do
begin
n := n + 1;
k := i*cols + j;
kh := i*cols + j + h;
if regression then
gamma0[h] := gamma0[h]
+ Sqr(HVectReadEl(resid,k,r1) - HVectReadEl(resid,kh,r2))
else
gamma0[h] := gamma0[h]
+ Sqr(HVectReadEl(pixel,k,r1) - HVectReadEl(pixel,kh,r2));
end; {for j}
gamma0[h] := gamma0[h]/(2*n);
end; {for h}
Assign(fo,fno+'.V00');
Rewrite(fo);
for h := 0 to max_lag do
Writeln(fo,h:3,gamma0[h]:10:2);
Close(fo);
Writeln;
{ Ninety degree variogram }
Write('Calculating ninety degree variogram...');
gamma90[0] := 0;
for h := 1 to max_lag do
begin
Mark_Time;
n := 0;
gamma90[h] := 0;
for j := 0 to cols-1 do
for i := 0 to (rows-h-1) do
begin
n := n + 1;
k := i*cols + j;
kh := (i+h)*cols + j;

```



```

        if regression then
            gamma90[h] := gamma90[h]
                        + Sqr(HVectReadEl(resid,k,r1) - HVectReadEl(resid,kh,r2))
        else
            gamma90[h] := gamma90[h]
                        + Sqr(HVectReadEl(pixel,k,r1) - HVectReadEl(pixel,kh,r2));
        end; {for i}
        gamma90[h] := gamma90[h]/(2*n);
    end; {for h}
    Assign(fo,fno+'.V90');
    Rewrite(fo);
    for h := 0 to max_lag do
        Writeln(fo,h:3,gamma90[h]:10:2);
    Close(fo);
    Writeln;
    if regression then
        begin
            HArrFree(data);
            HArrFree(zest);
            HArrFree(coef);
        end; {if regression}
{ Compute Model Coefficients (Zero Degree) }
    if model > 0 then
        begin
            num_iv := 1;
            data := HMatDef(range+1,num_iv);
            gamma := HVectDef(range+1);
            gcoef := HVectDef(num_iv+1);
        { Initialize matrices }
        for i := 0 to range do
            HVectWrtEl(gamma,i,gamma0[i],result);
        for i := 0 to range do
            case model of
                1 : HVectWrtEl(data,i,(1.5 - 0.5*Sqr(i/range))*(i/range),result);
                2 : HVectWrtEl(data,i,Sqrt(i),result);
                3 : HVectWrtEl(data,i,1-Exp(-i/range),result);
            end; {case}
        if nugget then
            begin
                HMultipleReg(data,gamma,gcoef,nil,TRUE,nil,result);
                nug := HVectReadEl(gcoef,0,result);
            end {if}
        else
            begin
                HMultipleReg(data,gamma,gcoef,nil,FALSE,nil,result);
                nug := 0;
            end; {else}
        gc := HVectReadEl(gcoef,1,result);
        end; {if model > 0}
{ Generate GNU Plot file }
    Assign(fo,fno+'.GNU');
    Rewrite(fo);
    if latex then
        begin
            Writeln(fo,'set term eepic');
            Writeln(fo,'set output "',fno,'2.tex"');

```

```

    end {if}
else
    Writeln(fo,'set term vgalib');
    Writeln(fo,'set size 1,1');
    Writeln(fo,'set nokey');
    Writeln(fo,'set xrange [0:',max_lag,']');
    Writeln(fo,'set yrange [0:5500]');
    Writeln(fo,'set tics out');
    Writeln(fo,'set xlabel "h"');
    Writeln(fo,'set ylabel "$\gamma(h)$");
    Write (fo,'set title "Variogram (Offset ',
        ThreeDigit(row_offset),',',
        ThreeDigit(col_offset));
if regression then
    if second_order then
        Writeln(fo,'; Second Order)')
    else
        Writeln(fo,'; First Order)')
else
    Writeln(fo,'; None)');
if regression then
    Write (fo,'plot ',var_res:8:2,', "k',
        ThreeDigit(row_offset),'-',
        ThreeDigit(col_offset),'.v00" w linesp, "k',
        ThreeDigit(row_offset),'-',
        ThreeDigit(col_offset),'.v90" w linesp')
else
    Write (fo,'plot ',variance:8:2,', "k',
        ThreeDigit(row_offset),'-',
        ThreeDigit(col_offset),'.v00" w linesp, "k',
        ThreeDigit(row_offset),'-',
        ThreeDigit(col_offset),'.v90" w linesp');
if model > 0 then
    begin
        Write(fo,' ',gc:8:3);
        case model of
            1 : Write(fo,'*(1.5*(x/',range,')-0.5*(x/',range,')**3)');
            2 : Write(fo,'*sqrt(x)');
            3 : Write(fo,'*(1-exp(-x/',range,'))');
        end; {case}
        if nugget then
            Writeln(fo,' + ',nug:8:3)
        else
            Writeln(fo);
        end {if}
    else
        Writeln(fo);
    Close(fo);
    HArrFree(data);
    HArrFree(gamma);
    HArrFree(gcoef);

{ Set up Kriging Equations }
if kriging = 0 then
    start := 1 {Simple kriging}
else

```

```

    start := 3; {Universal kriging}
    dim := Sqr(neighborhood) + start;
    AMat := HMatDef(dim,dim);
    TRHS := HVectDef(dim);
    MRHS := HVectDef(dim);
    LRHS := HVectDef(dim);
    TSol := HVectDef(dim);
    MSol := HVectDef(dim);
    LSol := HVectDef(dim);
    AMatInv := HMatDef(dim,dim);
    for i := 0 to start-1 do
        for j := 0 to start-1 do
            HMatWrtEl(AMat,i,j,0,result);
        for i := start to dim-1 do
            begin
                HMatWrtEl(AMat,0,i,1,result);
                HMatWrtEl(AMat,i,0,1,result);
            end; {for i}
        if kriging = 1 then
            begin
                n := 2;
                for i := 1 to neighborhood do
                    for j := 1 to neighborhood do
                        begin
                            n := n + 1;
                            HMatWrtEl(AMat,n,1,i,result);
                            HMatWrtEl(AMat,n,2,j,result);
                            HMatWrtEl(AMat,1,n,i,result);
                            HMatWrtEl(AMat,2,n,j,result);
                        end; {for j}
                    end; {else}
                for i := 0 to dim-(start + 1) do
                    for j := 0 to dim-(start + 1) do
                        begin
                            d := Sqrt(Sqr((i mod neighborhood) - (j mod neighborhood))
                                + Sqr((i div neighborhood) - (j div neighborhood)));
                            HMatWrtEl(AMat,i+start,j+start,Variogram(d),result);
                        end; {for j}
                    end; {for i}
                { Set up Middle RHS for kriging equations }
                HVectWrtEl(MRHS,0,1,result);
                if kriging = 1 then
                    begin
                        HVectWrtEl(MRHS,1,2.5,result);
                        HVectWrtEl(MRHS,2,2.5,result);
                    end;
                k := start;
                for i := 1 to 4 do
                    for j := 1 to 4 do
                        begin
                            d := Sqrt(Sqr(i - 2.5) + Sqr(j - 2.5));
                            HVectWrtEl(MRHS,k,Variogram(d),result);
                            k := k + 1;
                        end;
                    end;
                HGaussJordan(AMat,MRHS,MSol,AMatInv,det,cond,maxerr,result);
                if debug then
                    begin

```

```

    HMatSaveASC(AMatInv,fno+'.AMI',12,6,result);
    HMatSaveASC(MRHS,fno+'.RHM',12,6,result);
    HMatSaveASC(MSol,fno+'.WTM',12,6,result);
    end; {if debug}
{ Set up Top RHS for kriging equations }
HVectWrtEl(TRHS,0,1,result);
if kriging = 1 then
    begin
        HVectWrtEl(TRHS,1,2.0,result);
        HVectWrtEl(TRHS,2,2.5,result);
    end;
k := start;
for i := 1 to 4 do
    for j := 1 to 4 do
        begin
            d := Sqrt(Sqr(i - 2.0) + Sqr(j - 2.5));
            HVectWrtEl(TRHS,k,Variogram(d),result);
            k := k + 1;
        end;
HGaussJordan(AMat,TRHS,TSol,AMatInv,det,cond,maxerr,result);
if debug then
    begin
        HMatSaveASC(TRHS,fno+'.RHT',12,6,result);
        HMatSaveASC(TSol,fno+'.WTT',12,6,result);
    end; {if debug}
{ Set up Left RHS for kriging equations }
HVectWrtEl(LRHS,0,1,result);
if kriging = 1 then
    begin
        HVectWrtEl(LRHS,1,2.5,result);
        HVectWrtEl(LRHS,2,2.0,result);
    end;
k := start;
for i := 1 to 4 do
    for j := 1 to 4 do
        begin
            d := Sqrt(Sqr(i - 2.5) + Sqr(j - 2.0));
            HVectWrtEl(LRHS,k,Variogram(d),result);
            k := k + 1;
        end;
HGaussJordan(AMat,LRHS,LSol,AMatInv,det,cond,maxerr,result);
if debug then
    begin
        HMatSaveASC(LRHS,fno+'.RHL',12,6,result);
        HMatSaveASC(LSol,fno+'.WTL',12,6,result);
    end; {if debug}
HArrFree(AMat);
HArrFree(AMatInv);
HArrFree(LRHS);
HArrFree(TRHS);
HArrFree(MRHS);
k := 0;
for i := 0 to neighborhood-1 do
    for j := 0 to neighborhood-1 do
        begin
            wL[i,j] :=HVectReadEl(LSol,k+start,r1);

```

```

      wT[i,j] :=HVectReadEl(TSol,k+start,r1);
      wM[i,j] :=HVectReadEl(MSol,k+start,r1);
      k := k + 1;
    end; {for j}
  HArrFree(LSol);
  HArrFree(TSol);
  HArrFree(MSol);
  rdim := rows * sub_sample;
  cdim := cols * sub_sample;
  KSOL := HMatDef(rdim,cdim);
  CSOL := HMatDef(rdim,cdim);
  for si := 0 to rdim-1 do
    for sj := 0 to cdim-1 do
      begin
        mi := si mod sub_sample; di := si div sub_sample;
        mj := sj mod sub_sample; dj := sj div sub_sample;
        if (mi = 0) and (mj = 0) then
          { * Read original image/residual value * }
          begin
            k := di*cols + dj;
            cpix := HVectReadEl(pixel,k,r1);
            if regression then
              kpix := HVectReadEl(resid,k,r1)
            else
              kpix := HVectReadEl(pixel,k,r1);
            end {Replace with original value}
          else if ((di > 0) and (di < rows-2)) and
            ((dj > 0) and (dj < cols-2)) then
            { * Point to estimate is within borders for neighborhood size * }
            begin
              { * Set up neighborhood * }
              for i := 0 to neighborhood-1 do
                for j := 0 to neighborhood-1 do
                  begin
                    kh := (di-1+i)*cols + (dj-1+j);
                    cn[i,j] := HVectReadEl(pixel,kh,r1);
                    if regression then
                      kn[i,j] := HVectReadEl(resid,kh,r1)
                    else
                      kn[i,j] := HVectReadEl(pixel,kh,r1);
                    end; {for j}
                  end { * Estimate pixel value * }
                if (mi <> 0) and (mj <> 0) then
                  begin { * It's a middle position * }
                    cpix := (cn[0,0]+cn[0,3]+cn[3,0]+cn[3,3])
                      - 5*(cn[0,1]+cn[0,2]+cn[1,0]+cn[1,3]+cn[2,0]+
                        cn[2,3]+cn[3,1]+cn[3,2])
                      - 5*(cn[1,1]+cn[1,2]+cn[2,1]+cn[2,2]));
                    cpix := cpix/64;
                    kpix := 0;
                    for i := 0 to neighborhood-1 do
                      for j := 0 to neighborhood-1 do
                        kpix := kpix + wM[i,j]*kn[i,j];
                      end { * Middle * }
                    else if (mj <> 0) then
                      begin { * It's a top position * }

```

```

    cpix := 5*(cn[1,1]+cn[1,2]) - cn[1,0] - cn[1,3];
    cpix := cpix/8;
    kpix := 0;
    for i := 0 to neighborhood-1 do
        for j := 0 to neighborhood-1 do
            kpix := kpix + wT[i,j]*kn[i,j];
        end {* Top *}
    else
        begin {* It must be a left position *}
            cpix := 5*(cn[1,1]+cn[2,1]) - cn[0,1] - cn[3,1];
            cpix := cpix/8;
            kpix := 0;
            for i := 0 to neighborhood-1 do
                for j := 0 to neighborhood-1 do
                    kpix := kpix + wL[i,j]*kn[i,j];
                end; {else} (* Left *)
            end {else if}
        else {*** In border area ***}
            begin
                cpix := 0;
                kpix := 0;
            end;
        {* Add regression equation, if required *}
        if regression then
            begin
                if second_order then
                    reg := c[0] + c[1]*sj/2 + c[2]*si/2 + c[3]*Sqr(sj/2) + c[4]*Sqr(si/2)
                else
                    reg := c[0] + c[1]*sj/2 + c[2]*si/2;
                    kpix := reg - kpix;
                end; {if regression}
                HMatWrtEl(CSOL,si,sj,cpix,r1);
                HMatWrtEl(KSOL,si,sj,kpix,r1);
            end; {for sj}
        HArrFree(pixel);
        HArrFree(resid);

        Write('Calculating statistics... ');
        Assign(fbo,fno+'.ORI');
        Reset(fbo);
        sum_c := 0; sum_c2 := 0; bias_c := 0;
        sum_k := 0; sum_k2 := 0; bias_k := 0;
        n := 0;
        for si := 0 to rdim-1 do
            begin
                Mark_Time;
                for sj := 0 to cdim-1 do
                    begin
                        Read(fbo,pixel_o);
                        mi := si mod sub_sample; di := si div sub_sample;
                        mj := sj mod sub_sample; dj := sj div sub_sample;
                        if ((di > 0) and (di < rows-2)) and
                            ((dj > 0) and (dj < cols-2)) and
                            ((mi <> 0) or (mj <> 0)) then
                            begin
                                pixel_c := HMatReadEl(CSOL,si,sj,r1);

```

```

    pixel_k := HMatReadEl(KSOL,si,sj,ri);
    n := n + 1;
    dif_c := (pixel_o - pixel_c);
    dif_k := (pixel_o - pixel_k);
    bias_c := bias_c + dif_c;
    bias_k := bias_k + dif_k;
    sum_c := sum_c + Abs(dif_c);
    sum_k := sum_k + Abs(dif_k);
    sum_c2 := sum_c2 + Sqr(dif_c);
    sum_k2 := sum_k2 + Sqr(dif_k);
  end; {if}
end; {for j}
end; {for i}
HArrFree(KSOL);
HArrFree(CSOL);
mean_c := sum_c/n;
stdv_c := sqrt((n*sum_c2 - Sqr(sum_c))/(n*(n-1)));
mean_k := sum_k/n;
stdv_k := sqrt((n*sum_k2 - Sqr(sum_k))/(n*(n-1)));
z_value := (mean_c-mean_k)/(sqrt((sqr(stdv_k)/n + sqr(stdv_c)/n)));
Writeln;
Writeln('Cubic Error');
Writeln(' Mean = ',mean_c:5:2,' (',(bias_c/n):5:2,')');
Writeln(' StDv = ',stdv_c:5:2);
Writeln('Kriging Error');
Writeln(' Mean = ',mean_k:5:2,' (',(bias_k/n):5:2,')');
Writeln(' StDv = ',stdv_k:5:2);
Writeln;
Writeln('Z value = ',z_value:5:2);
Writeln('      n = ',n);

```

END.

E.2 Quinn-Curtis Routine Description

The following is a brief description of the Quinn Curtis procedures used in the program above (22:).

- HMatDef/HVecDef creates a matrix/vector of type REAL.
- HMatWrtEl/HMatReadEl writes or reads one element from a real matrix.
- HVecWrtEl/HMatReadEl writes or reads one element from a real vector.
- HMultipleReg fits a least squares multiple regression equation to a data set. It chooses a model which minimizes the sum of squares of the distances between the observed responses and one predicted by the fitted model.

- **HStatAnalysis** performs a statistical analysis of regression results to include standard error, multiple correlation coefficient, coefficient of determination, as well as significance of regression.
- **HVectMean** determines the mean of a vector.
- **HVectStDev** determines the standard deviation of a vector.
- **HArrFree** makes available memory space used by an array.
- **HGaussJordan** solves a system of linear equations using Gauss-Jordan method with partial pivoting. Returns the inverse of the original matrix as well as its determinant and solution.

Bibliography

1. Bernstein, Ralph. *All-Digital Precision Processing of ERTS Images, Final Report* Goddard Space Flight Center, 1975.
2. Bernstein, Ralph. "Digital Image Processing of Earth Observation Sensor Data" *IBM Journal of Research and Development* Vol. 20, No. 1, January 1976.
3. Billingsley, Fred C. *et al.* "Data Processing and Reprocessing," *Manual of Remote Sensing* 719-792. Falls Church, VA: American Society of Photogrammetry, 1983.
4. Christensen, Ronald *Linear Models for Multivariate, Time Series, and Spatial Data*. Springer-Verlag, 1991.
5. Clark, Isobel. *Practical Geostatistics*. London: Elsevier Applied Science, 1987.
6. Cressie, Noel. "Geostatistics," *The American Statistician*, 43(4):197-202 (November 1989).
7. Cressie, Noel. "The Origins of Kriging," *Mathematical Geology* Vol. 22, No. 3, 239-252, 1990.
8. David, Michel. *Geostatistical Ore Reserve Estimation*, New York: Elsevier Scientific Publishing Company, 1977.
9. Davis, John C. *Statistics and Data Analysis in Geology* (Second Edition). New York: John Wiley and Sons, 1986.
10. Evans, Howard E. and James J. Lange. Staff notes distributed in PHYS 521, Space Surveillance. School of Engineering, Air Force Institute of Technology (AU), Wright-Patterson AFB OH, Version B, May 1985.
11. Evans, Howard E. and James J. Lange. Staff notes distributed in PHYS 621, Electro-Optical Space Systems Technology. School of Engineering, Air Force Institute of Technology (AU), Wright-Patterson AFB OH, January 1989.
12. Freund, John E. *et al.* *Probability and Statistics for Engineers* (Fourth Edition). Prentice-Hall, Inc., 1990.
13. Gonzalez, Rafael C. and Richard E. Woods. *Digital Image Processing*. Addison-Wesley Publishing Company Inc., 1992.
14. Hord, R. Michael. *Digital Image Processing of Remotely Sensed Data*. Academic Press, 1982.
15. Huijbregts, Ch. J. and A. G. Journel. *Mining Geostatistics*. Academic Press, 1978.
16. Lillesand, Thomas M. and Ralph W. Kiefer. *Remote Sensing and Image Interpretation* (Second Edition). New York: John Wiley and Sons, 1987.
17. Mather, Paul M. *Computer Processing of Remotely-Sensed Images, an Introduction*. John Wiley and Sons, 1987.
18. Matheron, G. "Principles of Geostatistics," *Economic Geology*, 58:1246-1266 (1963).
19. McGee, Donald W., *The Application of Statistical Kriging to Improve Satellite Imagery Resolution*. MS Thesis, AFIT/GSO/ENS/91D-13. School of Engineering, Air Force Institute of Technology (AU), Wright-Patterson AFB OH, December 1991.
20. Moik, Johannes G., *Digital Processing of Remotely Sensed Images*. National Aeronautics and Space Administration, SP-431, 1980.
21. Neter, John *et al.* *Applied Linear Statistical Models* (Third Edition). Richard D. Irwin, Inc., 1990.

22. Quinn-Curtis, Inc. *The Huge Virtual Array and Numerical Analysis Toolbox for Turbo Pascal*, IPC-TP-030, Version 2.0, 1991.

Vita

Captain David John Blaufuss was born in Emporia, Kansas on April 5, 1962. He graduated from Osage City High School, Osage City, Kansas as a member of the National Honor Society and Bausch-Lomb science award winner. He graduated from Emporia State University, with honors, with a Bachelor of Science degree in Physics in 1984. Captain Blaufuss is a member of Sigma Pi Sigma national physics honor society and Kappa Mu Epsilon national mathematics honor society. He attended officer training school and was commissioned a second lieutenant in the United States Air Force on December 17, 1985. Captain Blaufuss joined Air Force Systems Command and was stationed at Peterson Air Force Base, Colorado where he took part in the activation of the Consolidated Space Operations Center. He entered into Planner/Analyst (PA) training for the Defense Satellite Communications System, Phase III (DSCS III) satellite system. Captain Blaufuss became the only DSCS III PA to maintain a highly-qualified rating throughout his tenure in the position. In 1990, he became the program lead for DSCS III, where he managed the transfer of the operational mission of the DSCS III constellation from Air Force Systems Command to Air Force Space Command. In May 1991, Captain Blaufuss entered the School of Engineering of the Air Force Institute of Technology to pursue a degree in Space Operations. He will separate from the Air Force in December 1992.

Permanent address: 633 Sunset Drive
Osage City, Kansas 66523

REPORT DOCUMENTATION PAGE			Form Approved OMB No. 0704-0188	
Public reporting burden for this collection of information is estimated to average 1 hour per response, including the time for reviewing instructions, searching existing data sources, gathering and maintaining the data needed, and completing and reviewing the collection of information. Send comments regarding this burden estimate or any other aspect of this collection of information, including suggestions for reducing this burden, to Washington Headquarters Services, Directorate for Information Operations and Reports, 1215 Jefferson Davis Highway, Suite 1204, Arlington, VA 22202-4302, and to the Office of Management and Budget, Paperwork Reduction Project (0704-0188), Washington, DC 20503.				
1. AGENCY USE ONLY (Leave blank)	2. REPORT DATE December 1992	3. REPORT TYPE AND DATES COVERED Master's Thesis		
4. TITLE AND SUBTITLE ANALYSIS OF KRIGING APPLIED TO RESOLUTION ENHANCEMENT OF DIGITAL SATELLITE IMAGERY		5. FUNDING NUMBERS		
6. AUTHOR(S) David J. Blaufuss, Captain, USAF				
7. PERFORMING ORGANIZATION NAME(S) AND ADDRESS(ES) Air Force Institute of Technology, WPAFB OH 45433-6583		8. PERFORMING ORGANIZATION REPORT NUMBER AFIT/GSO/ENS/92D-3		
9. SPONSORING/MONITORING AGENCY NAME(S) AND ADDRESS(ES)		10. SPONSORING/MONITORING AGENCY REPORT NUMBER		
11. SUPPLEMENTARY NOTES				
12a. DISTRIBUTION / AVAILABILITY STATEMENT Approved for public release; distribution unlimited		12b. DISTRIBUTION CODE		
13. ABSTRACT (Maximum 200 words) To aid the viewer in interpreting the information contained in an image, spatial resolution of the image can be increased. One way to increase the resolution is to improve the optics and sensors of the imaging system. Another is to process the data on the ground by computer. Enhancement techniques can be employed to alter the image and extract necessary data. Current techniques to manipulate and enlarge an image are nearest-neighbor, bilinear interpolation, and cubic convolution which can give greater clarity and readability. To satisfy the growing demand for quality (high-resolution) remotely sensed images, new techniques to enhance images need to be developed. Kriging is the geostatistical spatial estimation technique developed by Matheron that optimally predicts spatial data using observations at nearby locations. This research investigates the application of kriging as a technique of digital image resolution enhancement by adapting its use for the personnel computer and validating its capability and reliability. Twenty-seven percent of the images tested produced significantly lower means for kriging than cubic convolution with 45 percent of the kriged images producing lower variances.				
14. SUBJECT TERMS kriging, semi-variogram, variogram, resolution, cubic convolution, bilinear interpolation, nearest neighbor		15. NUMBER OF PAGES 138		
		16. PRICE CODE		
17. SECURITY CLASSIFICATION OF REPORT Unclassified	18. SECURITY CLASSIFICATION OF THIS PAGE Unclassified	19. SECURITY CLASSIFICATION OF ABSTRACT Unclassified	20. LIMITATION OF ABSTRACT UL	